Image Cover Sheet

CLASSIFICATION	SYSTEM NUMBER
UNCLASSIFIED	499040

TITLE

ACOUSTIC PROPERTIES OF SONAR DOME MATERIALS

System Number:

Patron Number:

Requester:

Notes:

DSIS Use only:

Deliver to:

ADA399040.PDF [Page: 3 of 112]

National Defence
Research and Development Branch

Défense nationale
Bureau de recherche et développement

DREA CR/96/420

ACOUSTIC PROPERTIES OF SONAR DOME MATERIALS

by
Quanshun Liu — Jacques Y. Guigné

GUIGNÉ INTERNATIONAL LIMITED
685 St. Thomas Line
Paradise, Newfoundland, Canada
A1L 1C1

CONTRACTOR REPORT

Prepared for

Defence Research Establishment Atlantic

Centre de Recherches pour la Défense Atlantique

Canada

THIS IS AN UNEDITED REPORT ON SCIENTIFIC OR TECHNICAL WORK CONTRACTED BY THE DEFENCE RESEARCH ESTABLISHMENT ATLANTIC OF THE RESEARCH AND DEVELOPMENT BRANCH OF THE DEPARTMENT OF NATIONAL DEFENCE, CANADA.

THE CONTENTS OF THE REPORT ARE THE RESPONSIBILITY OF THE CONTRACTOR, AND DO NOT NECESSARILY REFLECT THE OFFICIAL POLICIES OF THE DEPARTMENT OF NATIONAL DEFENCE.

PLEASE DIRECT ENQUIRIES TO:

THE CHIEF,
DEFENCE RESEARCH ESTABLISHMENT ATLANTIC,
P.O. BOX 1012,
DARTMOUTH, NOVA SCOTIA, CANADA
B2Y 3Z7

National Defence
Research and Development Branch

Défense nationale
Bureau de recherche et développement

DREA CR/96/420

ACOUSTIC PROPERTIES OF SONAR DOME MATERIALS

by
Quanshun Liu — Jacques Y. Guigné

GUIGNÉ INTERNATIONAL LIMITED
685 St. Thomas Line
Paradise, Newfoundland, Canada
A1L 1C1

Scientific Authority Jeffrey P. Szabo
J.P. Szabo

W7707-4-2930/01-HAL
Contract Number

May 1996

CONTRACTOR REPORT

Prepared for

Defence Research Establishment Atlantic

Centre de Recherches pour la Défense Atlantique

Canada

The correct citation for this report is:

Liu, Q. and Guigné, J.Y., 1996, "Acoustic Properties of Sonar Dome Materials." DREA Contractor Report CR/96/420.

ABSTRACT

The acoustic properties of composite panels made from high strength polyethylene Spectra Fiber were compared to conventional glass fiber composites, and to the double walled stainless steel design currently used in the C5 Sonar Dome. Characterization consisted of insertion loss measurements from 0-40 kHz using a parametric array projector, and "self noise" measurements from 0-6 kHz. All the panels but the cyanate-based 4H Spectra Fiber composite panel tested had very low insertion losses (<1 dB) below 10 kHz at normal incidence. Apart from the epoxy-based 4H panel, the Spectra Fiber composite panels had lower insertion losses, and less angular dependence of the insertion loss, than both the glass fiber composites and the double walled stainless steel panel in the 0-40 kHz range. Of the two different resin systems examined, epoxy and cyanate ester, the cyanate ester resin based composite panels had slower water uptake rates than the epoxy panels, but there was no significant difference in the insertion losses below 10 Hz. In general, the angular dependence of the insertion losses below 10 kHz was minimal with the exception of the 4H epoxy Spectra Fiber panel, which had a slightly higher angular dependence. Aging the composite panels in water resulted in some slightly reduced insertion losses, with the exception of the 4H cyanate Spectra Fiber panel. The self noise experiments consisted of measuring the radiated sound produced by a mechanically excited panel placed at the air/water interface in a reverberant tank. Comparison of the composite panels to the stainless steel dome section was complicated by the rigidity of the stainless steel structure, which produced few modes in the frequency range studied.

RÉSUMÉ

Les propriétés acoustiques des panneaux de composite de Spectra Fiber de polyéthylène à haute résistance ont été comparées à celles des composites classiques de fibre de verre, de même qu'à celles des panneaux d'acier inoxydable à double paroi employés à l'heure actuelle dans le dôme sonar C5. La caractérisation consistait à prendre des mesures de l'affaiblissement d'insertion de 0 à 40 kHz au moyen d'un projecteur paramétrique en réseau et des mesures de "bruit propre" de 0 à 6 kHz. Le taux d'affaiblissement d'insertion de tous les panneaux mis à l'essai, à l'exception du panneau en composite de Spectra Fiber 4H à base de cyanate, était très faible (<1 dB) à moins de 10 kHz à un angle d'incidence perpendiculaire. À l'exception du panneau 4H à base d'époxy, les panneaux de composite de Spectra Fiber avaient des taux d'affaiblissement d'insertion plus faibles et une dépendance angulaire de l'affaiblissement d'insertion moins marquée que celle des composites de fibre de verre et du panneau en acier inoxydable à double paroi dans l'intervalle de 0 à 40 kHz. Des deux différentes résines employées, l'époxy et l'ester de cyanate, les panneaux constitués de composite à base d'ester de cyanate avaient des taux d'absorption d'eau moins élevés que ceux des panneaux en époxy, mais la différente entre les taux d'affaiblissement d'insertion n'était pas très élevée à moins de 10 kHz. De façon générale, la dépendance angulaire des taux d'affaiblissement d'insertion à moins de 10 kHz était minime, sauf dans le cas du panneau en époxy de Spectra Fiber 4H, qui présentait une dépendance angulaire légèrement plus élevée. Le vieillissement des panneaux de composites dans l'eau a permis d'obtenir des taux d'affaiblissement d'insertion légèrement plus faibles, sauf dans le cas du panneau de cyanate de Spectra Fiber 4H. Les expériences portant sur le bruit propre consistaient à mesurer le son émis par un panneau exposé à une vibration mécanique à l'interface air-eau dans un réservoir réverbérant. La comparaison des panneau de composite pour la section du dôme en acier inoxydable s'est avérée plus difficile en raison de la rigidité de la structure en acier inoxydable, ce qui a donné lieu à quelque modes de fréquences différents dans l'intervalle de fréquences étudiés.

PERFACE

Background

The C5 Sonar Dome currently used on Canadian naval vessels is made from double walled stainless steel, which corrodes and is expensive to fabricate. Director Maritime Combat Systems (DMCS) is investigating composite materials as an alternative to the stainless steel domes in hopes of reducing maintenance costs and improving the acoustic properties of the dome material. In this study, the acoustic properties of composite materials made from two different reinforcing fibers, Spectra Fiber® and glass, were compared to the double walled stainless steel design used in the C5 dome.

Principal Results

The principal test used to characterize the materials was insertion loss, i.e., the reduction in sonar signal resulting from insertion of a test panel between projector and receiver. Both the composite and stainless steel panels tested had very low insertion losses ($<$ 1 dB) in the frequency range 0 - 10 kHz, but the Spectra Fiber composites clearly had better acoustic properties in the 10 - 40 kHz frequency range than either the glass fiber composites or the double walled stainless steel panel. Aging the samples in water did not appreciably alter the insertion losses. The "self noise" characteristics of the composite panels were comparable to the double walled stainless steel panel, but it was suggested that full scale tests would be more conclusive.

Significance of Results

The results indicate that from an acoustic point of view, Spectra or glass fiber reinforced plastics would be as good as, and probably better than, the double walled stainless steel currently used in C5 sonar domes.

Future Plans

In addition to studying the mechanical properties of glass and Spectra reinforced composites, DREA may be asked to comment on the effect of impact damage on the acoustic properties of the composite panels and the effect of thickness on the insertion loss.

by J.P. Szabo
DREA Scientific Authority

TABLE OF CONTENTS

ABSTRACT ii

PREFACE iii

LIST OF FIGURES v

LIST OF PHOTOGRAPHS viii

LIST OF TABLES viii

LIST OF APPENDICES ix

1.0 INTRODUCTION 1

2.0 MATERIALS AND METHODOLOGY 2
2.1 TEST PANELS 2
2.2 EXPERIMENTAL METHODS 3
2.2.1 Insertion Loss 3
2.2.2 Weight Change Rate During Aging 13
2.2.3 Self Noise Evaluation 14

3.0 RESULTS AND DISCUSSIONS 24
3.1 INSERTION LOSS 24
3.1.1 Insertion Loss of Panels Before Aging 24
3.1.2 Insertion Loss of Panels After Aging 24
3.1.3 Weight Change After Aging 25
3.1.4 Insertion Loss of Sonar Window 26
3.1.5 Angle of Incidence 26
3.2 SELF NOISE EVALUATION 26
3.2.1 Frequency Response Function 26
3.2.2 Driving Force and Radiated Pressure 28

4.0 CONCLUSIONS 30

ACKNOWLEDGMENTS 30

REFERENCES 31

LIST OF FIGURES

Figure 1. The basic components of the experimental arrangement for insertion loss measurements 9
Figure 2. Experimental arrangements for measuring the insertion loss 10
Figure 3. Time history and Hilbert Transform envelope of a transmitted signal 11
Figure 4. Insertion loss versus frequency for a 20 gauge stainless steel plate 12
Figure 5. Example of FRF and phase of an epoxy-based 4H Spectra Fiber composite panel21
Figure 6. Data from an epoxy-based 4H Spectra Fiber composite panel under pseudo random mode 22
Figure 7. Epoxy-based 4H Spectra Fiber composite panel in free run mode triggered by HP 3314A Function Generator 23
Figure 8. Insertion loss of an epoxy-based 8H Spectra Fiber composite panel before aging 35
Figure 9. Insertion loss of an epoxy-based 4H Spectra Fiber composite panel before aging 36
Figure 10. Insertion loss of a cyanate-based 8H Spectra Fiber composite panel before aging 37
Figure 11. Insertion loss of a cyanate-based 4H Spectra Fiber composite panel before aging 38
Figure 12. Insertion loss of an epoxy-based 8H GRP panel before aging 39
Figure 13. Insertion loss of a cyanate-based 8H GRP panel before aging 40
Figure 14. Insertion loss of an epoxy-based 8H Spectra Fiber composite panel after aging 42
Figure 15. Insertion loss of an epoxy-based 4H Spectra Fiber composite panel after aging 43
Figure 16. Insertion loss of a cyanate-based 8H Spectra Fiber composite panel after aging 44
Figure 17. Insertion loss of a cyanate-based 4H Spectra Fiber composite panel after aging 45
Figure 18. Insertion loss of an epoxy-based 8H GRP panel after aging 46
Figure 19. Insertion loss of a cyanate-based 8H GRP panel after aging 47
Figure 20. Insertion loss measurement of a double walled stainless steel sonar window . . 49
Figure 21. Insertion loss measurement of a 20 gauge stainless steel plate 50
Figure 22. Insertion loss versus angle of incidence for a 10 mm thick epoxy-based 8H Spectra Fiber composite panel 52
Figure 23. Insertion loss versus angle of incidence for a 10 mm thick epoxy-based 4H Spectra Fiber composite panel 53

P499040.PDF [Page: 11 of 112]

Figure 24. Insertion loss versus angle of incidence for a 10 mm thick cyanate-based 8H Spectra Fiber composite panel 54
Figure 25. Insertion loss versus angle of incidence for a 10 mm thick cyanate-based 4H Spectra Fiber composite panel 55
Figure 26. Insertion loss versus angle of incidence for a 10 mm thick epoxy-based 8H GRP panel 56
Figure 27. Insertion loss versus angle of incidence for a 10 mm thick cyanate-based 8H GRP panel 57
Figure 28. Insertion loss versus angle of incidence for a 20 gauge stainless steel plate . . . 58
Figure 29. Insertion loss versus angle of incidence for a 60 mm thick double walled stainless steel sonar window 59
Figure 30. Frequency response function and phase of an epoxy-based 8H Spectra Fiber composite panel 61
Figure 31. Pressure, force and radiation measurements of an epoxy-based 8H Spectra Fiber composite panel under pseudo random mode 62
Figure 32. Pressure, force and radiation measurements of an epoxy-based 8H Spectra Fiber composite panel under free run mode 63
Figure 33. Frequency response function and phase of an epoxy-based 4H Spectra Fiber composite panel 65
Figure 34. Pressure, force and radiation measurements of an epoxy-based 4H Spectra Fiber composite panel under pseudo random mode 66
Figure 35. Pressure, force and radiation measurements of an epoxy-based 4H Spectra Fiber composite panel under free run mode 67
Figure 36. Frequency response function and phase of a cyanate-based 8H Spectra Fiber composite panel 69
Figure 37. Pressure, force and radiation measurements of a cyanate-based 8H Spectra Fiber composite panel under pseudo random mode 70
Figure 38. Frequency response function and phase of a cyanate-based 4H Spectra Fiber composite panel 72
Figure 39. Pressure, force and radiation measurements of a cyanate-based 4H Spectra Fiber composite panel under pseudo random mode 73
Figure 40. Pressure, force and radiation measurements of a cyanate-based 4H Spectra Fiber composite panel under free run mode 74
Figure 41. Frequency response function and phase of an epoxy-based 8H GRP panel . . . 76
Figure 42. Pressure, force and radiation measurements of an epoxy-based 8H GRP panel under pseudo random mode 77

P499040.PDF [Page: 12 of 112]

Figure 43. Pressure, force and radiation measurements of an epoxy-based 8H GRP panel under free run mode 78
Figure 44. Frequency response function and phase of a cyanate-based 8H GRP panel 80
Figure 45. Pressure, force and radiation measurements of a cyanate-based 8H GRP panel under pseudo random mode 81
Figure 46. Pressure, force and radiation measurements of a cyanate-based 8H GRP panel under free run mode 82
Figure 47. Frequency response function and phase of a double walled stainless steel sonar window with one wall immersed in water 84
Figure 48. Pressure, force and radiation measurements of a double walled stainless steel sonar window under pseudo random mode with one wall immersed in water 85
Figure 49. Pressure, force and radiation measurements of a double walled stainless steel sonar window under free run mode with one wall immersed in water . 86
Figure 50. Frequency response function and phase of a double walled stainless steel sonar window with two layers of walls immersed in water 87
Figure 51. Pressure, force and radiation measurements of a double walled stainless steel sonar window under pseudo random mode with two layers of walls immersed in water 88
Figure 52. Pressure, force and radiation measurements of a double walled stainless steel sonar window under free run mode with two layers of walls immersed in water 89

LIST OF PHOTOGRAPHS

Photograph 1. Top: Flume tank (top) in the Marine Institute of the Memorial University of Newfoundland. Bottom: Electronics for acoustic property measurements and test panel preparation 6

Photograph 2. Transmitter, hydrophones, optical positioning beam and other tools 7

Photograph 3. Protractor on the optical beam (top) and truncator line up with transmitter in the tank (bottom) 8

Photograph 4. Top: The reverberant tank for self noise measurements Bottom: B & K 8103 hydrophone in position for pressure measurements . . 15

Photograph 5. Shaker is tightened to the fluid-loaded panel 16

Photograph 6. Electronics for measurements of FRF, force and pressure 17

LIST OF TABLES

Table 1. List of tested panels and calibration plate 2

Table 2. The dimension of the reverberant tank 14

Table 3. PA7D power amplifier calibration values 19

Table 4. Panel weight measurements before and after aging 25

Table 5. Modal frequencies of test panels and sonar window 27

Table 6. Radiation signal gain and loss frequency points (Hz) in 0 to 3000 Hz range . . . 29

P499040.PDF [Page: 14 of 112]

LIST OF APPENDICES

Appendix A. Calibration chart for B&K hydrophone Type 8103, Serial No. 1049463 . . . 91

Appendix B. Calibration chart for B&K hydrophone Type 8103, Serial No. 1049464 . . . 92

Appendix C. Beam pattern of transmitter GILTX500 after truncator. Fc=500 kHz, Fm=10 kHz, signal received by a B&K 8103 hydrophone 93

Appendix D. Signal level and distance off truncator, transmitter to truncator distance is 100 cm. Transmitter: GILTX500, hydrophone: B&K 8103. Fc=500 kHz, Fm=10 kHz 94

Appendix E. System calibration chart for insertion loss measurements 95

1.0 INTRODUCTION

The two main functions of a sonar dome are to protect hull-mounted sonar equipment from physical damage as a ship moves through the water, and to displace the turbulent boundary layer away from the ship hull to reduce flow noise. Ideally, the dome should have a minimal effect on the propagation of sound from the target to the ship and from the ship to the target. Conventional sonar domes are of all-metal construction with a thin stainless steel window or two steel walls separated with stiffeners, as in the C5 Dome used in the Canadian Navy. Generally speaking, the insertion loss increases with frequency, thickness, and density of the dome materials. Thus, sonar dome materials should be as thin and as light as possible. This may be achieved by using materials for dome construction that have a low insertion loss. Unfortunately, materials which have low insertion losses, such as elastomers, are usually not stiff enough to be self-supporting and do not have the required strength for sonar domes. One solution is to use fibre-reinforced plastic (FRP) composite materials with high strength-to-weight ratios, which enable thin panels with relatively low insertion loss to be used. In addition to low insertion loss, FRPs may offer better noise characteristics than metallic structures due to higher internal damping, since the dome itself may contribute to the noise level via flow excitation of resonances within the structure.

This research project focuses on the acoustic characterization of several candidate materials being considered as sonar dome construction materials. In addition to metallic-based panels and glass-reinforced materials, composites reinforced with Spectra Fiber were examined. Spectra Fiber, from Allied Signal Corporation, is polyethylene prepared in such a manner that it is highly crystalline, with the crystals aligned along the fiber axis. Examination of the acoustic properties of Spectra Fiber panels is part of a larger effort to develop Spectra Fiber sonar domes, sponsored by Chief Research and Development, and Director Maritime Combat Systems. This report presents the experimentally obtained results of insertion loss and self noise evaluation on four Spectra Fiber composite panels, two glass reinforced panels (GRP) and one double walled stainless steel sonar window.

2.0 MATERIALS AND METHODOLOGY

2.1 TEST PANELS

Spectra Fiber composite panels were prepared by Advanced Composite Technology (ACT), Sparks, Nevada using two different resin systems and two different weaves. The resin systems used for the prepregs were based on either a cyanate ester (BTCY-3) or an epoxy, Shell EPON 828 (BT250E). The plasma treated Spectra Fiber reinforcing fibers were configured in either a 985-8H satin weave or a 988-4H satin weave, as shown in Table 1.

Table 1. List of Test Panels and Calibration Plate

Sample Identification		Weave	Dimensions (mm)
Spectra Fiber Composite Panels			
985PT/BT250E	(Epoxy-based)	8H	1005 x 1005 x 10
988PT/BT250E	(Epoxy-based)	4H	1005 x 1005 x 10
985PT/BTCY-3	(Cyanate-based)	8H	1005 x 1005 x 10
988PT/BTCY-3	(Cyanate-based)	4H	1005 x 1005 x 10
GRP Panels			
7H5100LN016/001	(Epoxy-based)	8H	1020 x 1080 x 10
7H5100LN016/002	(Cyanate-based)	8H	1010 x 1255 x 10
Stainless Steel Sonar Window			914 x 914 x 60
Standard Calibration Panel	(20 gauge SS plate)		1219 x 1168 x 0.92

In each case, the panels contained 50% $\pm$ 2% by weight resin. Glass reinforced composite panels (GRP) were fabricated by ACT using the same resin systems (cyanate or epoxy) as the Spectra Fiber panels, using an 8H satin weave.

2.2 EXPERIMENTAL METHODS

2.2.1 Insertion Loss

This investigation required acoustic measurements of sound, propagated at a normal incidence to a panel immersed in water. The use of a parametric source was strategic to the study. With conventional sources, measurements on panels of limited size are affected by diffraction from the edges of the test panels. At low frequencies, approaching 1 kHz, diffraction is most pronounced, making it difficult to resolve the diffracted signal from the main transmitted signal (Piquette, 1994). To minimize such effects, the energy at the edge must be reduced. With conventional acoustic transmission, it is very difficult to generate small spot insonification at low frequencies; directionality is a function dictated by transmission frequency and transducer size.

In view of this, a parametric source was designed and developed with a small beam cross-section. The basic principles of a parametric source can be found in Westervelt (1963, 1960), Clay and Medwin (1977), Berktay *et al.* (1979), Humphrey and Berktay (1985) and Humphrey (1992, 1985). Briefly, when two intense sound waves of slightly different frequencies are generated coaxially in water, they interact to produce secondary signals that contain a band of frequencies. These include both the sum and difference frequencies. Of particular importance are the low difference frequency signals generated. These signals possess many attractive attributes suited for material testing which include narrow beamwidth, no side lobes, and broadband capabilities even at the lower kilohertz range. Therefore, material testing in a small tank is possible with parametric arrays since diffraction and side lobe interference problems are made negligible. In addition, the broad bandwidth inherent in the parametric source allows material testing over a wide range of frequencies to be executed with a single small transducer (Szabo, *et al.*, 1992, Whelan, *et al.*, 1993).

In the experiments, a process called "self-demodulation" was used to create the secondary signals of the parametric array. In this method, a pulse-modulated carrier wave is

radiated from the acoustic transducer with nonlinear interactions occurring in the water among all the frequencies radiated to yield a band of secondary lower frequencies.

The source for the study involved a wideband transducer which was 80 mm in diameter and had a resonance of 500 kHz (GILTX500), driven by a modulated carrier waveform obtained from the transmitting electronics. A short carrier pulse with a smooth envelope was transmitted. A "raised cosine bell" was generated as the modulating function. A Brüel and Kjær (B&K) hydrophone Type 8103 which has a flat frequency response up to 100 kHz (see Appendix B for its calibration chart), was used as a receiver.

For our application, the parametric source was deliberately truncated within the Rayleigh distance by placing a "lowpass acoustic filter" (truncator) across the primary beam at one meter from the transducer. This approach attenuated the higher frequency primary waves while transmitting the low-frequency, secondary waves without significant loss. The truncator design was not a trivial task, but involved careful matching of characteristics of the primary beam to minimize spreading of the secondary wave after termination. Distances between hydrophones and panels had to be considered in the design of the truncator panel. A plate made of 20 gauge stainless steel was used as a truncator.

A large test tank was needed to deal with the low frequency measurements. The Flume Laboratory located at the Memorial University of Newfoundland's Marine Institute was an ideal site for low frequency material evaluation. The Flume Laboratory consists of a large, rectangular concrete windowed tank; 21.5 meters long, 8 meters wide and 4 meters deep (Photo 1). The transmission and reception electronics were placed on a bench of the bridge over the flume tank. The surface of the bridge was covered by sponge type acoustical damping sheets to reduce the noise from the bridge created by walking or moving. Photos 2 and 3 show the transmitter, receivers, positioning and angular measurement device.

The transmission electronics is described here. A Hewlett Packard (HP) 3311A function generator was used to trigger a Wavetek 20 MHz pulse/function generator to create the modulation envelope. The envelope signal was mixed with a carrier signal from an HP 8601A

generator/sweeper using a Hatfield Instruments Type 1754 modulator. The modulator output was fed to the transducer (GILTX500) via an HP 461A buffer amplifier and an ENI model 2100L RF power amplifier. The modulation frequency was set at 10 kHz for all insertion loss measurements.

The signal from a B & K 8103 hydrophone was fed into a B & K charge amplifier Type 2635 for signal conditioning. It was then bandpass filtered (300 Hz to 50 kHz) via a Krohn-Hite Model 3550 analog filter before being digitized by a Datalab DL912 Transient Recorder. For most tests, a sampling period of 0.5 μs (sampling frequency 2 MHz) was selected. A portable 486-33MHz PC-III computer was used to transfer the data from the Datalab DL912 Transient Recorder for storage and post-processing.

The general geometry used in the study is shown in Figures 1 and 2. A reference signal was first acquired; the transmitted signal was then recorded with the test panel placed between the truncator and hydrophone. The insertion loss of a panel was defined in terms of the complex incident sound pressure and complex transmitted sound pressure:

$$IL = 20\log_{10}\left|\frac{\textit{incident sound pressure } p_i}{\textit{transmittted sound pressure } p_t}\right| = 20\log_{10}\frac{1}{|T|} \qquad (1)$$

where T is the complex transmission coefficient.

Computations of the complex reflection and transmission coefficient were performed in the frequency domain via the Fast Fourier Transform (FFT). In each case, the complex Fourier coefficients for each pulse were used in the division. In addition, the Hilbert Transform was employed to better display and calculate changes in the waveform shape. Such a response analysis involves taking the imaginary part of the signal along with the real part. The resulting analytic signal is displayed as a time envelope. Upon being squared, the envelope is proportional to the acoustic energy. Such transformed data allows for precise time representation of both the peak values and instantaneous phases of the signal. The Hilbert-

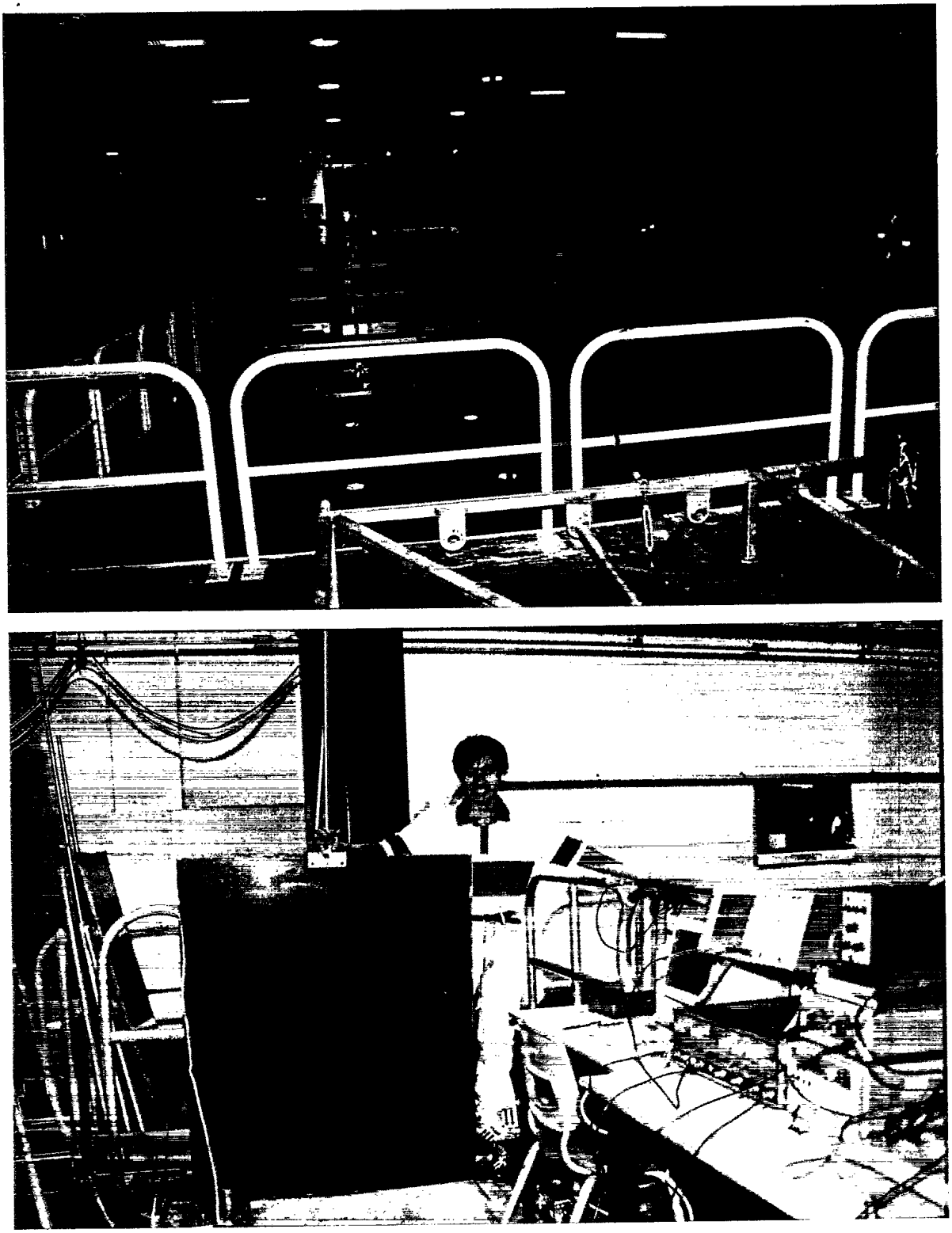

Photograph 1. Top: Flume Tank in the Marine Institute of the Memorial University of Newfoundland, Bottom: Electronic for acoustic property measurements and test panels

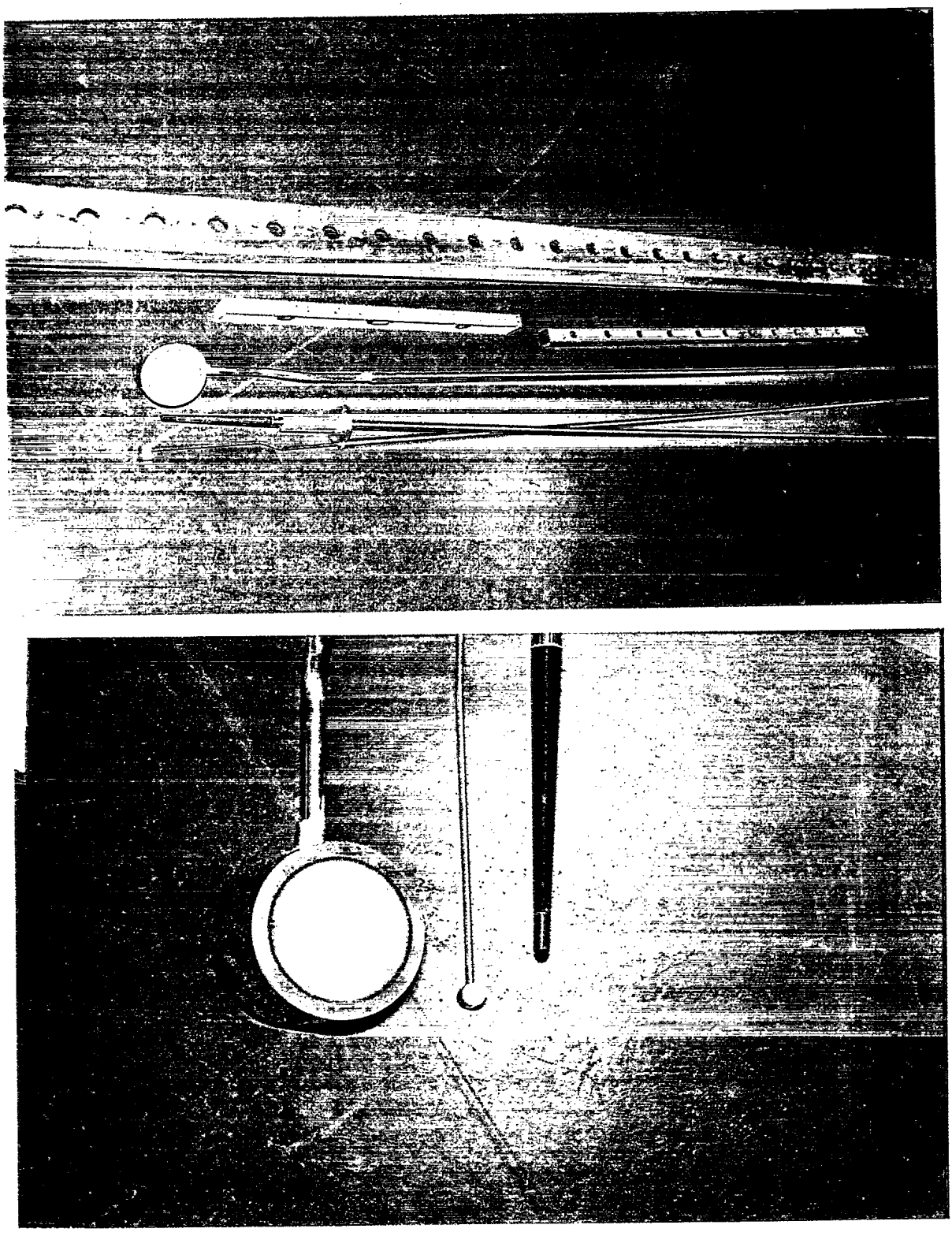

Photograph 2. Transmitter, hydrophones, optical positioning beam, and other tools

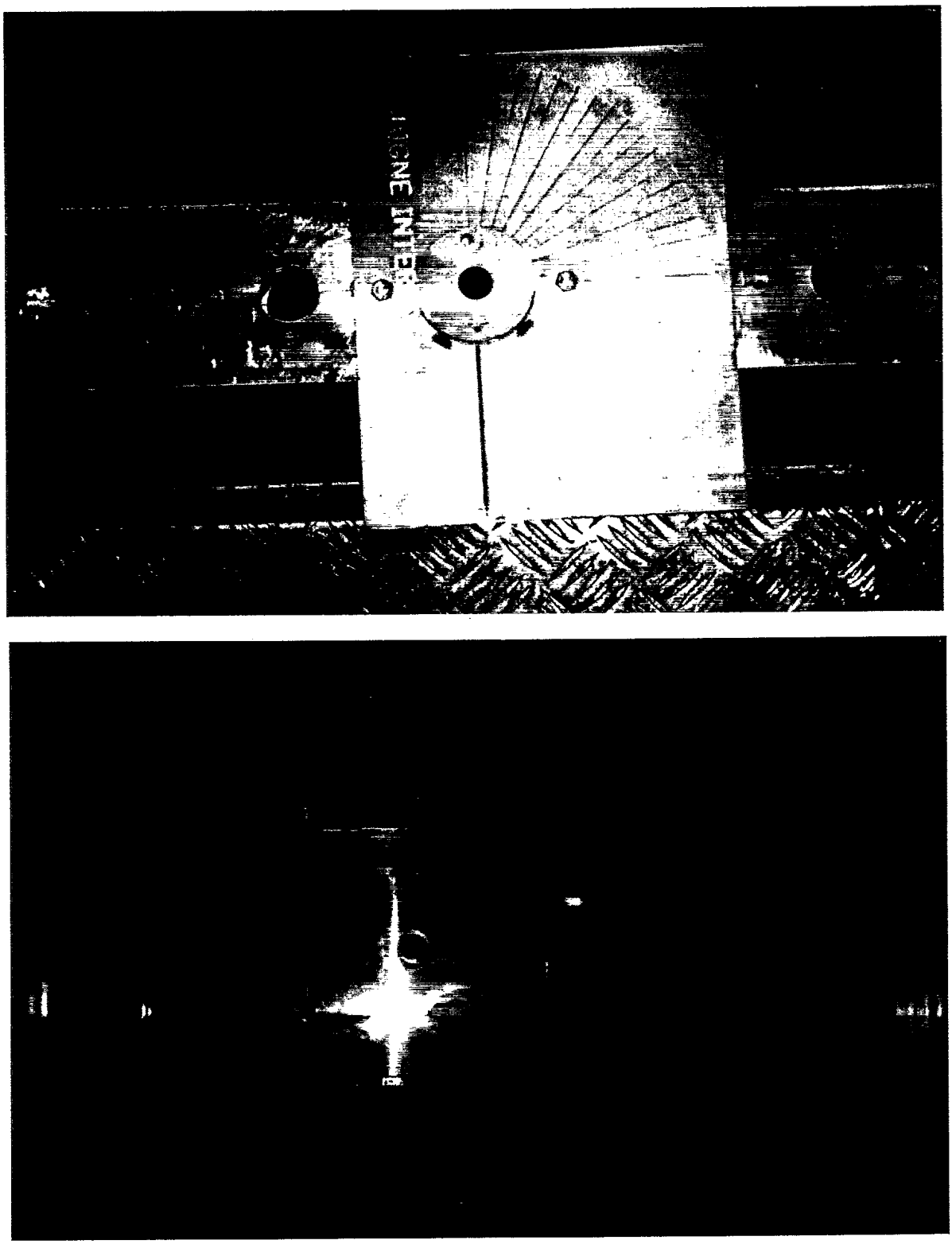

Photograph 3. Protractor on the positioning beam (top) and truncator was lined up with transmitter in the Flume Tank (bottom)

transformed series were detrended and the energy envelopes were log transformed (see Figure 3). Guigné *et al.* (1991) and Guigné and Chin (1989) provide details on the application of the Hilbert Transform to underwater acoustics.

The beam pattern of the transmitter GILTX500 after truncator is shown in Appendix C. System calibration results are summarized in Appendices D and E. A comparison between theoretical result and experimental result for a 20 gauge stainless steel calibration plate is given in Figure 4. Overall the two curves are well matched.

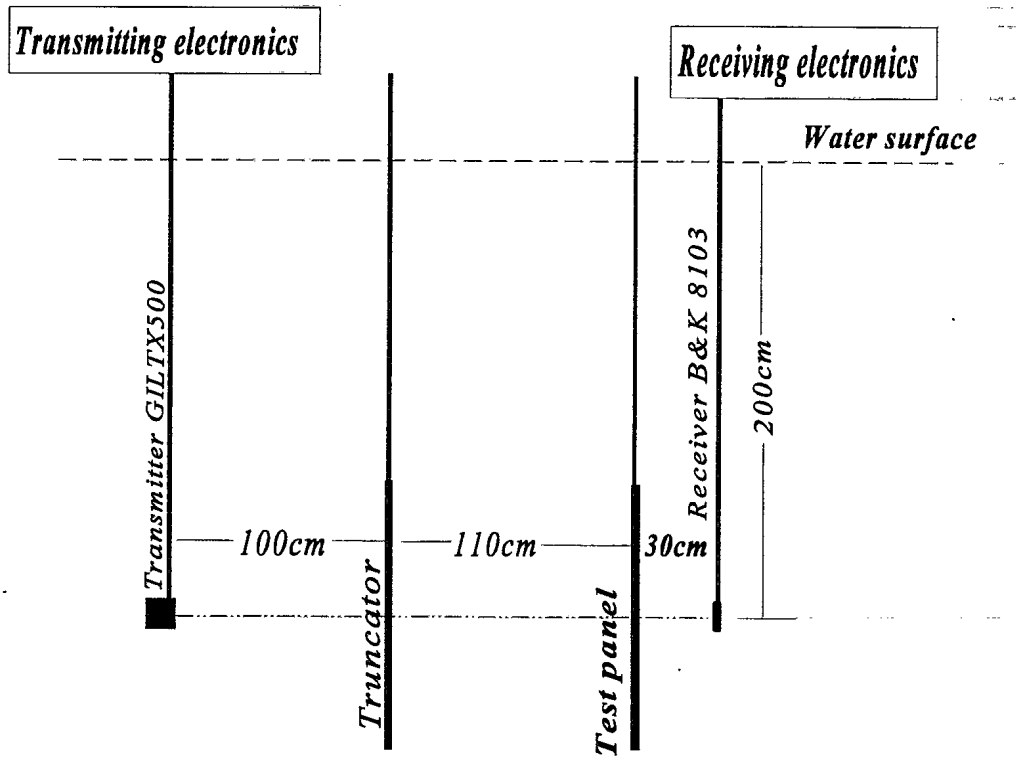

Figure 1. The basic components of the experimental arrangement for carrying out insertion loss measurements

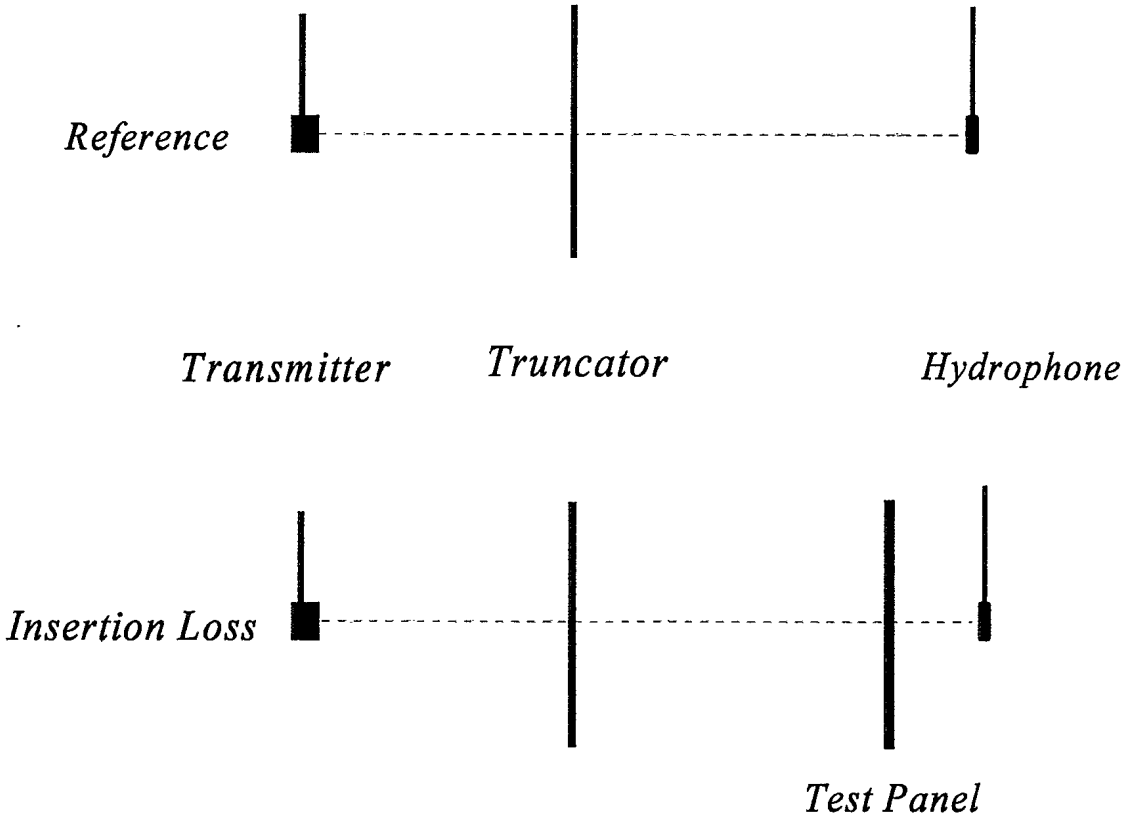

Figure 2. Experimental arrangements for measuring the insertion loss

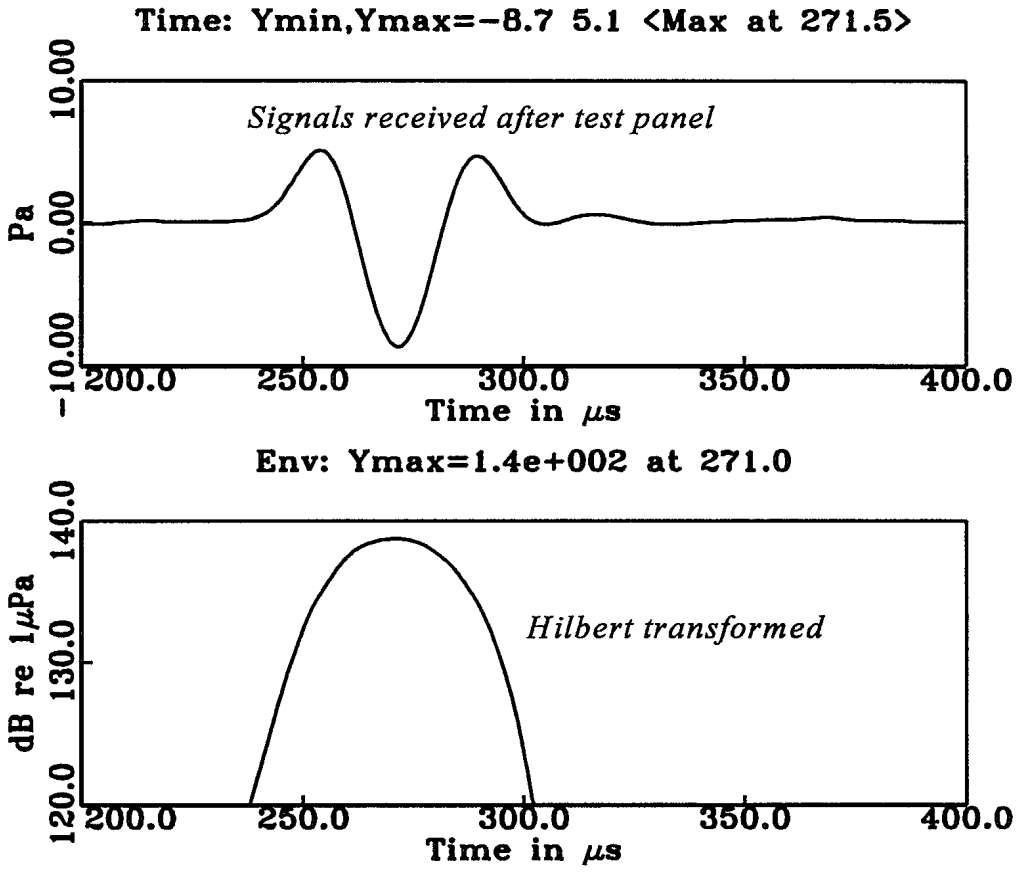

Figure 3. Time history and Hilbert Transform envelope of a transmitted signal

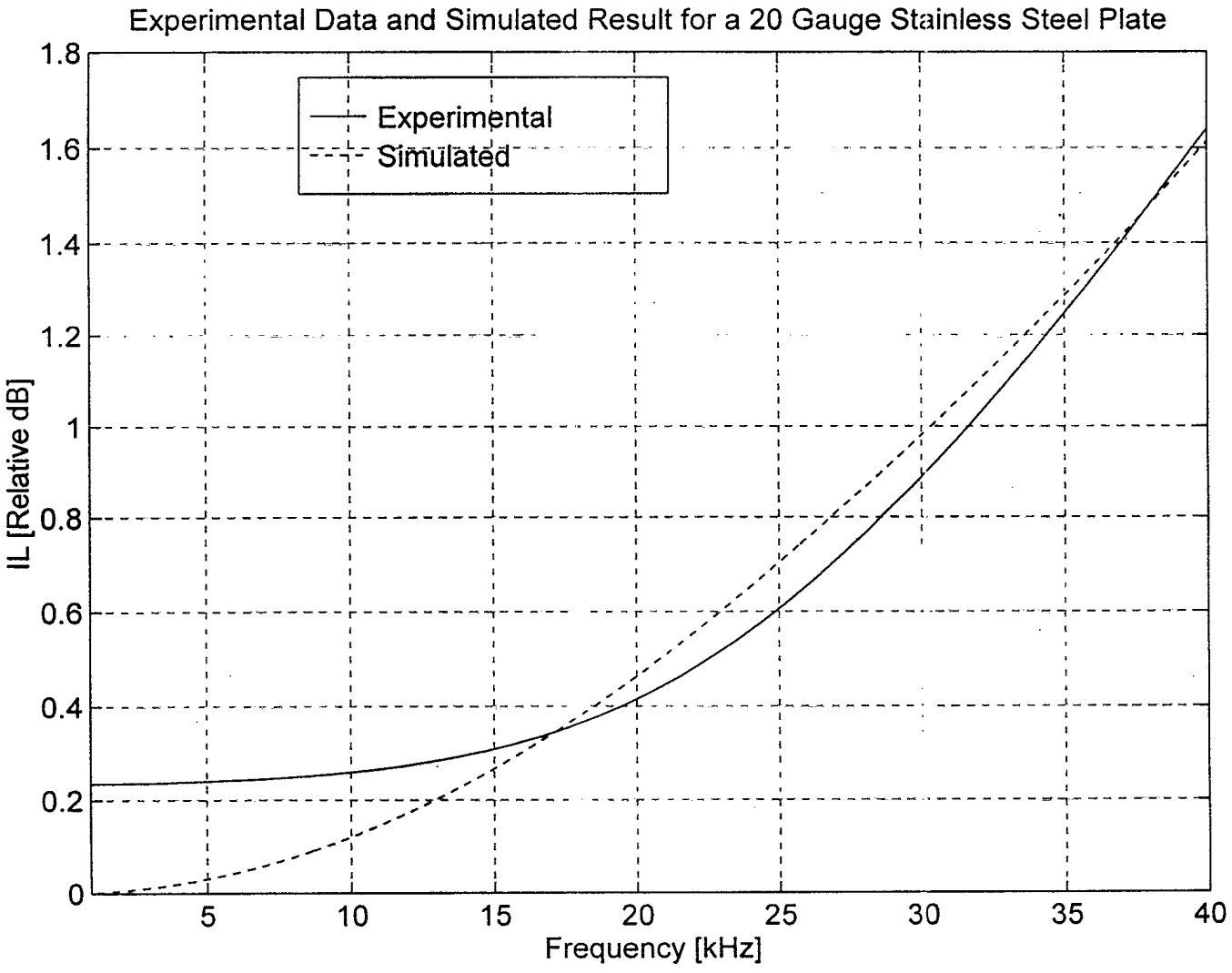

Figure 4. Graph of insertion loss versus frequency for a 20 gauge stainless steel plate at normal incidence.

2.2.2 Weight Change Rate During Aging

The dry weight of each panel was determined on a Fairbanks scale. Two readings were taken for averaging. Panels were then submerged to 2.5 meter depth for freshwater aging in the acoustics tank of the Canadian Centre for Marine Communications (CCMC) at the Marine Institute of Newfoundland. The water temperature was 11 °C at panel aging depth. Four Spectra Fiber composite panels were aged beginning on March 21, 1995. Due to late arrival, the two GRP panels were started aging on May 9, 1995. All of those six panels were aged in water until July 7, 1995. During the aging period, wet weights of panels were measured twice. The procedure for weight change rate measurements was as follow:

Panels were retrieved and drained for 10 minutes. The surface of the panels was wiped with paper towels to make sure there was no water adhered to the panel. The panels were weighed in 20 minutes and in one hour respectively after retrieval. Weight change rates were calculated based on Equation 2,

$$\text{Weight Change Rate (R)} = (W_2 - W_1)/(W_1 \times T) \qquad (2)$$

where, W_2 is the new weight in grams, W_1 is the previous weight in grams, and T is the time interval in days.

2.2.3 Self Noise Evaluation

A brief summary of the experimental method is given here. For more detail, the reader is asked to refer to C.A. Hamm, "Evaluation of Noise Reduction Coatings: Experimental Design", DREA Contractor Report CR/96/417.

Experiments for self noise evaluation were conducted in the Underwater Acoustics Lab of Guigné International Limited. The dimensions of the tank used for this experiment were 172 cm in length, 152 cm in width and 163 cm in depth. The volume of the tank was 4.26 m^3. In order to increase the frequency range of reverberance, a special designed reverberant chamber (0.9 m^3) was built to fit in the GIL tank. This chamber had no parallel surfaces (Photo 4). The dimensions are shown in Table 2.

Table 2. The Outside Dimensions of the Reverberant Chamber*

(in centimeters)

	Panel 1	Panel 2	Panel 3	Panel 4
Top edge	121	123	115	120
Bottom edge	103	103	106	95
Left edge	75	77	79	74
Right edge	74	75	77	79

* *Bottom panel dimensions are 102, 102, 105 and 94*

The chamber was constructed with 1/2" plywood panels. The surfaces of the internal walls were lined with 1" thick styrofoam and randomly attached pyramid-shape styrofoam pieces of different sizes to reduce standing wave patterns and enhance reverberance. This was partially attained by having no parallel surfaces in the chamber. The chamber extended an upper frequency limit of the reverberance from 1.2 kHz in the 4.26 m^3 tank to 3.0 kHz in the reverberant chamber.

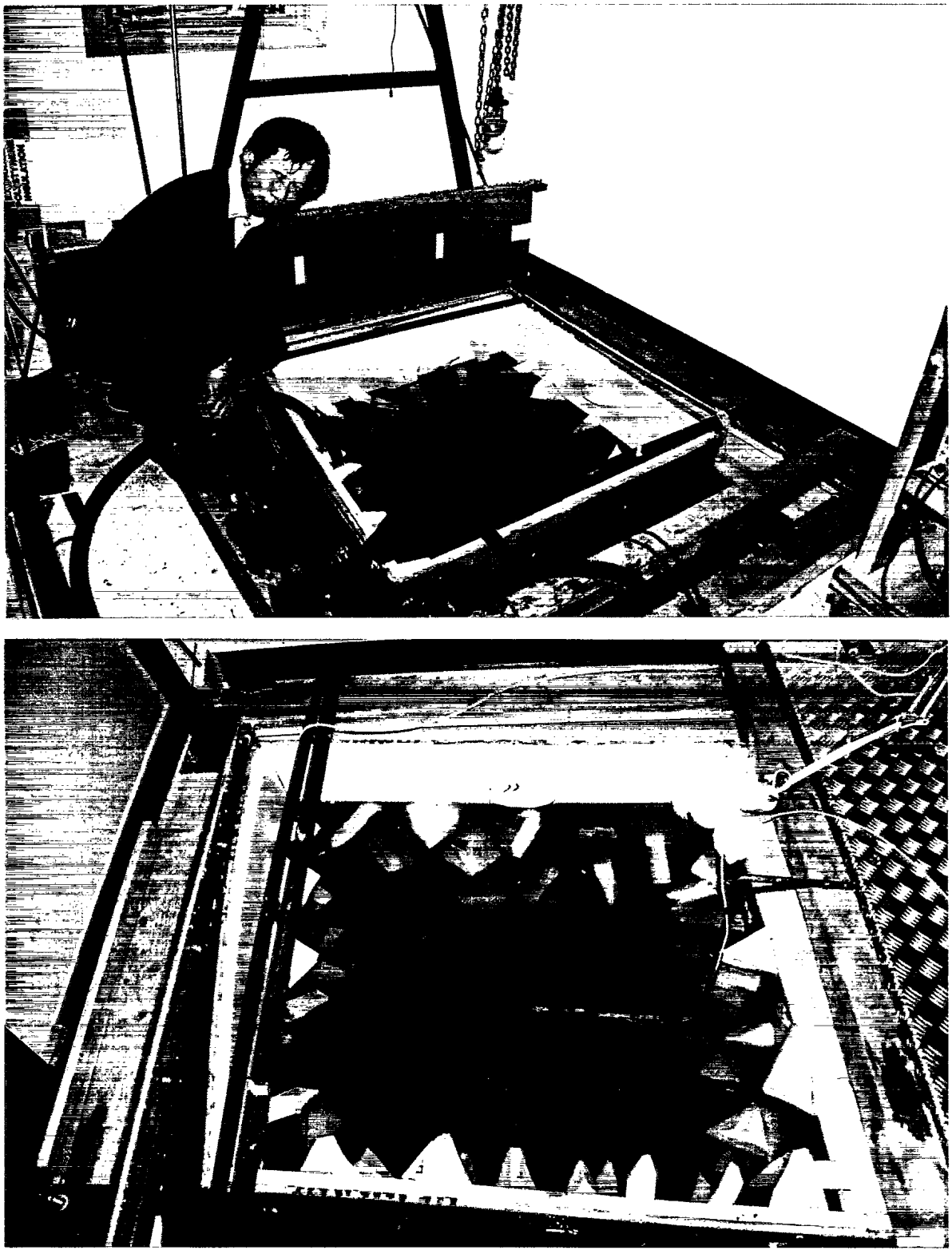

Photograph 4. Top: Reverberance chamber for self noise measurements
Bottom: B&K 8103 hydrophone in position for pressure measurement

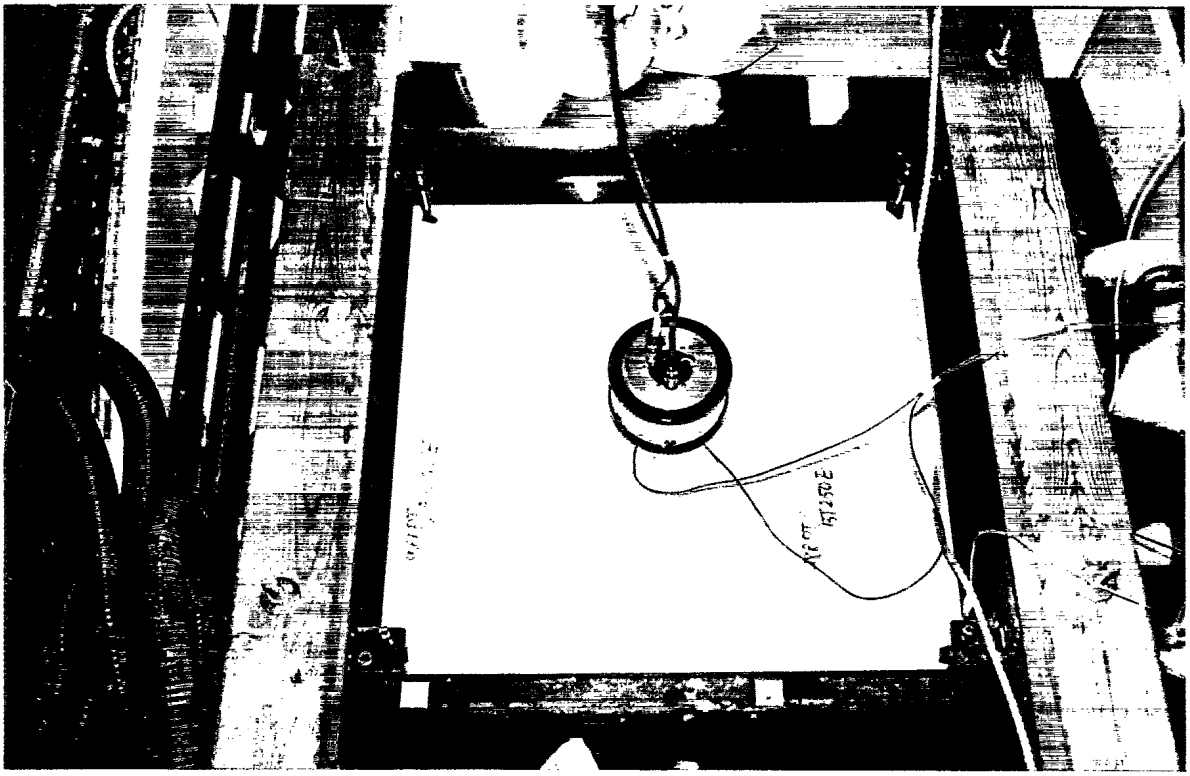

Photograph 5. Shaker is tightened to the fluid-loaded panel

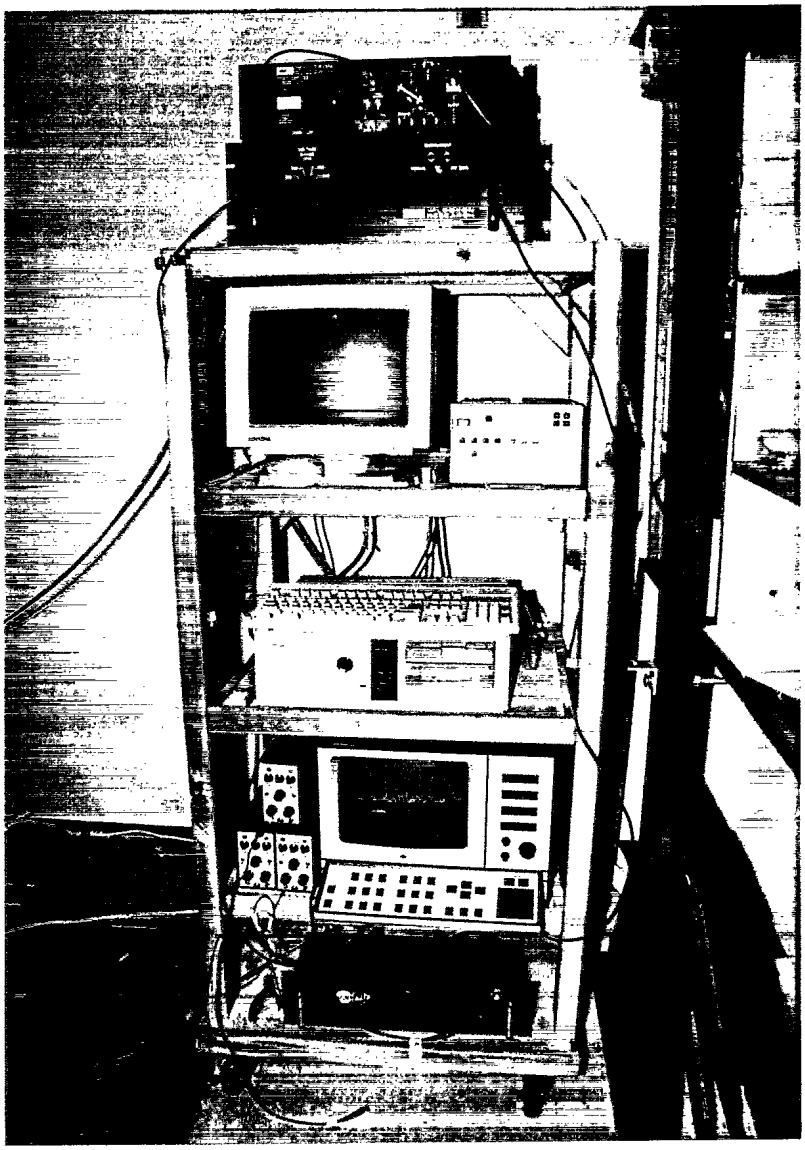

Photograph 6. Electronic for measurements of FRF, force and pressure

The basic geometry for this test involved submerging the test panel halfway at the air-water interface, with a mechanical excitation source on the air side, and sound receiver (B & K 8103 hydrophone) in the water below the plate. One basic measurement of reverberation is the uniformity of the sound field within the volume housing the sound source. That is, if the volume is truly reverberant, the sound field should be homogeneous and isotropic. There may be exceptions very near boundaries.

All of the panels and sonar windows were cut to 2' x 2'. There was a 3/8" threaded hole at the center of the panel to adapt the Wilcoxon Research Model F4/F7 shaker which was used to excite the panels. Since the test materials, especially Spectra Fiber composite panels, were not sufficiently firm to withstand the forces imposed upon it by the shaker apparatus, a minor modification of the shaker adapter was necessary. Specifically, the smaller adapter was replaced by a 3/8" in diameter stainless steel bolt utilizing a 1" diameter head and a 1" diameter washer. The surface of the test panel in contact with water was wetted with mild soap water to reduce the formation air bubbles at the material-water interface, fixed to the supporting frame and immersed in the water of the tank (Photo 5). Air bubbles beneath the panel were then cleared and the panel was leveled. The shaker was attached to the adapter on the test panel and tightened by a spanner wrench.

Photo 6 shows the measurement instrument in the Acoustics Lab. The Wilcoxon Research Model PA7D Power Amplifier obtained input signals from a signal generator and output amplified signals to a Model F4/F7 Dual Shaker System via the Model N7C Matching Network. Radiated pressure (P) measurement were taken by using a B & K 8103 hydrophone (Appendix A) to acquire an acoustic signal, which was passed to a B & K Model 2032 Dual Channel Signal Analyzer via a signal conditioning charge amplifier B & K Type 2635. Control of the 2032 was handled by an IBM compatible personal computer via an IEEE parallel interface. Data from three hydrophone positions were collected. Hydrophone Position 1 was 30 cm vertically under the shaking point. Positions 2 and 3 were 28 cm under the panel and were 15 cm away from the shaking point horizontally.

The Frequency Response Function (FRF) H(ω), equal to the ratio of acceleration A (ω) to force F (ω) in the frequency domain, was used to describe the mechanical behavior.

$$H(\omega) = A(\omega)/F(\omega) \tag{3}$$

The FRF measurement setting used on the 2032 was 1/H1 and is defined by Brüel & Kjær as

$$1/H1 = F/a \tag{4}$$

where F and a are spectra of driving point force and driving point acceleration, respectively. Measurements were made using an accelerometer and a force transducer contained inside the Wilcoxon impedance head. The force transducer was located at the point where the force was applied to the mechanical system. Figure 4 is an example of 1/H1 measured at the center of a panel. The upper plot is the magnitude of 1/H1 in dB. The lower plot is the phase of 1/H1 in degrees. The frequency range was set from 0 to 6400 Hz which was generated by a B & K 2032 pseudo random signal generator. FRF, force and pressure data were averaged over 200 spectra.

Since the PA7D power amplifier does not have visual indicators or locking mechanisms, power output calibrations were necessary for repeat experiments and comparisons. The values are given in Table 3.

Table 3. PA7D Power Amplifier Calibration Values

Frequency (Hz)	Input V_{pp} (volts) (sine wave)	Output V_{pp} (volts)	
		Channel A (F4)	Channel B (F7)
1000	0.6	4.25	0.3625
5000	0.6	4.187	0.4

For the double walled sonar dome panel, the shaker under pseudo random excitation was not being strong enough to activate the panel. A Hewlett Packard 3314A Function Generator was used to provide a constant amplitude swept-sine signal in the frequency range

64.7 to 6000 Hz to the PA7D power amplifier under free run mode. The number of samples for averaging was 2000 in this case.

Two sets of data for force and radiated pressure measurements from the same panel under free run (swept sine) and pseudo random trigger mode are shown here as examples (Figures 5, 6 and 7). Figure 5 shows that there are 15 modal frequencies in 0 to 6 kHz frequency range. This was determined by examining the phase spectrum and identifying frequencies where the phase crossed 90°. Figures 6 and 7 are data from pseudo random mode and free run trigger mode on the B & K 2032 Signal Analyzer respectively. Modal frequencies could be easily seen in data of both radiated pressure and force especially at the low frequency end. Data from the swept sine source (HP3314A Function Generator) is 15 dB higher than data acquired by a pseudo random mode. However, the trends of the radiation efficiency are very similar to each other.

The radiation efficiency is defined here in terms of radiated pressure per unit input force. It should be noted that each of the pressure and force quantities are functions of frequency.

$$\Delta dB_{pF} = 10\log_{10}\left\lfloor p_{radiated}\right\rfloor - 10\log_{10}\left\lfloor F_{applied}\right\rfloor \qquad (5)$$

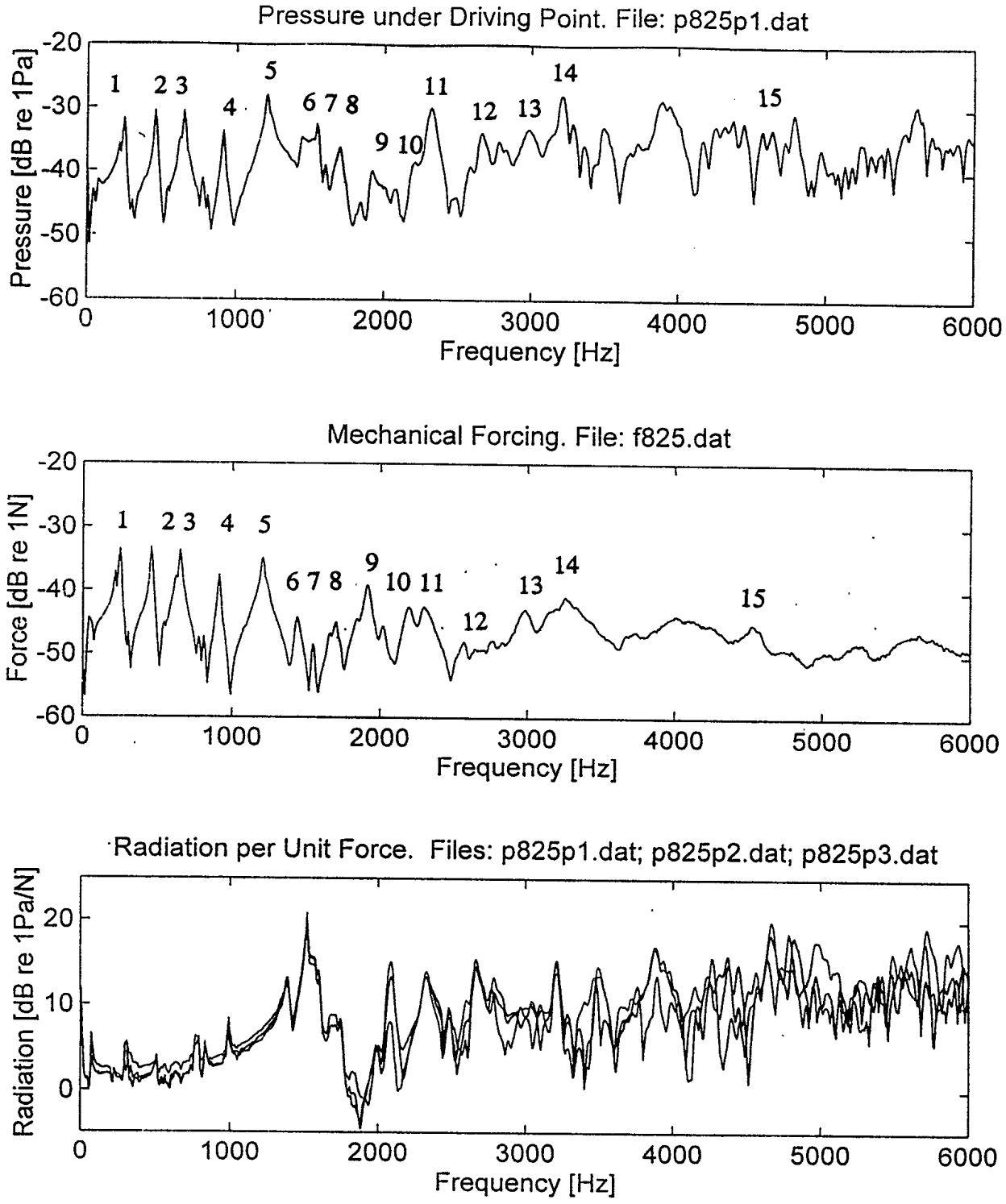

Figure 5. Example of FRF and phase of an epoxy-based 4H Spectra Fiber composite panel

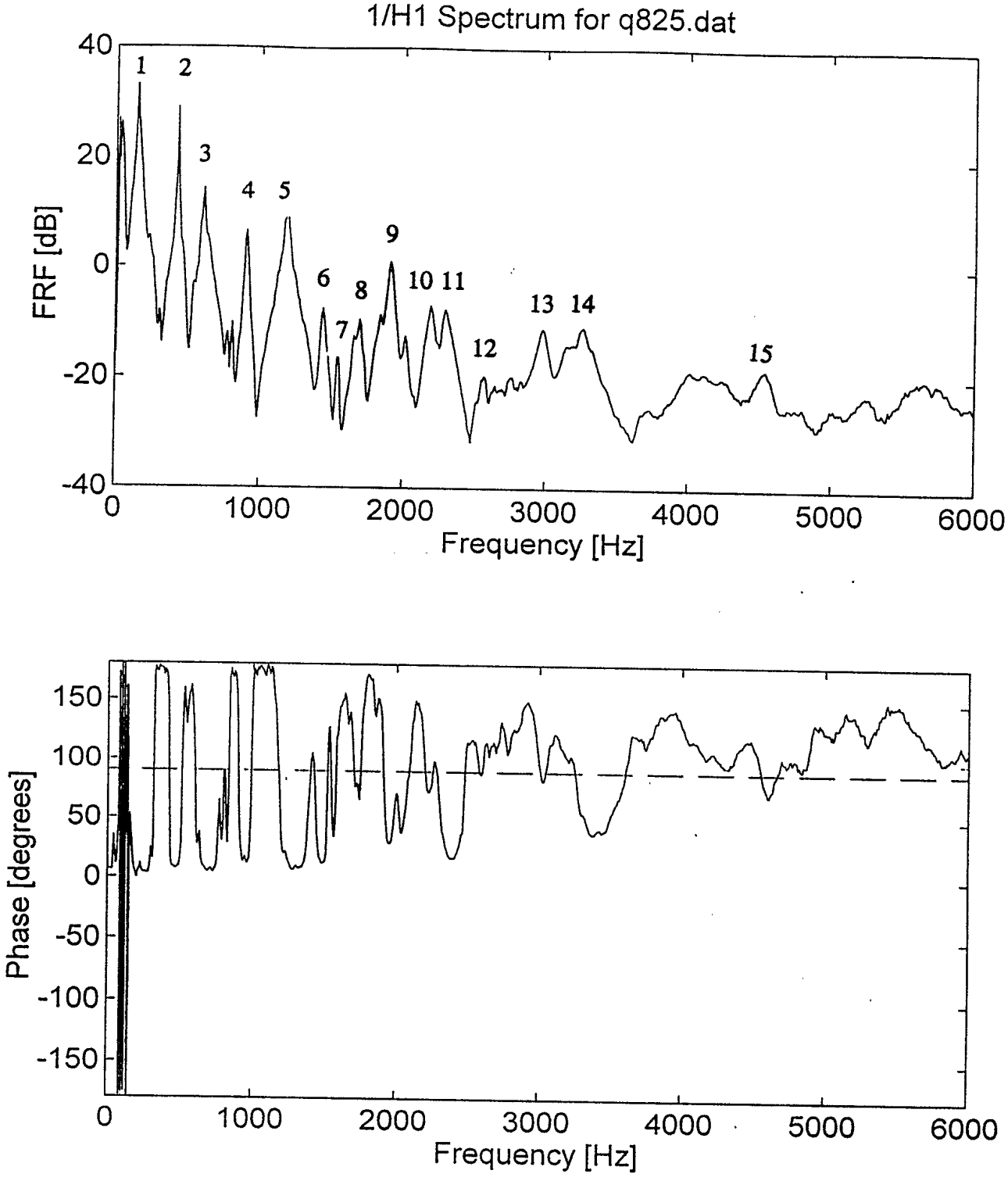

Figure 6. Data from an epoxy-based 4H Spectra Fiber composite panel under pseudo random mode

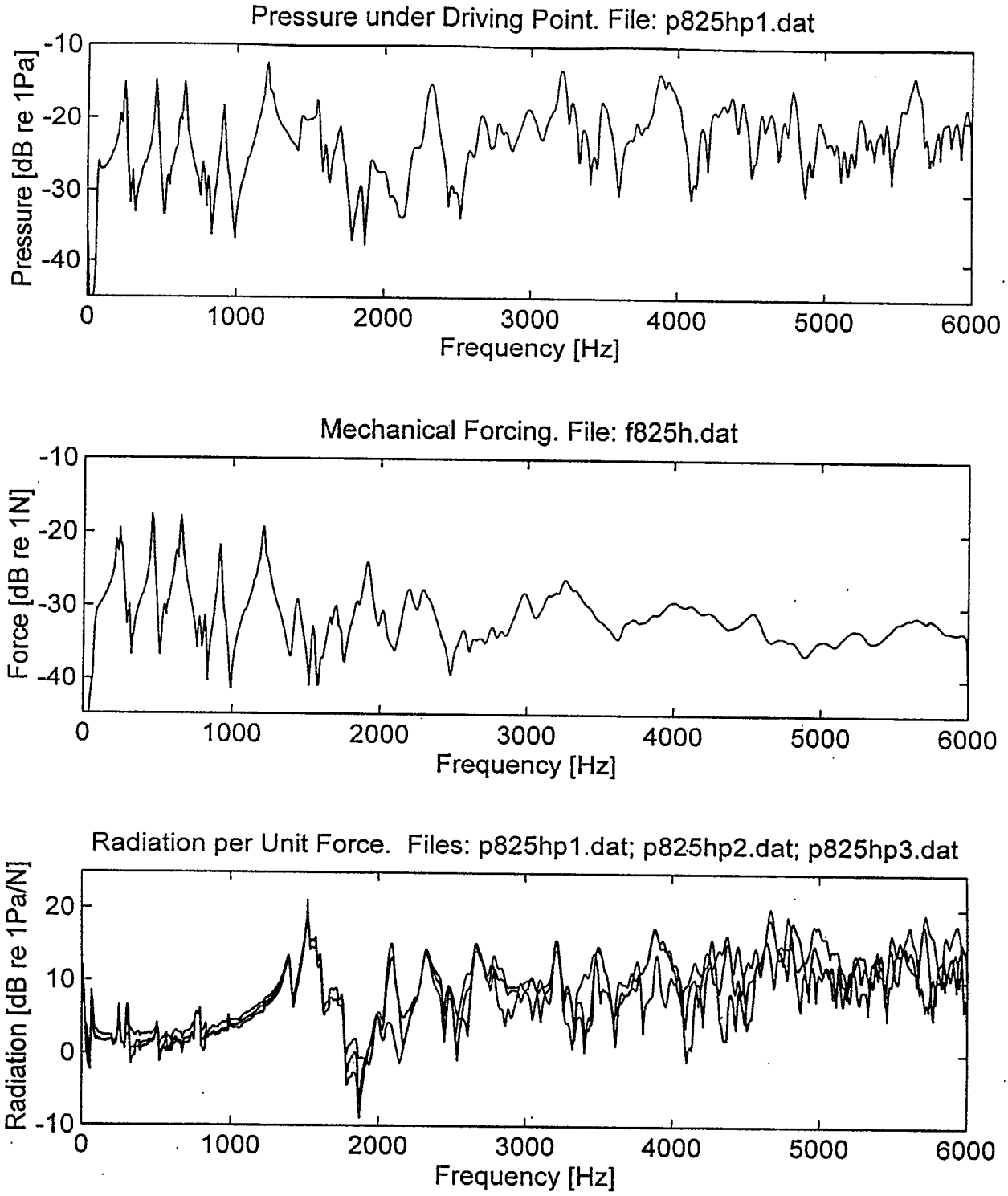

Figure 7. Epoxy-based 4H Spectra Fiber composite panel measured under free run mode

3.0 RESULTS AND DISCUSSIONS

3.1 INSERTION LOSS

3.1.1 Insertion Loss of Panels Before Aging

Ideally, the properties of a sonar dome would be such as to allow acoustic radiation to propagate through with minimal reflection, absorption, or distortion. Results of the insertion loss from six panels are presented through Figure 8 to Figure 13. All four Spectra Fiber composite panels (Figures 8, 9, 10 and 11) have less than 1 dB insertion loss in the 0 to 30 kHz frequency range. Note that the epoxy-based 4H and cyanate-based 8H Spectra Fiber composite panel have their insertion losses less than 0.5 dB in the 1 to 25 kHz frequency range. In contrast GRP panels (Figures 12 and 13) had losses that increased more sharply with frequency, with values of 2.5 - 3.5 dB at the higher end of the frequency range examined (40 kHz). The insertion loss of a thin (0.92 mm) stainless steel panel is shown for comparison in Figure 21. Note how the waveshape is altered considerably compared with the Spectra Fiber composite panels.

3.1.2 Insertion Loss of Panels After Aging

Results of the insertion loss from six panels after aging are shown in Figures from 14 to 19. The epoxy-based 8H Spectra Fiber composite panel had a relatively flat insertion loss, less than 1 dB up to 37 kHz. A negative insertion loss occurred when frequency was lower than 5 kHz. This negative loss represents a signal gain. Thus, the signal level at the observation position is higher with the panel present than without the panel. The negative insertion loss has been observed in cases where the source and receiver are in close proximity, and has been attributed to the non-planar sound field that exists in this case (Humphrey and Berktay, 1985). The epoxy-based 4H Spectra Fiber composite panel showed very low and almost constant insertion losses. The cyanate-based 8H Spectra Fiber composite panel exhibits an insertion loss below 1 dB. Nevertheless, the cyanate-based 4H panel had a sharp increase

losses that increased when frequency was higher than 25 kHz and decreased slightly when the frequency was lower than 25 kHz. It is notable that epoxy-based GRPs had negative insertion loss and cyanate-based GRPs had a very low loss when the frequency is lower than 8 kHz.

There were no significant changes of insertion loss for epoxy-based 4H panel and cyanate-based 8 H panel after aging. The insertion losses of other panels were lower except for the cyanate ester based 4H panel where the IL increased at frequencies less than 10 kHz.

3.1.3 Weight Change After Aging

Weight measurements of panels before and after aging are tabulated in Table 4. There were very small changes in weight after aging. Notwithstanding this, the epoxy-based panels absorbed more water than the cyanate-based panels.

Table 4. Panel Weight Changes after Aging

Panels	Dry kg	Wet kg	Change Rate (day^{-1})	Wet kg	Change Rate (day^{-1})	Average (day^{-1})
Date	21/03/95	08/06/95		10/07/95		
985PT/BT250E	10.510	10.570	$7.22X10^{-5}$	10.620	$1.48X10^{-4}$	$9.42X10^{-5}$
985PT/BTCY-3	9.870	9.900	$3.80X10^{-5}$	9.920	$6.31X10^{-5}$	$4.56X10^{-5}$
988PT/BT250E	10.370	10.460	$1.10X10^{-4}$	10.490	$8.96X10^{-5}$	$1.04X10^{-4}$
988PT/BTCY-3	10.130	10.160	$3.74X10^{-5}$	10.180	$6.15X10^{-5}$	$4.44X10^{-5}$
GRP (Epoxy)	20.370 09/05/95	20.440	$1.15X10^{-4}$	20.480	$3.05X10^{-5}$	$8.70X10^{-5}$
GRP (Cyanate)	20.690 09/05/95	20.740	$8.05X10^{-5}$	20.760	$3.01X10^{-5}$	$5.45X10^{-5}$

3.1.4 Insertion Loss of Sonar Window

The insertion loss of a stainless steel sonar window was around 1 dB below 10 kHz (Figure 20), but it increased dramatically when the frequency was above 10 kHz.

3.1.5 Angle of Incidence

Insertion loss measurements on 6 composite panels, one double walled stainless steel sonar window and one 20 gauge stainless calibration plate were carried out at 0°, 30°, and 60° from normal incidence (Figures from 22 to 29). The insertion loss of Spectra Fiber composite panels fluctuated within 1 dB for non-normal incidence except the epoxy-based 4H panel, which was sensitive to angular changes. For both epoxy-based and cyanate-based GRP panels, insertion losses decreased as the angle to the normal increased. There was very little loss at 60°. Small changes were found at 30° for the 20 gauge stainless steel calibration plate. However, the insertion loss fluctuated with frequency at 60°. The insertion loss of the sonar window varied less than 1 dB as the angle of incidence was changed for the frequency range studied.

3.2 SELF NOISE EVALUATION

3.2.1 Frequency Response Function

The range of frequencies examined was 0 to 6 kHz (Figures 30, 33, 36, 38, 41, 44, 47 and 50). The modal frequencies are those where the magnitude of $1/H(\omega)$ peaks and the phase crosses 90°. Table 5 lists the modal frequencies for six panels and a sonar window. Modes are distinct at frequencies lower than 4 kHz. Modes appear small but are still detectable in the frequency range from 4 to 6 kHz. There are similar modal frequencies among the Spectra Fiber composite panels (Figures 30, 33, 36 and 38). Fewer modal frequencies could be located in the cyanate panels. The cyanate-based 8H Spectra Fiber composite panel has 10 modes. The sonar window with both walls contacted with water had fewer modes than that of a single wall

immersed (Figures 47 and 50). The signals returned from sonar window were weak and noisy. It is assumed that it is difficult for shaker to activate such a sonar window, which is a very rigid structure when cut to these dimensions (50.8 x 50.8 x 6 cm).

Table 5. Modal Frequencies (Hz) of Test Panels and Sonar Window

Mode	Epoxy Composite		Cyanate Composite		8H GRP Panel		Sonar Window	
	8H	4H	8H	4H	Epoxy	Cyanate	One in	Two in
1	151	137	154	145	143	146	98	88
2	446	434	452	433	412	445	735	489
3	646	605	647	608	561	600	880	812
4	924	900	946	909	835	771	1007	1472
5	1205	1193	1231	1223	1116	909	1218	1550
6	1473	1438	1467	1579	1327	1206	1291	1943
7	1767	1553	1790	1637	1387	1408	1813	2274
8	1945	1706	1913	1752	1579	1519	2025	2541
9	2340	1918	2804	1942	1805	1708	2199	2839
10	2800	2200	3095	2340	2088	1860	2274	3007
11	3043	2282		2576	2480	2517	2361	
12	3330	2578		3061	2847	2811	2569	
13	4235	3001		3350	3092	3073	2830	
14	4640	3247			3901	3221	2898	
15		4551			4191	3691	3167	
16					4371		3481	
17					5644		3727	
18							4103	

3.2.2 Driving Force and Radiated Pressure

Both radiated pressure and driving force data are in good agreement with the frequency response function (FRF). Individual peaks could be matched among them at the same frequency (refer to Figures from 30 to 52). At the higher frequency end, there are not many features from the force data. However there is high level of noise in the pressure data when the frequencies were higher than 4 kHz, possibly because the tank is not reverberant enough at these frequencies.

It is recommended that a full scale shaker test be carried out to compare the self noise characteristics of the stainless steel dome and composite domes. The tests carried out under this contract are not conclusive enough to rank the panels in terms of self noise, especially at frequencies $>$ 4 kHz.

Peaks in the radiation efficiency were pronounced and had similar patterns among the 7 test samples except for the sonar window (Table 6). Neither cyanate 8H Spectra Fiber composite panel nor epoxy 8H GRP panel showed any peaks in the radiation efficiency around 2080 Hz.

Table 6. Radiation Efficiency Frequency Points (Hz) in 0 to 3000 Hz Range

$10\log_{10}(p/F)$	< 0 dB	> 10 dB			
Epoxy-based 8H Spectra Fiber composite	1900	1540	2090	2350	2625
Epoxy-based 4H Spectra Fiber composite	1900	1530	2080	2300	2670
Cyanate-based 8H Spectra Fiber composite	1900	1530		2311	2630
Cyanate-based 4H Spectra Fiber composite	1900	1530	2079	2320	2645
Epoxy-based 8H GRP	2036	1510		2273	2657
Cyanate-based 8H GRP	1900	1525		2295	2669
Sonar window one layer in water	1000	589	1220	1488	2068
Sonar window 2 layers in water	272	1522	2052		2610

4.0 CONCLUSIONS

From this experiment, it is clear that the Spectra Fiber composite panels have very low insertion losses compared to the glass fiber composites (GRP) of the same thickness, especially above 10 kHz. In particular, the epoxy-based panel and cyanate-based panel have remarkable responses producing very little wave-shape distortion and losses. In addition to being non-corroding and having high strength to weight ratios, their acoustic properties appear well-matched to the impedance of water, and appear well suited to low frequency propagation. Overall, it would appear that significant gains would be made using Spectra Fiber composite materials over glass fiber and metallic sonar domes, at frequencies greater than 10 kHz. However, stainless steel and GRP materials have low insertion loss at frequencies lower than 10 kHz.

Cyanate-based panels absorbed less water than that of epoxy-based panels during water aging treatment. Most tested aged panels reduced the insertion losses except the cyanate-based 4H Spectra Fiber composite one.

Results of force, pressure and FRF measurements were closely related to each other. It was recommended that large scale tests be carried out to compare the self noise characteristics of the stainless steel dome with the composite domes.

ACKNOWLEDGMENTS

This research was funded by the Department of National Defence of Canada under Contract No. W7707-4-2930/01-HAL. We wish to acknowledge the contributions of Voon Hong Chin who helped on a system calibration at the beginning of this project. Craig Hamm, Wali Li, Sandra Mercer, Wai Chi Siu and Hong Hai Liu provided many supports during experiments and data analyses. Dick Whittaker of the Industrial Research Assistance Program made the Flume Tank at the Marine Institute of Newfoundland available for this experiment.

REFERENCES

Berktay, H.O., B.V. Smith, H.B. Braithwaite and M. Whitehouse, 1979, Subbottom profilers with parametric sources, *Underwater Applications of Nonlinear Acoustics*, Institute of Acoustics, University of Bath, England, Session 1.2, pp. 1-10.

Clay, C.S., and H. Medwin, 1977, Acoustical Oceanography: Principles and Applications, *Wiley-Interscience*, New York, pp. 185-187.

Davies, H.G., 1971, Low frequency random excitation of water-loaded rectangular plates. *J. Sound Vib.*, **15**, 107-126.

Frendi, A., L. Maestrello, and A. Bayliss, 1994, Coupling between plate vibration and acoustic radiation. *J. Sound Vib.*, **177**, 207-226.

Gu, Y. And C.R. Fuller, 1993, Active control of sound radiation from a fluid-loaded retangular uniform plate. *J. Acoust. Soc. Am.*, **93**, 337-345.

Guigné, J.Y., J.P. Szabo and Q. Liu, 1995, Acoustic properties of sonar dome materials. in: Abstracts and summaries of the 2nd Canadian Forces/Crad Meeting on naval applications of materials technology, May 2-4, 1995. Halifax, Canada. 663pp.

Guigné, J.Y., N. Rukavina, P.H. Hunt and J.S. Ford, 1991, An acoustic parametric array for measuring the thickness and stratigraphy of contaminated sediments. *J. Great Lake Res.*, **17**, 120-131.

Guigné, J.Y. and V.H. Chin, 1989, Acoustic imaging of an inhomogeneous sediment matrix, *Marine Geophysical Research*, **11**, 301-317.

Hagedorn, P., 1994, A note on the vibrations of infinite elastic plates in contact with water. *J. Sound* Vib., **175,** 233-240.

Hagelberg, M.P., and R.D. Corsaro, 1985, A small pressurized vessel for measuring the acoustic properties of materials, *J. Acoust. Soc. Am.*, **77**, 1222.

Hamm, C.A., 1996, Evaluation of noise reduction coatings: experimental design. DREA Contract Report CR/96/417.

Humphery, V.F., 1992, Non-linear acoustics as a laboratory tool. *Proc. I.O.A.,* **14(3)**, 99-113.

Humphrey, V.F., 1985, The measurement of acoustic properties of specimens of limited size by use of a parametric source, *J. Sound Vib.,* **98**(1), 67-81

Humphrey, V.F., and H. O. Berktay, 1985, The transmission coefficient of a panel measured with a parametric source, *J. Sound Vib.*, **101**, 85-106.

Mikesa, E.E., and J.A. Behrens, 1986, Evaluation of transducer window materials, *J. Acoust. Soc. Am.*, **59**, 1294-1298.

Piquette, J.C., 1994, Direct measurements of edge diffraction from soft underwater acoustic panels. *J. Acoust. Soc. Am.* **95**, 3090-3099

Szabo, J.P., 1992, A forced vibration non-resonant method for the determination of complex modulus in the audio frequency range, Defense Research Establishment Atlantic, Technical Memorandum 92/201.

Szabo, J.P., J.Y. Guigné, and V.H. Chin, 1992, Dynamic mechanical and acoustic properties of a PVC-based commercial damping elastomer, *J. Acoust. Soc. Am.*, **90**, 2293.

Westervelt, P.J., 1960, Parametric end-fire array, *J. Acoust. Soc. Am.*, **32**, 934A.

Westervelt, P.J., 1963, Parametric acoustic array, *J. Acoust. Soc. Am.* **35,** 535-537.

Whelan, S.M., V.H. Chin and J.Y. Guigné, 1993, A multilayered model for simulation of acoustical parameters, Defense Research Establishment Atlantic, Contract Report 93/408, Distribution Limited.

INSERTION LOSS MEASUREMENTS BEFORE THE PANELS WERE AGED

Figure 8. Insertion loss of an epoxy-based 8H Spectra Fiber composite panel before aging 35

Figure 9. Insertion loss of an epoxy-based 4H Spectra Fiber composite panel before aging 36

Figure 10. Insertion loss of a cyanate-based 8H Spectra Fiber composite panel before aging 37

Figure 11. Insertion loss of a cyanate-based 4H Spectra Fiber composite panel before aging 38

Figure 12. Insertion loss of an epoxy-based 8H GRP panel before aging 39

Figure 13. Insertion loss of a cyanate-based 8H GRP panel before aging 40

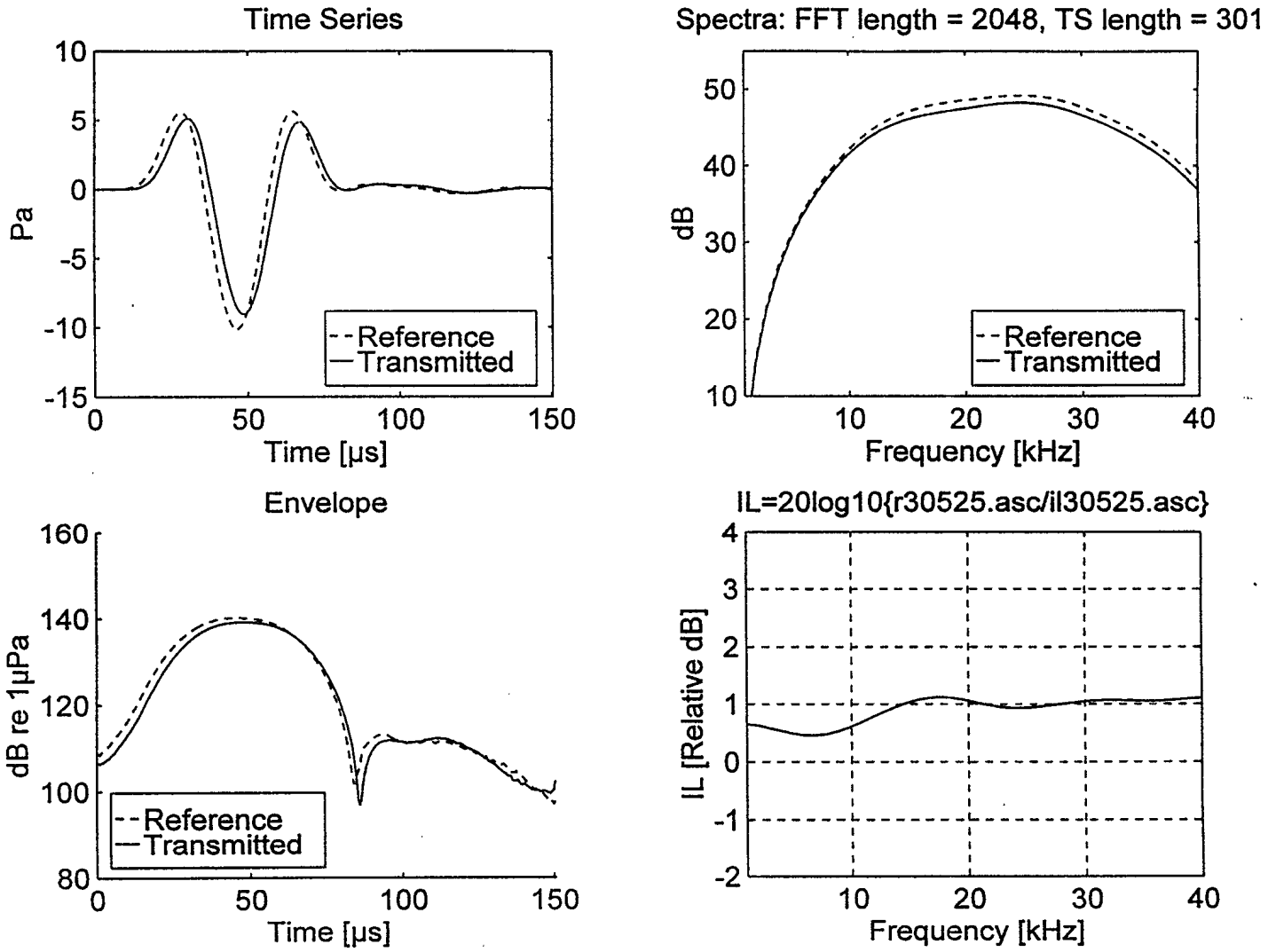

Figure 8. Insertion loss of an epoxy-based 8H Spectra Fiber composite panel before aging

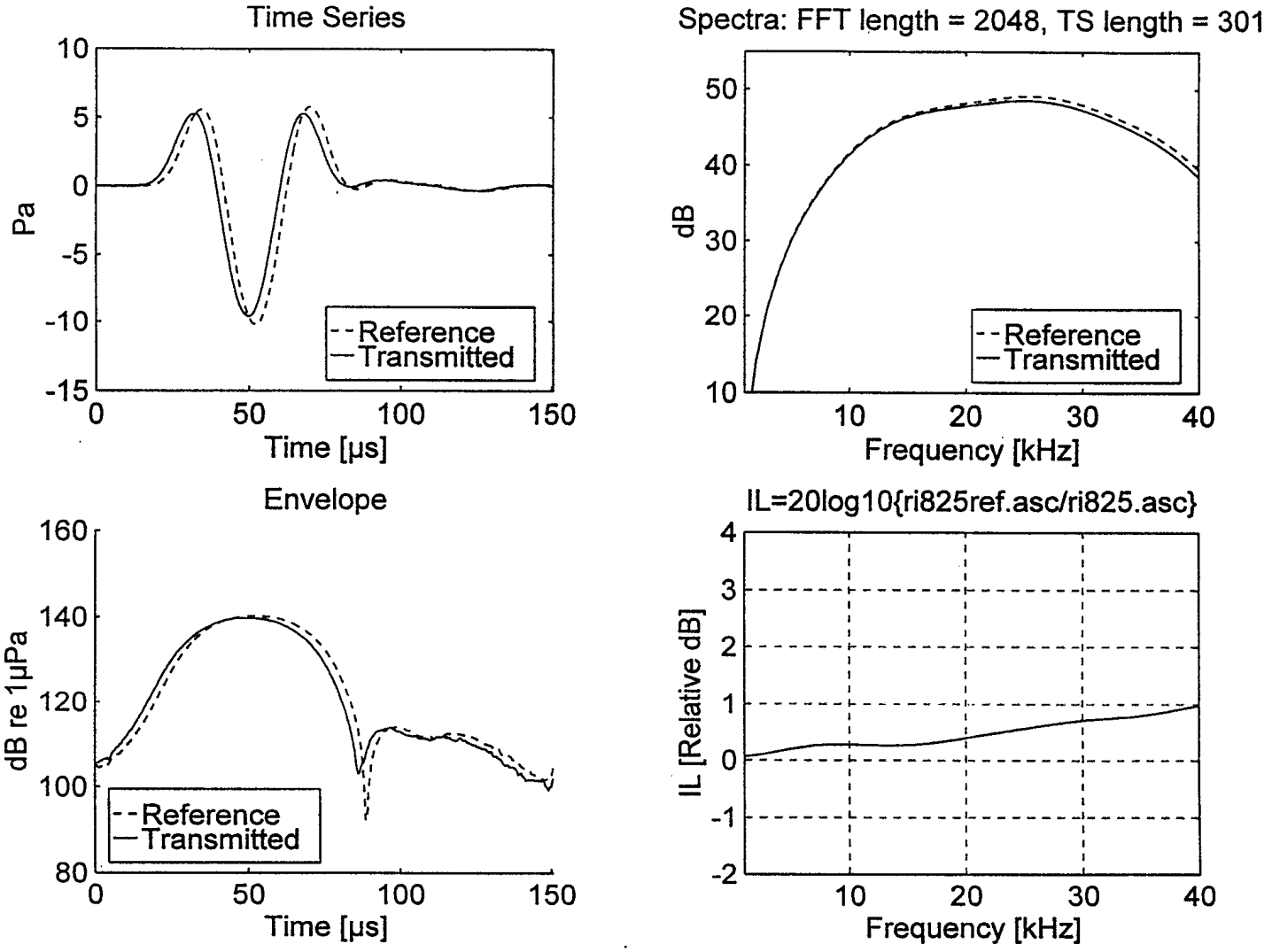

Figure 9. Insertion loss of an epoxy-based 4H Spectra Fiber composite panel before aging

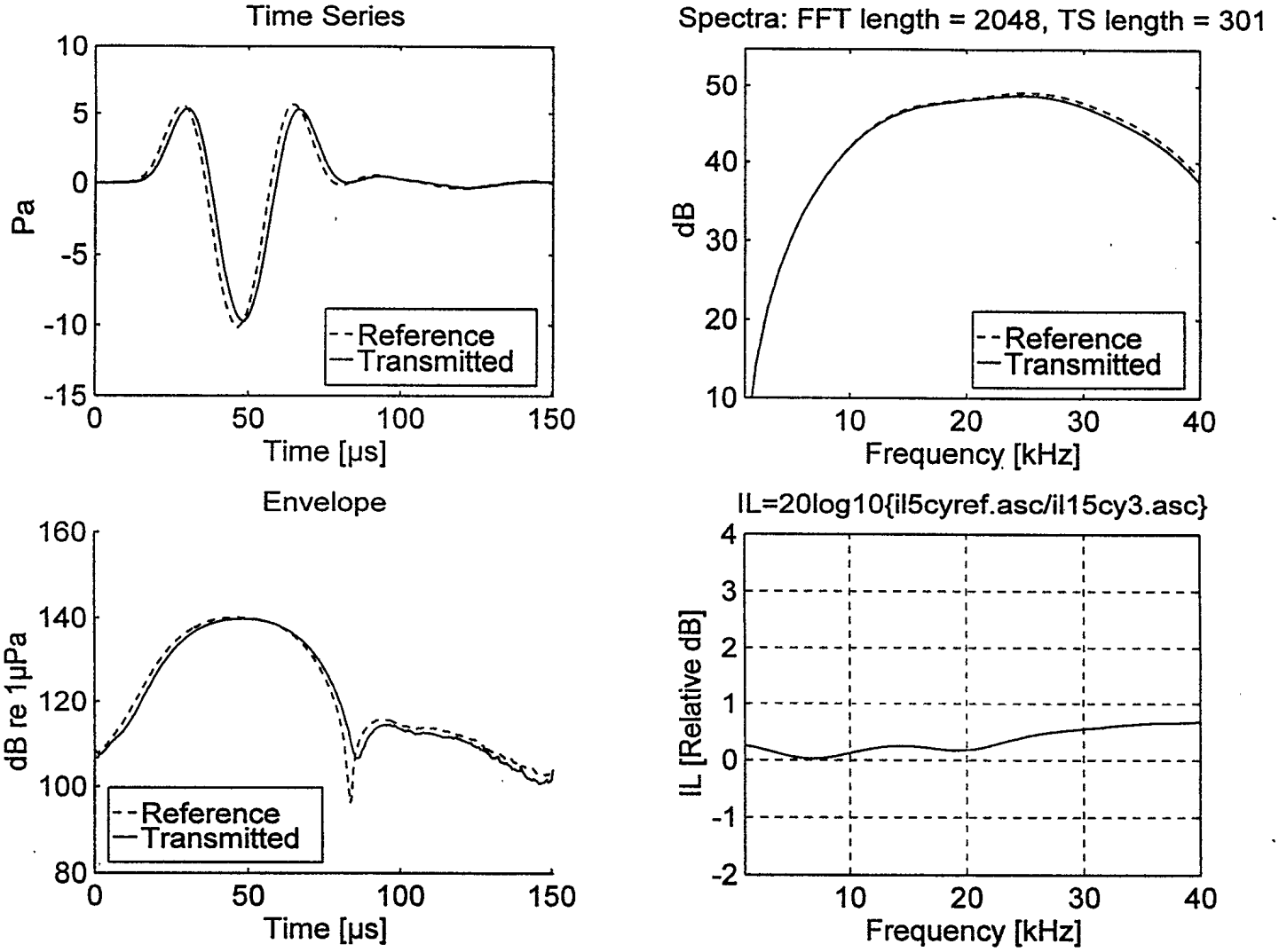

Figure 10. Insertion loss of a cyanate-based 8H Spectra Fiber composite panel before aging

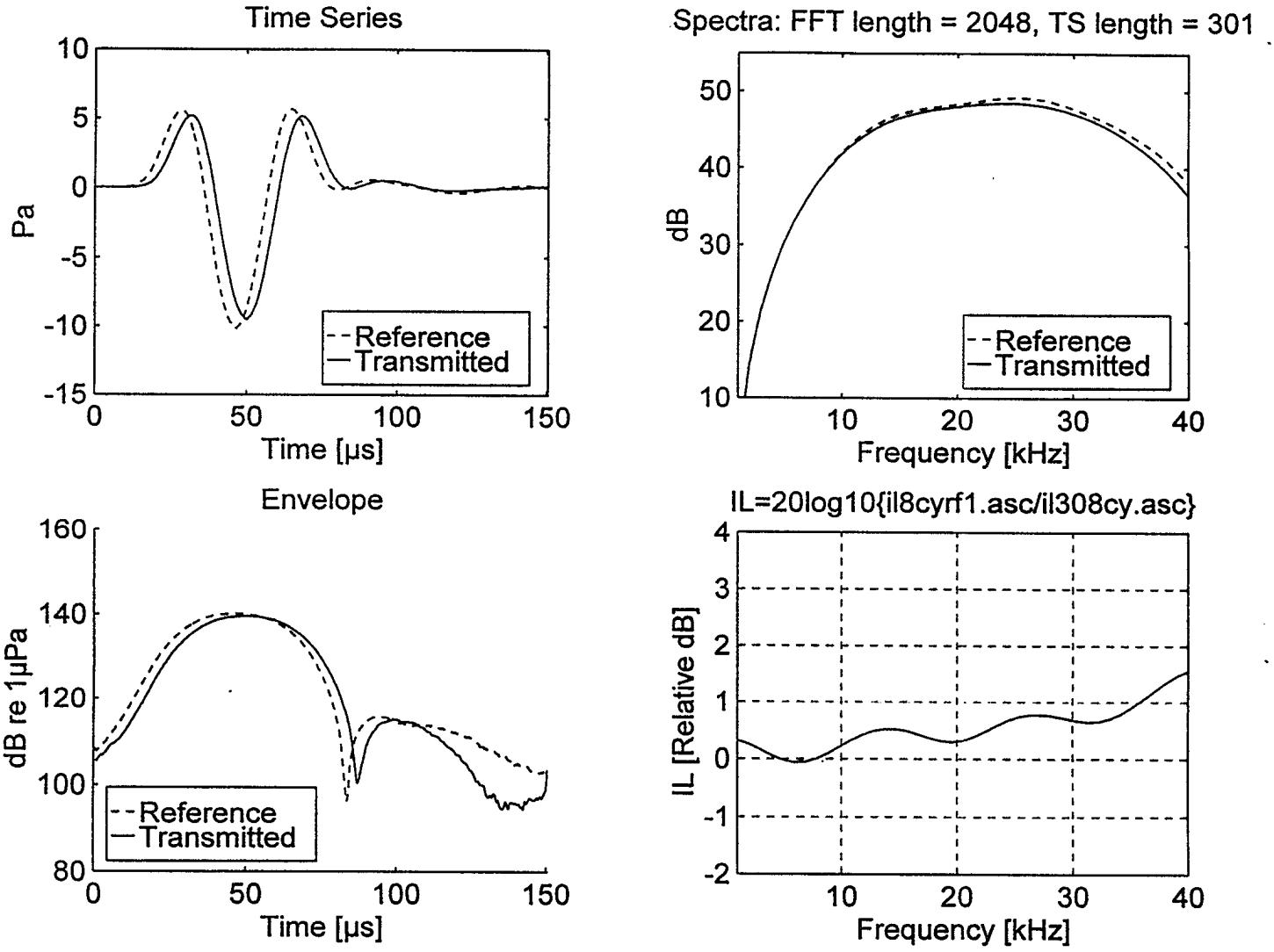

Figure 11. Insertion loss of a cyanate-based 4H Spectra Fiber composite panel before aging

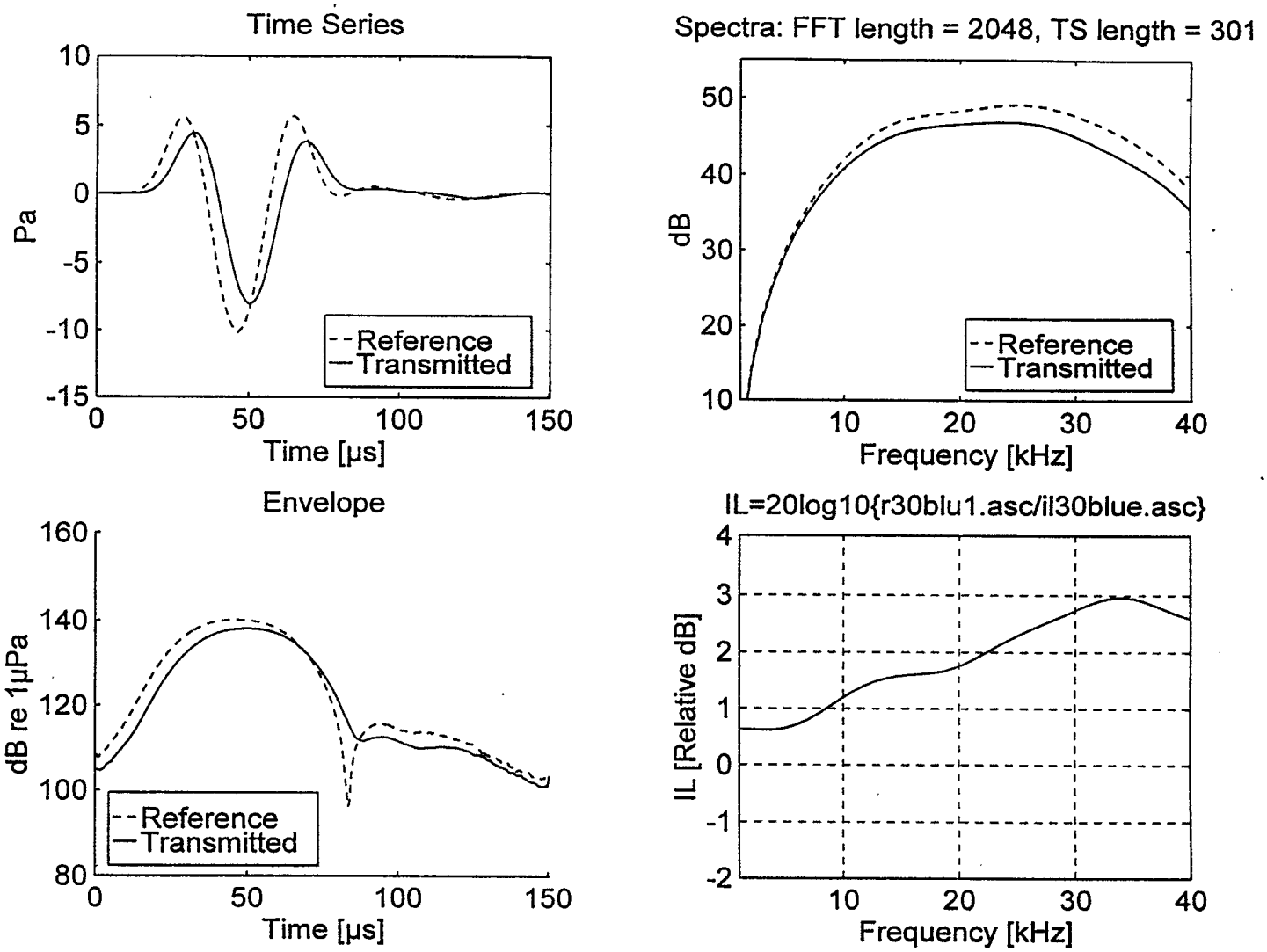

Figure 12. Insertion loss of an epoxy-based 8H GRP panel before aging

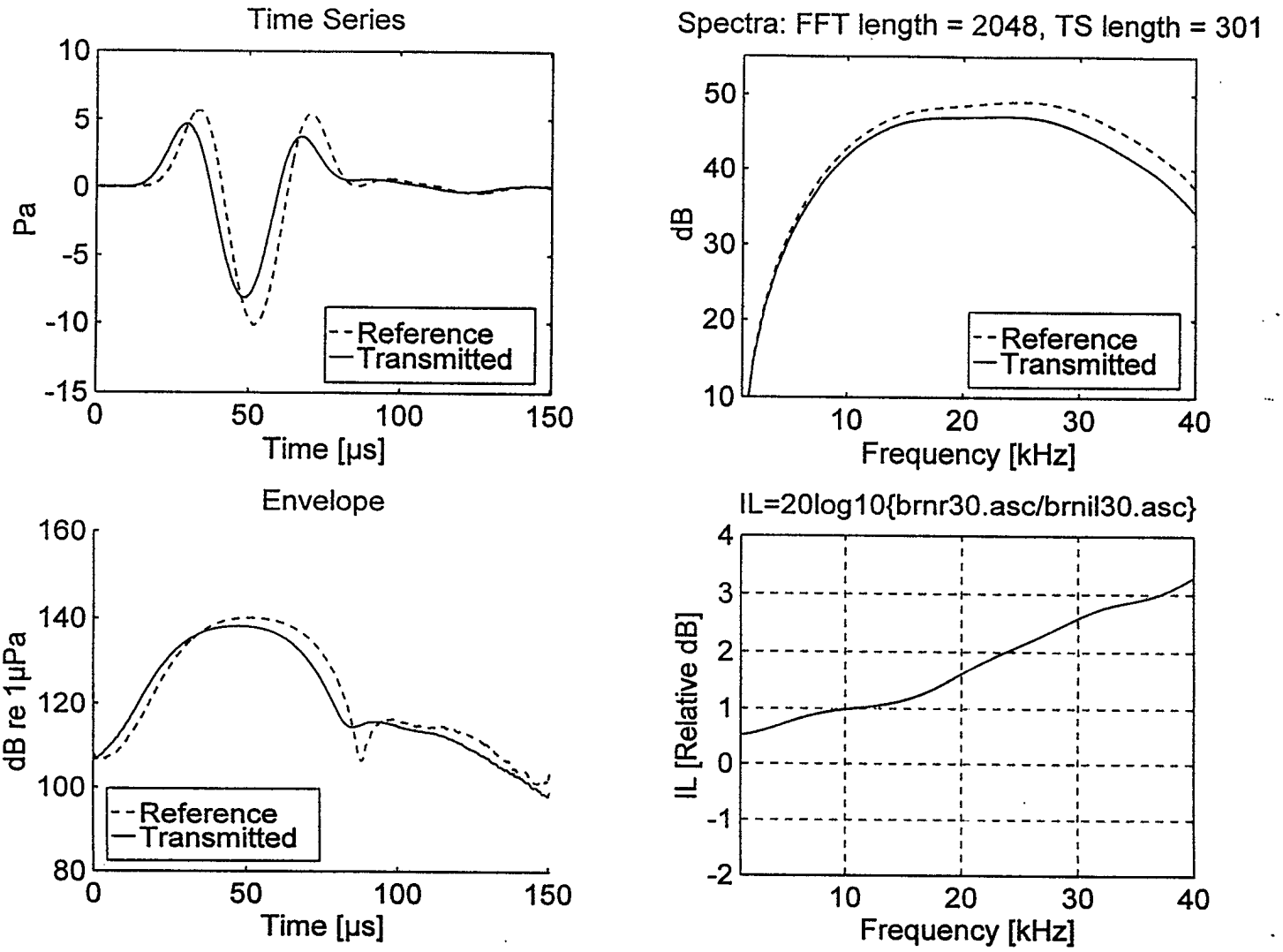

Figure 13. Insertion loss of a cyanate-based 8H GRP panel before aging

INSERTION LOSS MEASUREMENTS AFTER THE PANELS WERE AGED

Figure 14. Insertion loss of an epoxy-based 8H Spectra Fiber composite panel after aging 42

Figure 15. Insertion loss of an epoxy-based 4H Spectra Fiber composite panel after aging 43

Figure 16. Insertion loss of a cyanate-based 8H Spectra Fiber composite panel after aging 44

Figure 17. Insertion loss of a cyanate-based 4H Spectra Fiber composite panel after aging 45

Figure 18. Insertion loss of an epoxy-based 8H GRP panel after aging 46

Figure 19. Insertion loss of a cyanate-based 8H GRP panel after aging 47

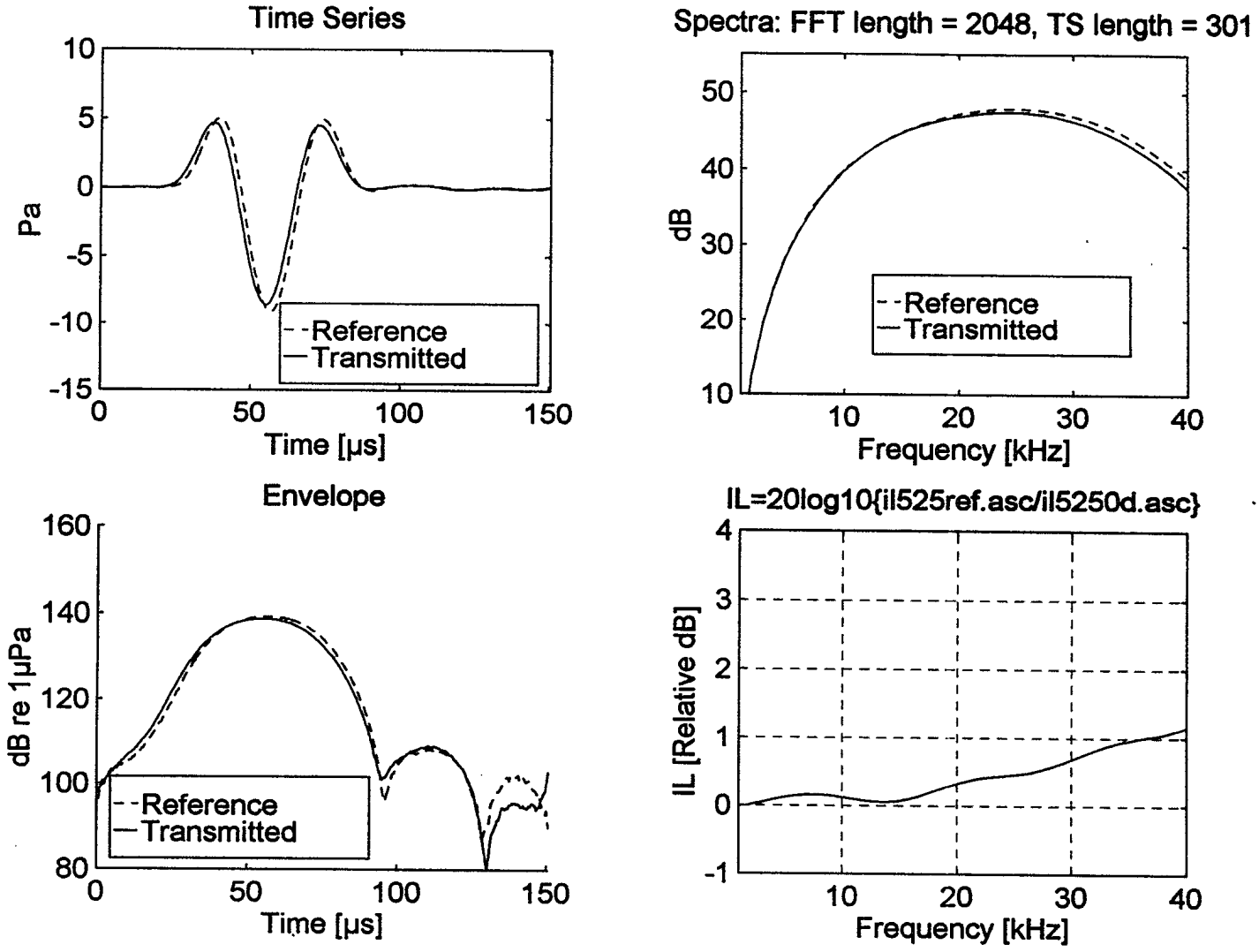

Figure 14. Insertion loss of an epoxy-based 8H Spectra Fiber composite panel after aging

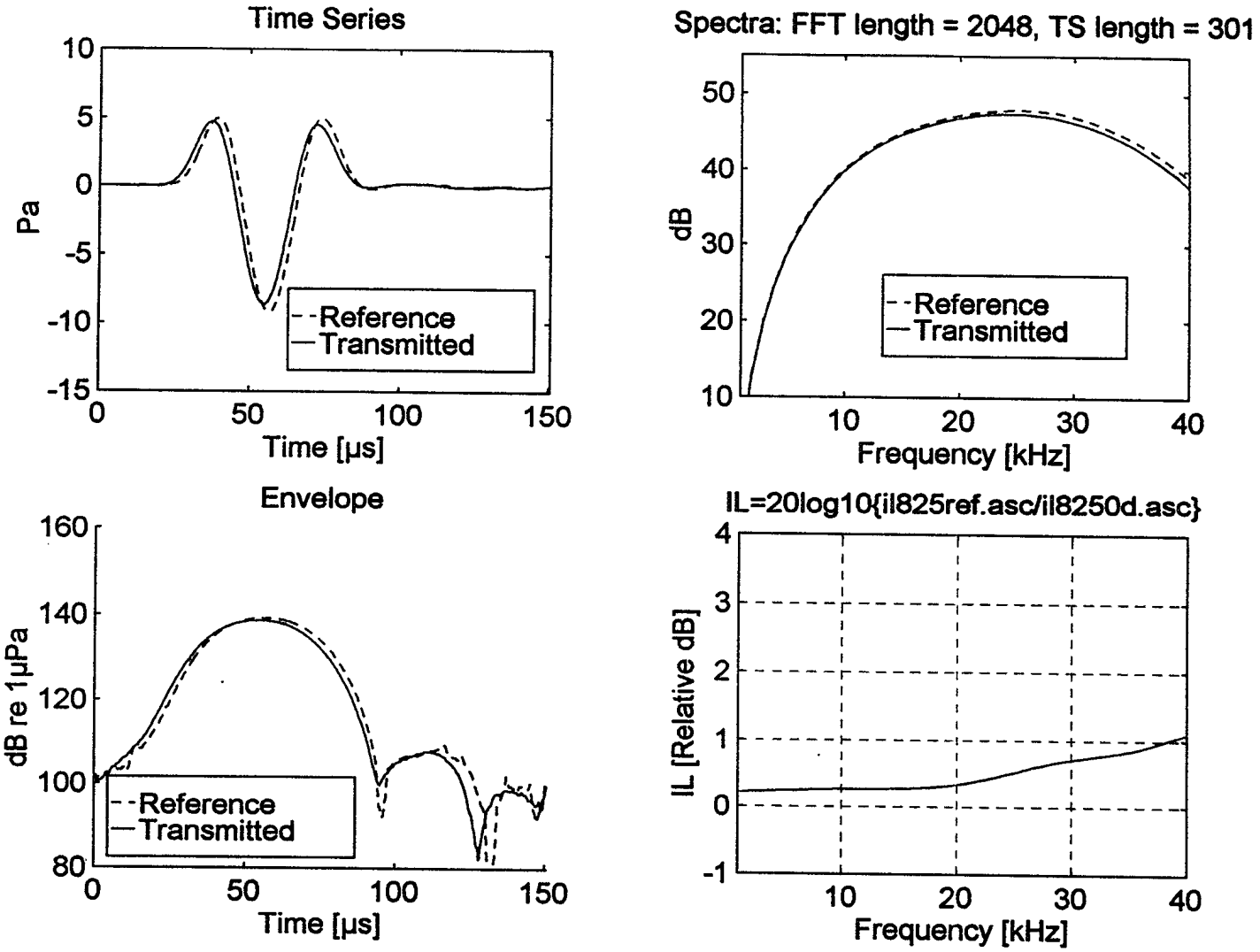

Figure 15. Insertion loss of an epoxy-based 4H Spectra Fiber composite panel after aging

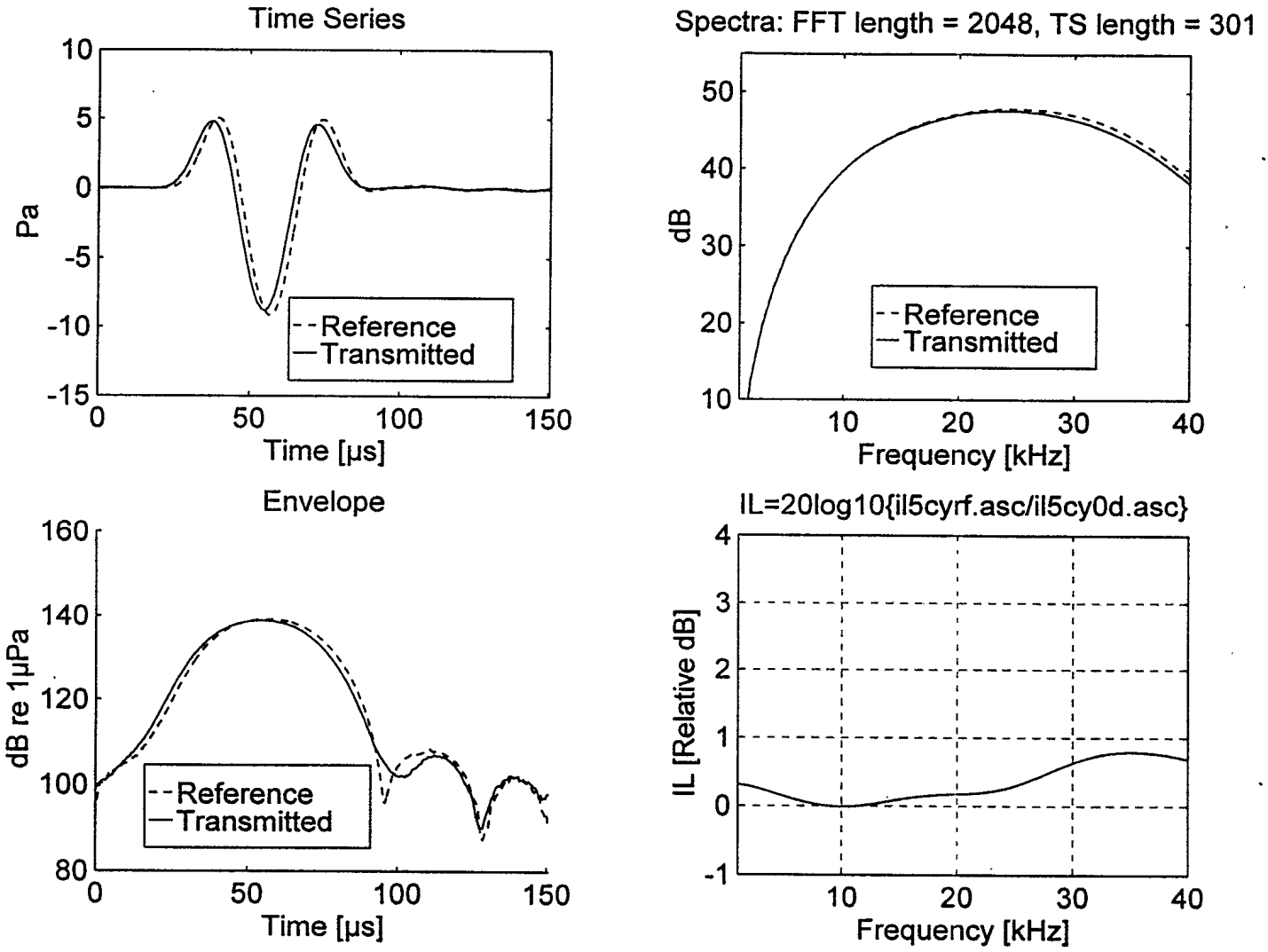

Figure 16. Insertion loss of a cyanate-based 8H Spectra Fiber composite panel after aging

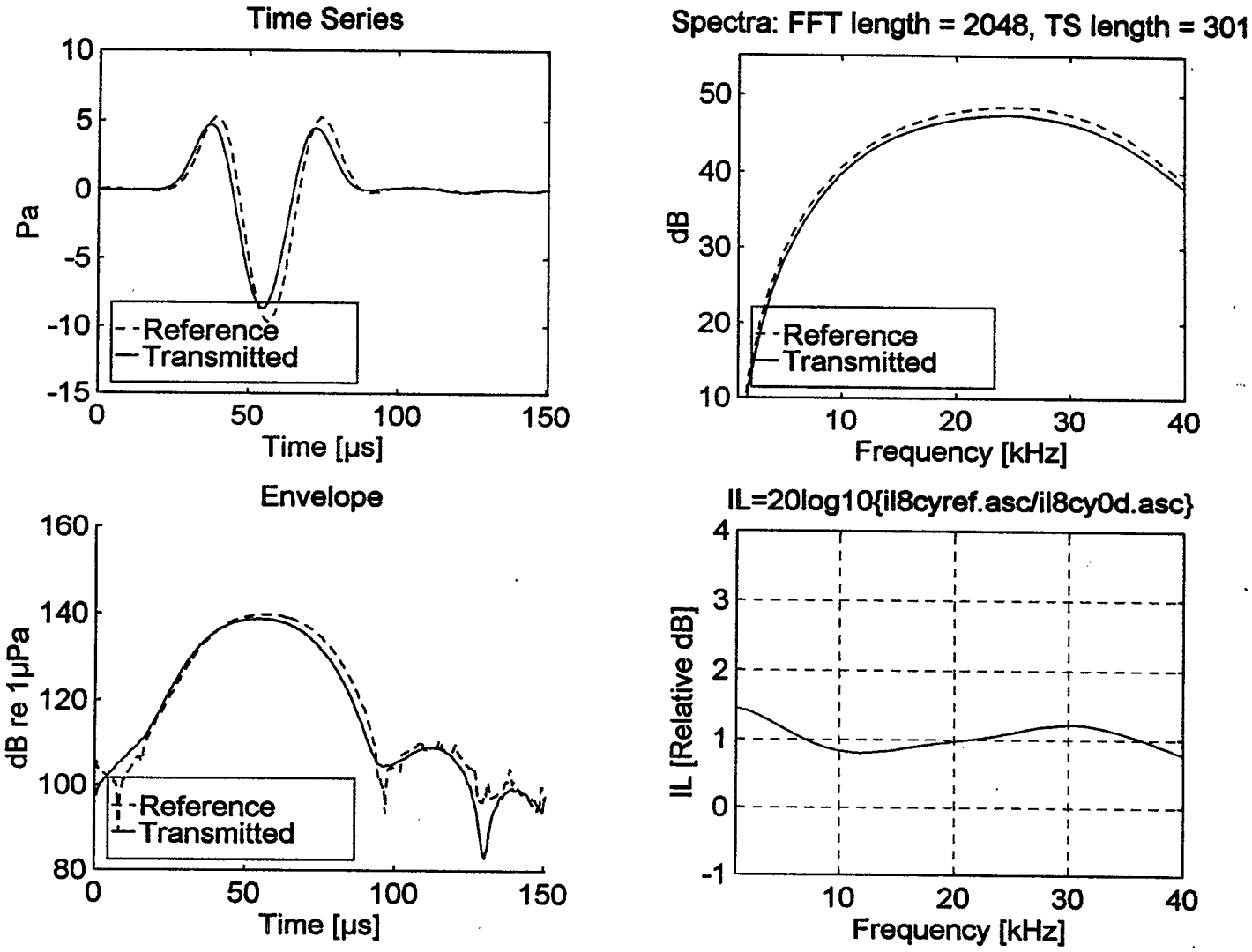

Figure 17. Insertion loss of a cyanate-based 4H Spectra Fiber composite panel after aging

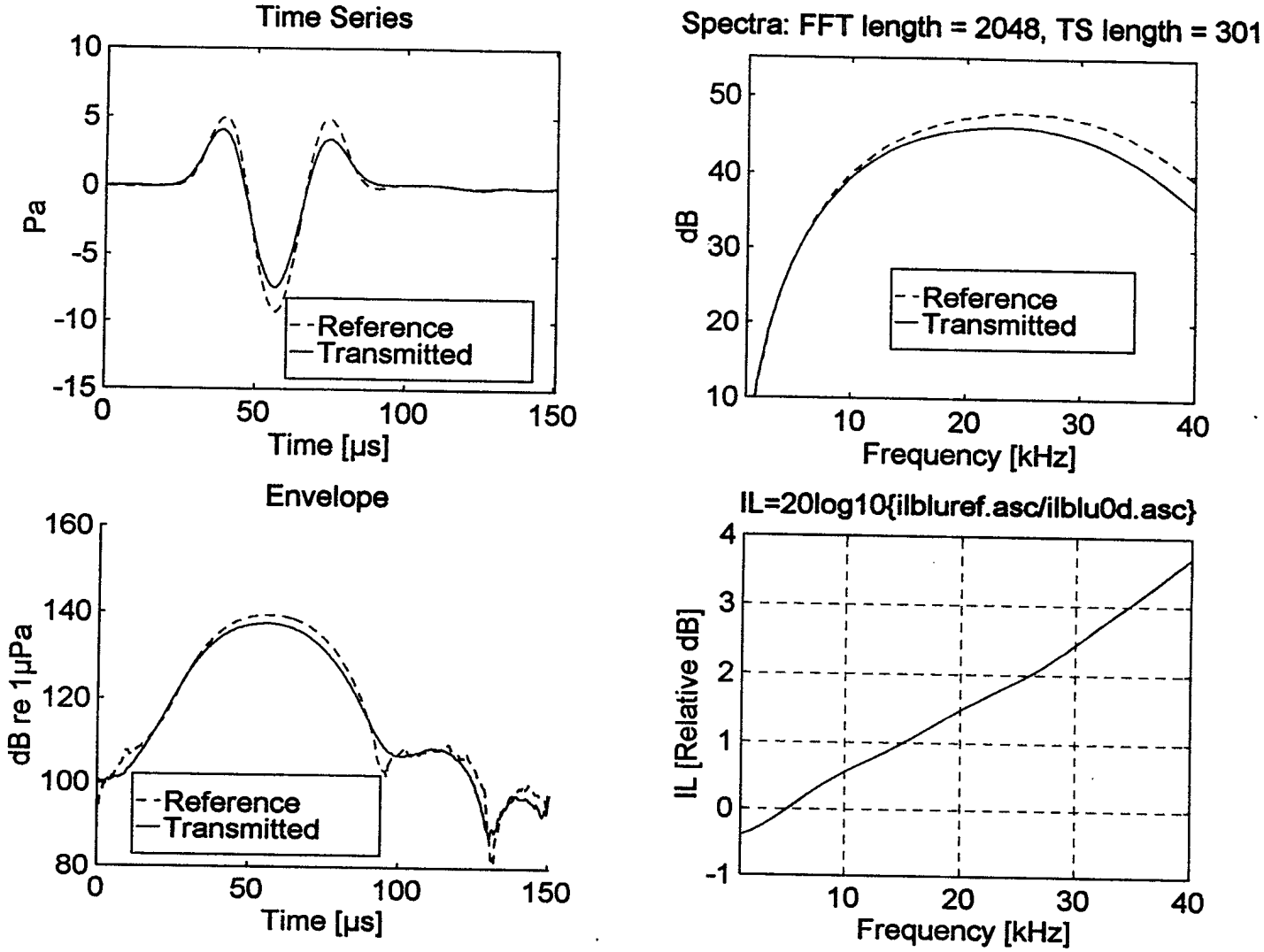

Figure 18. Insertion loss of an epoxy-based 8H GRP panel after aging

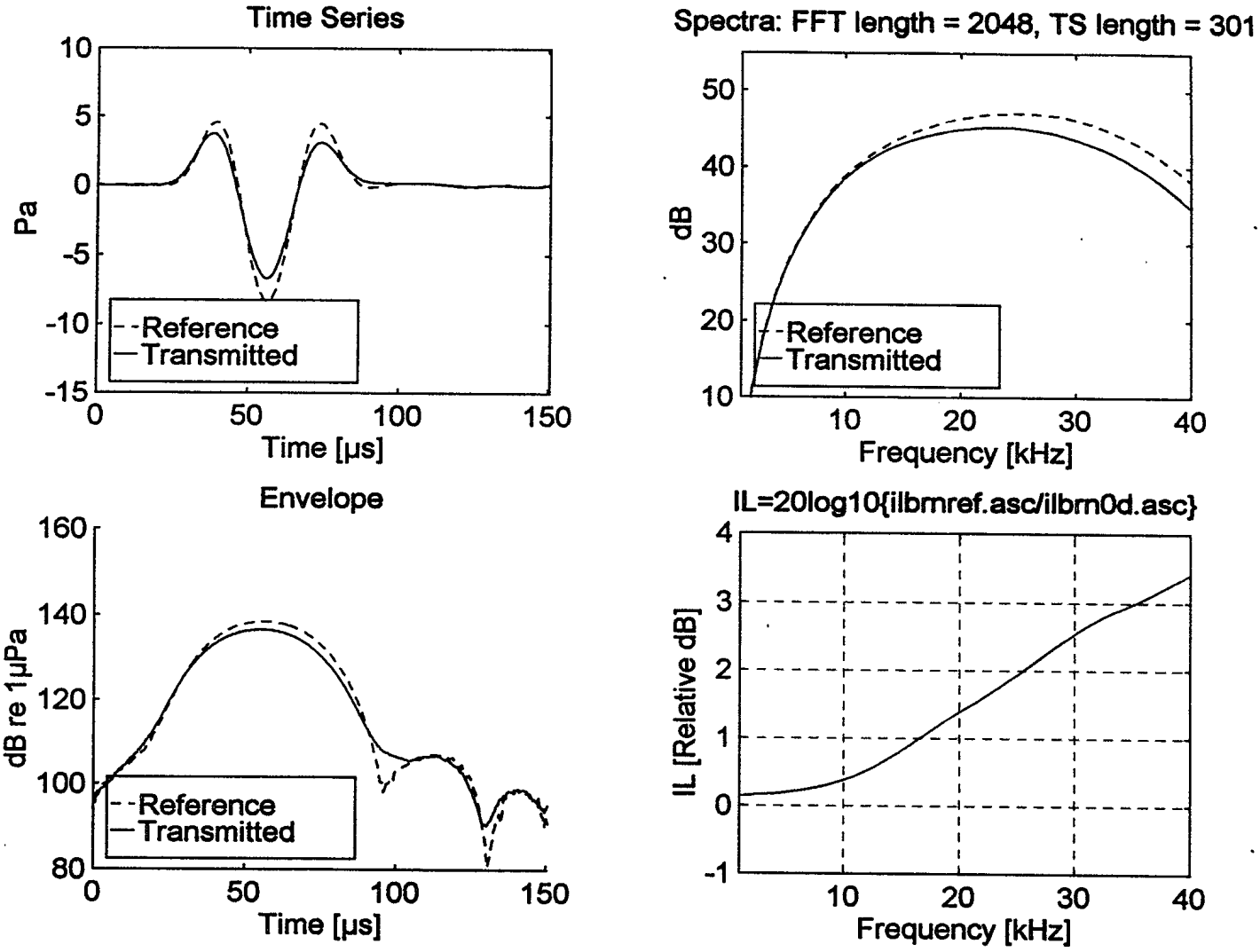

Figure 19. Insertion loss of a cyanate-based 8H GRP panel after aging

INSERTION LOSS MEASUREMENTS OF A STAINLESS STEEL SONAR WINDOW AND STAINLESS STEEL CALIBRATION PLATE

Figure 20. Insertion loss measurement of a double wall stainless steel sonar window . . . 49

Figure 21. Insertion loss measurement of a 20 gauge stainless steel plate 50

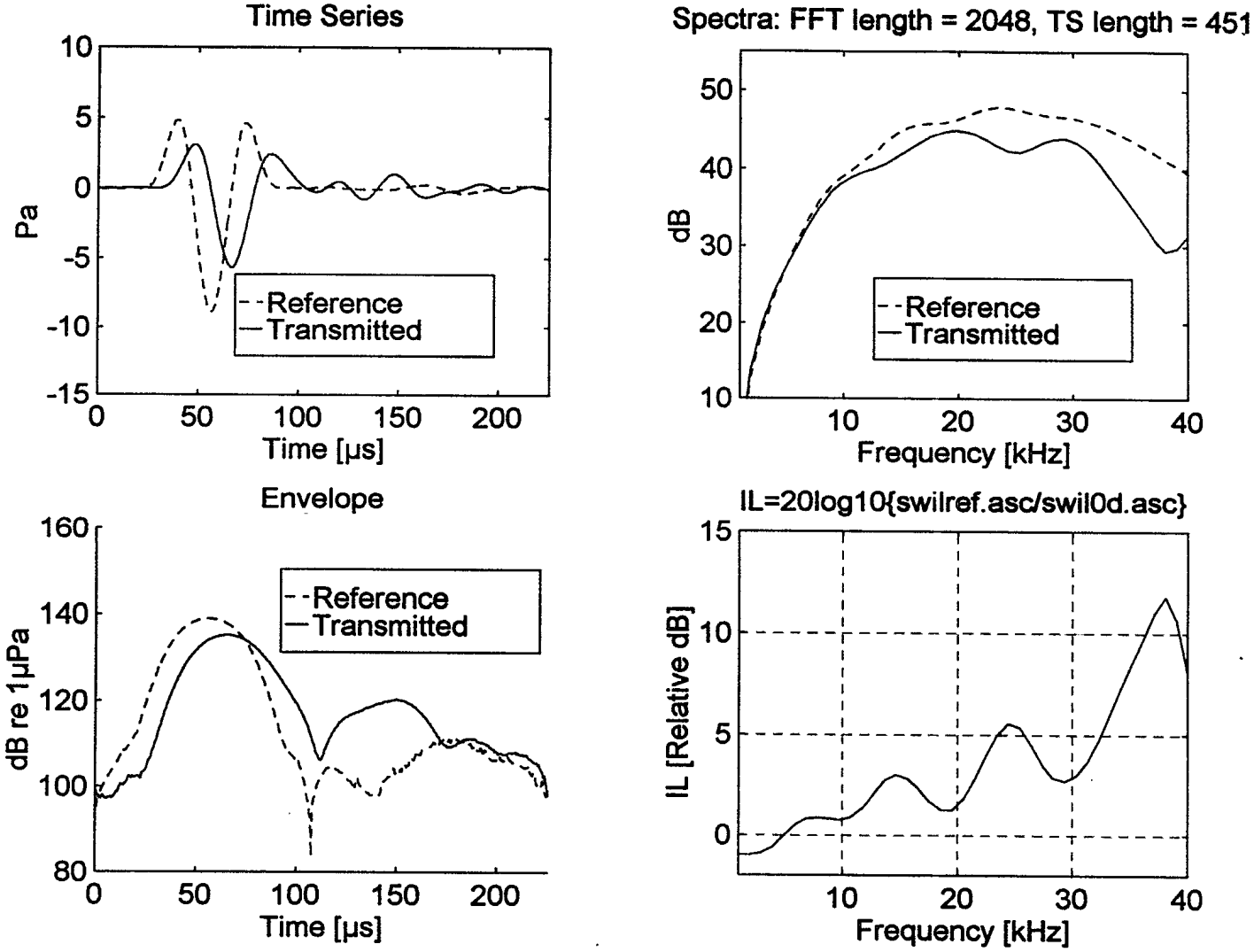

Figure 20. Insertion loss measurement of a double wall stainless steel sonar window

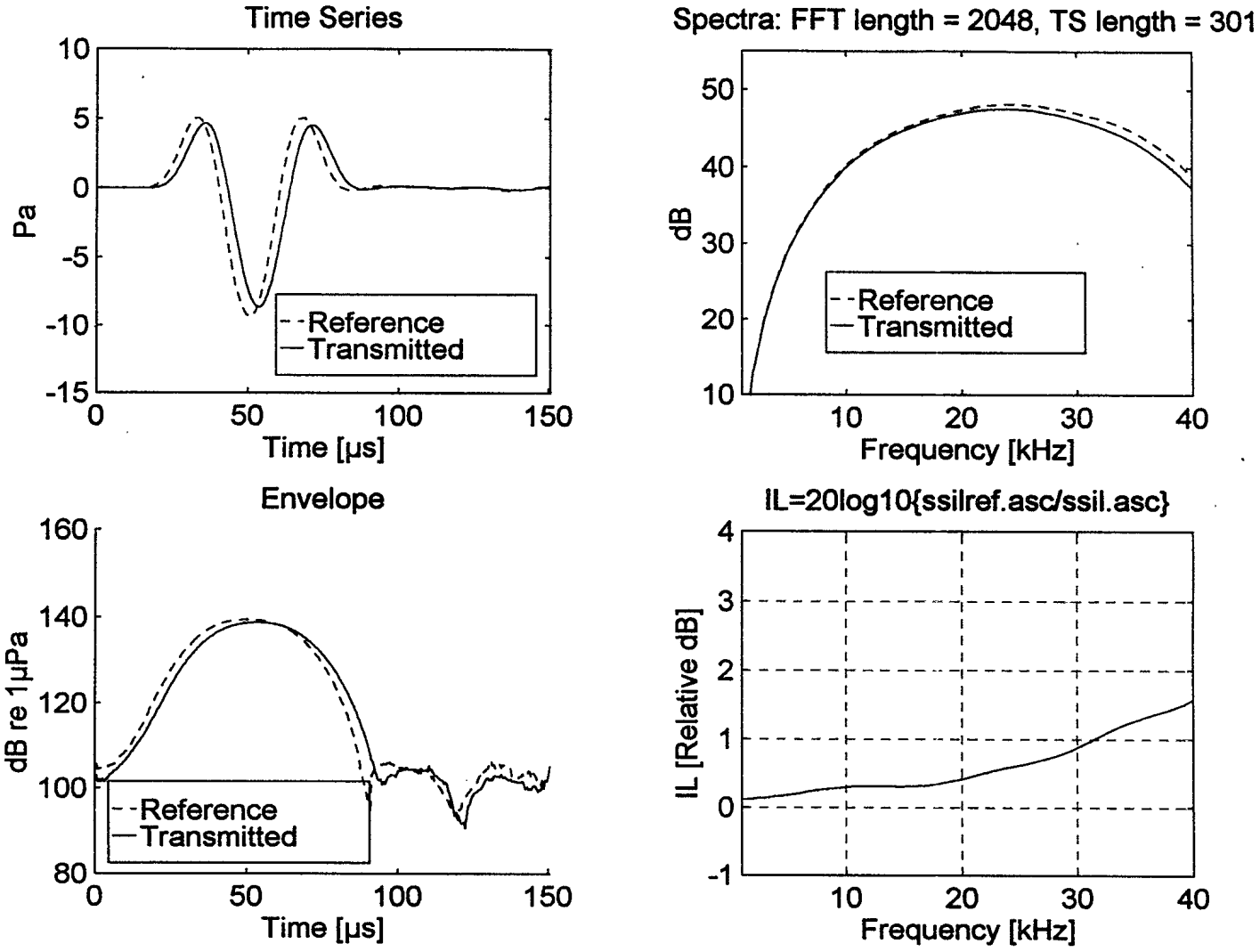

Figure 21. Insertion loss measurement of a 20 gauge stainless steel plate

INSERTION LOSS VERSUS ANGLE OF INCIDENCE

Figure 22. Insertion loss versus angle of incidence for a 10 mm thick epoxy-based 8H Spectra Fiber composite panel 52

Figure 23. Insertion loss versus angle of incidence for a 10 mm thick epoxy-based 4H Spectra Fiber composite panel 53

Figure 24. Insertion loss versus angle of incidence for a 10 mm thick cyanate-based 8H Spectra Fiber composite panel 54

Figure 25. Insertion loss versus angle of incidence for a 10 mm thick cyanate-based 4H Spectra Fiber composite panel 55

Figure 26. Insertion loss versus angle of incidence for a 10 mm thick epoxy-based 8H GRP panel 56

Figure 27. Insertion loss versus angle of incidence for a 10 mm thick cyanate-based 8H GRP panel 57

Figure 28. Insertion loss versus angle of incidence for a 20 gauge stainless steel plate . . 58

Figure 29. Insertion loss versus angle of incidence for a 60 mm thick double wall stainless steel sonar window 59

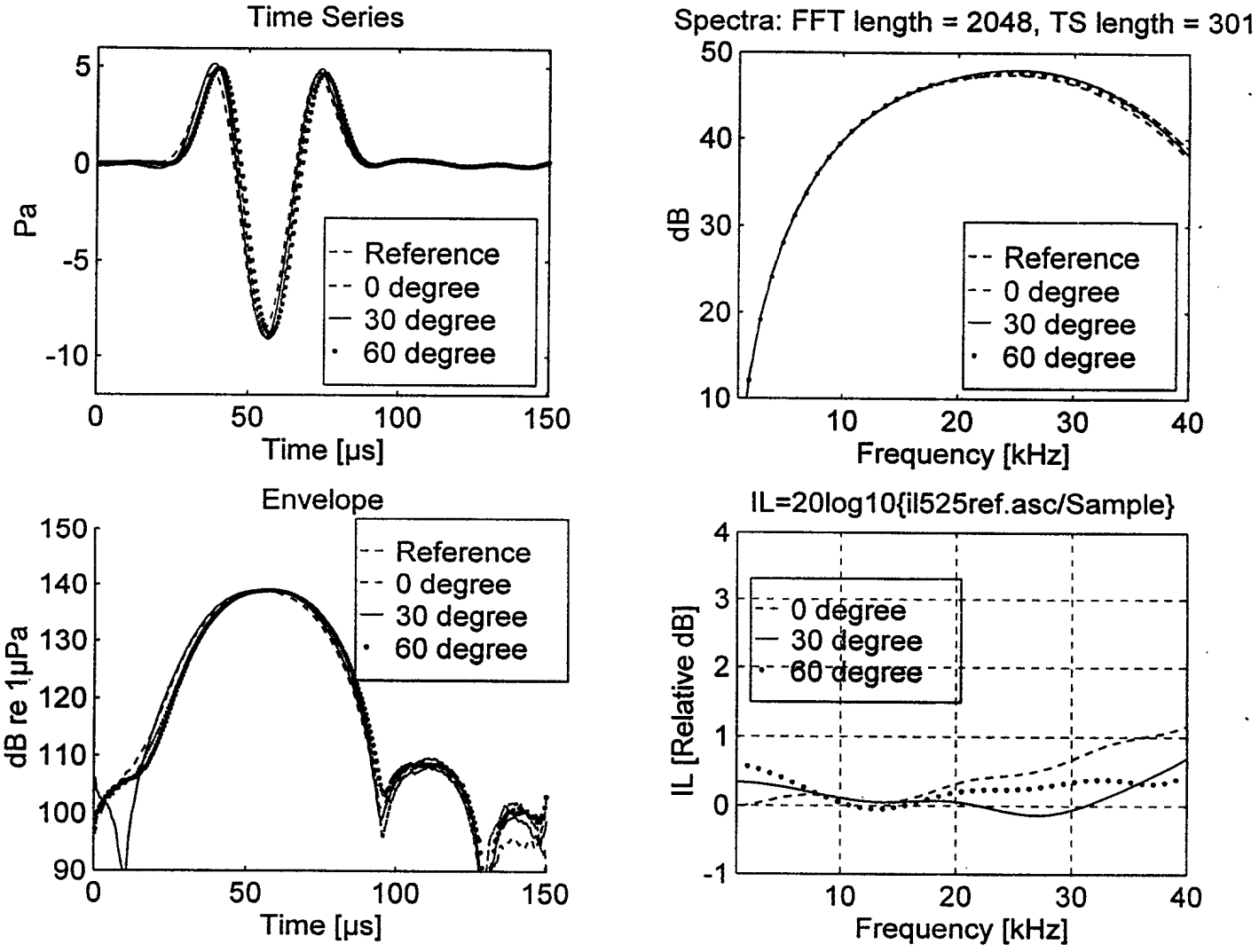

Figure 22. Insertion loss versus angle of incidence for a 10 mm thick epoxy-based 8H Spectra Fiber composite panel

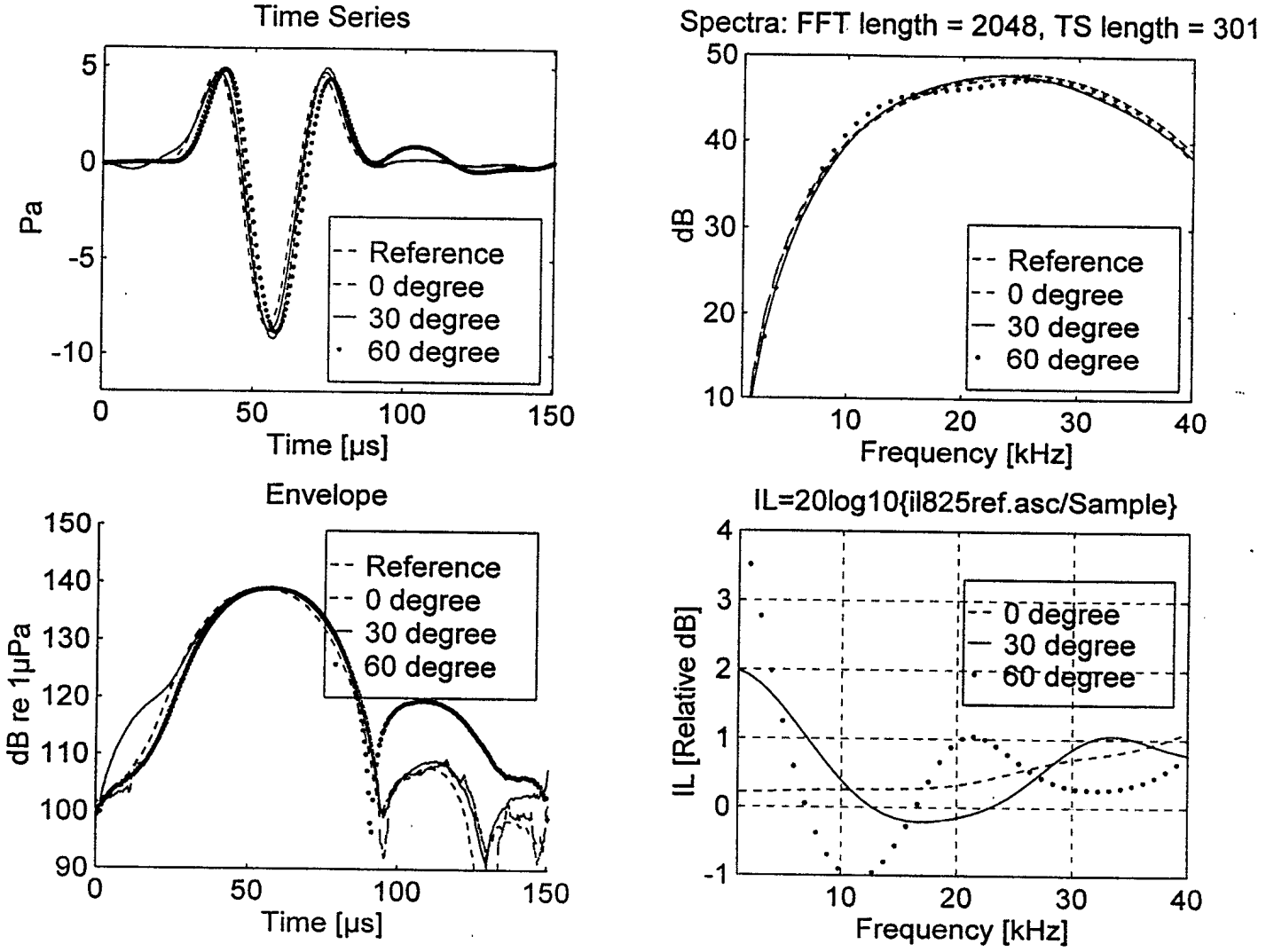

Figure 23. Insertion loss versus angle of incidence for a 10 mm thick epoxy-based 4H Spectra Fiber composite panel

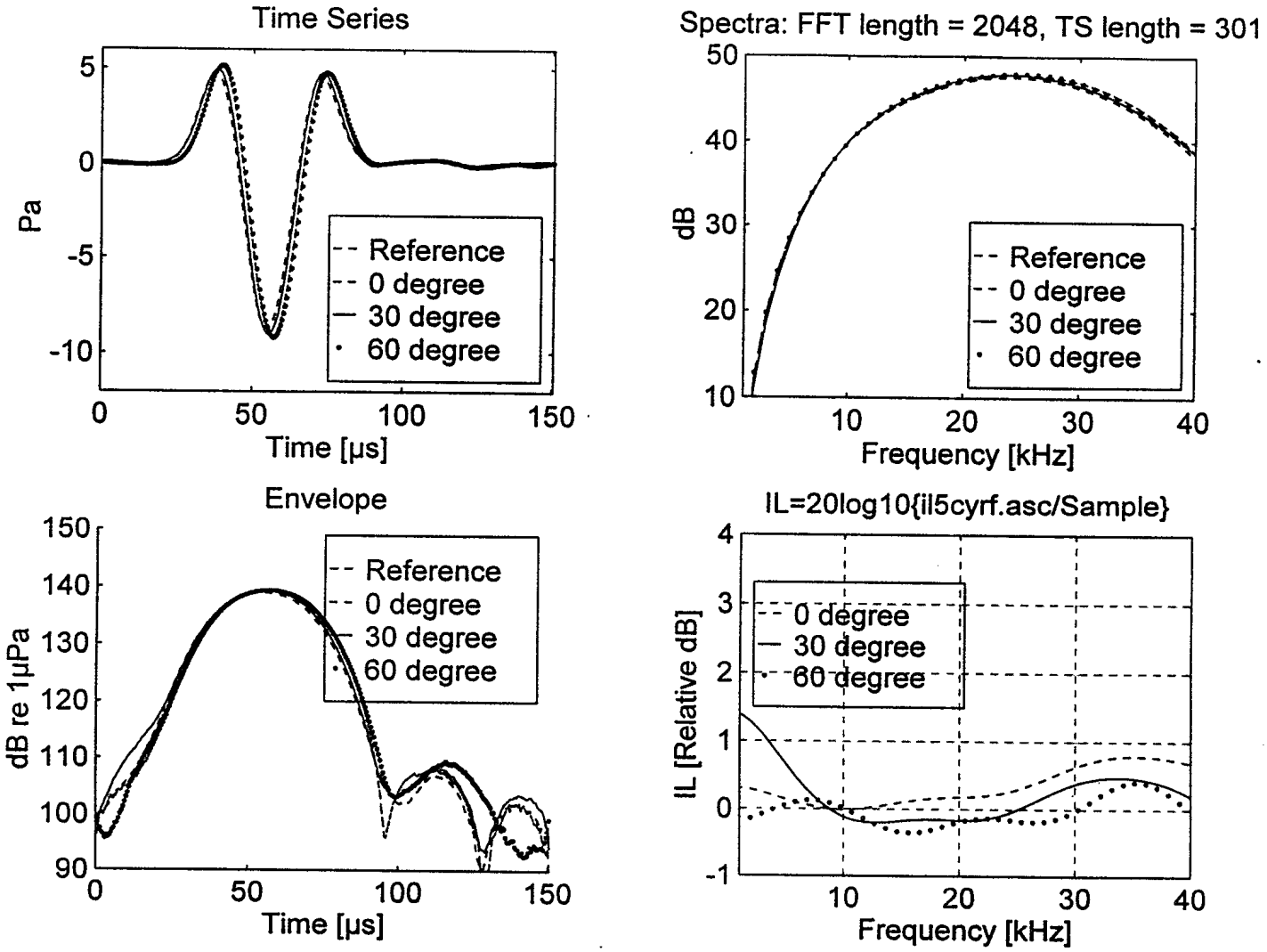

Figure 24. Insertion loss versus angle of incidence for a 10 mm thick cyanate-based 8H Spectra Fiber composite panel

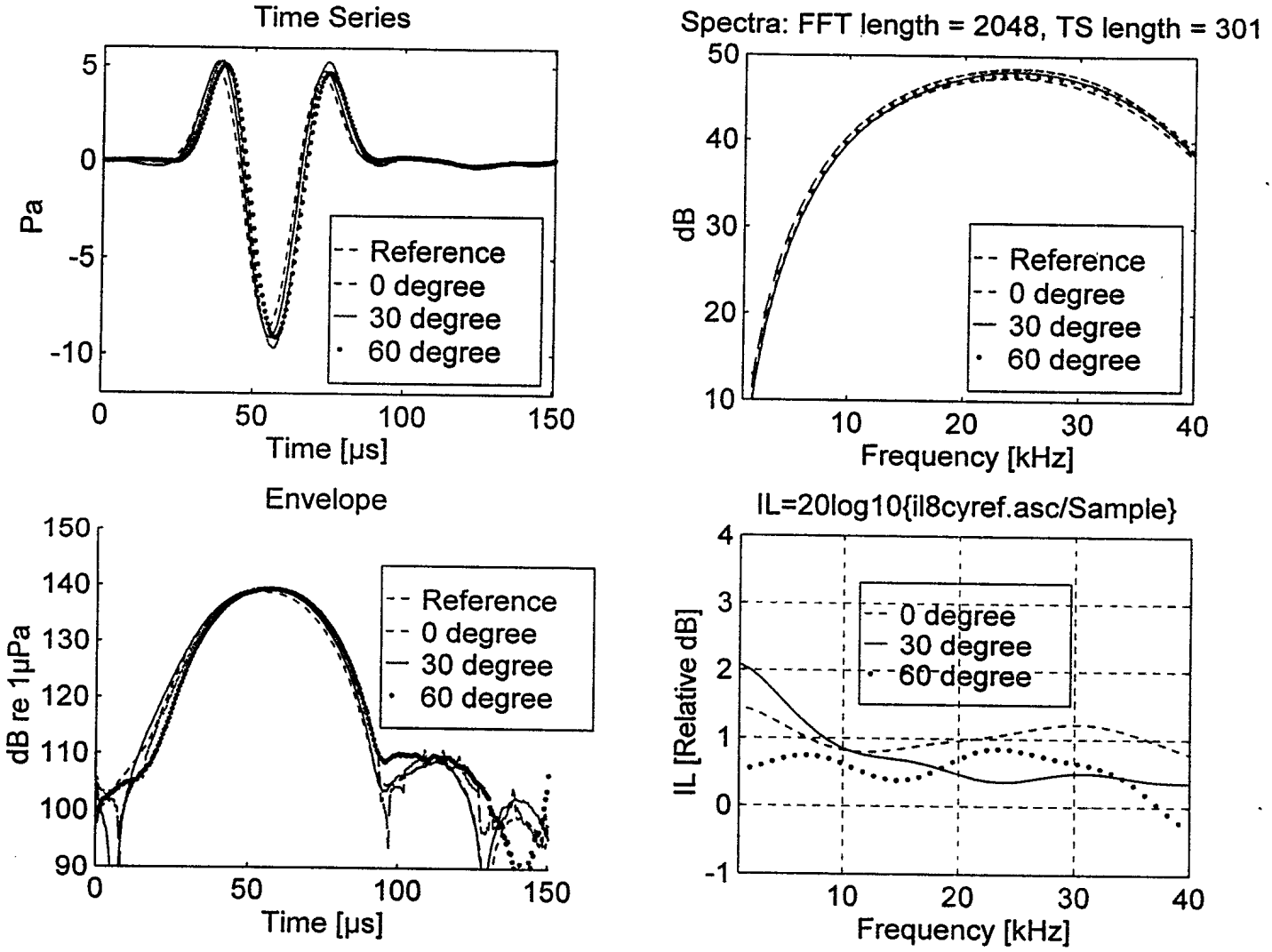

Figure 25. Insertion loss versus angle of incidence for a 10 mm thick cyanate-based 4H Spectra Fiber composite panel

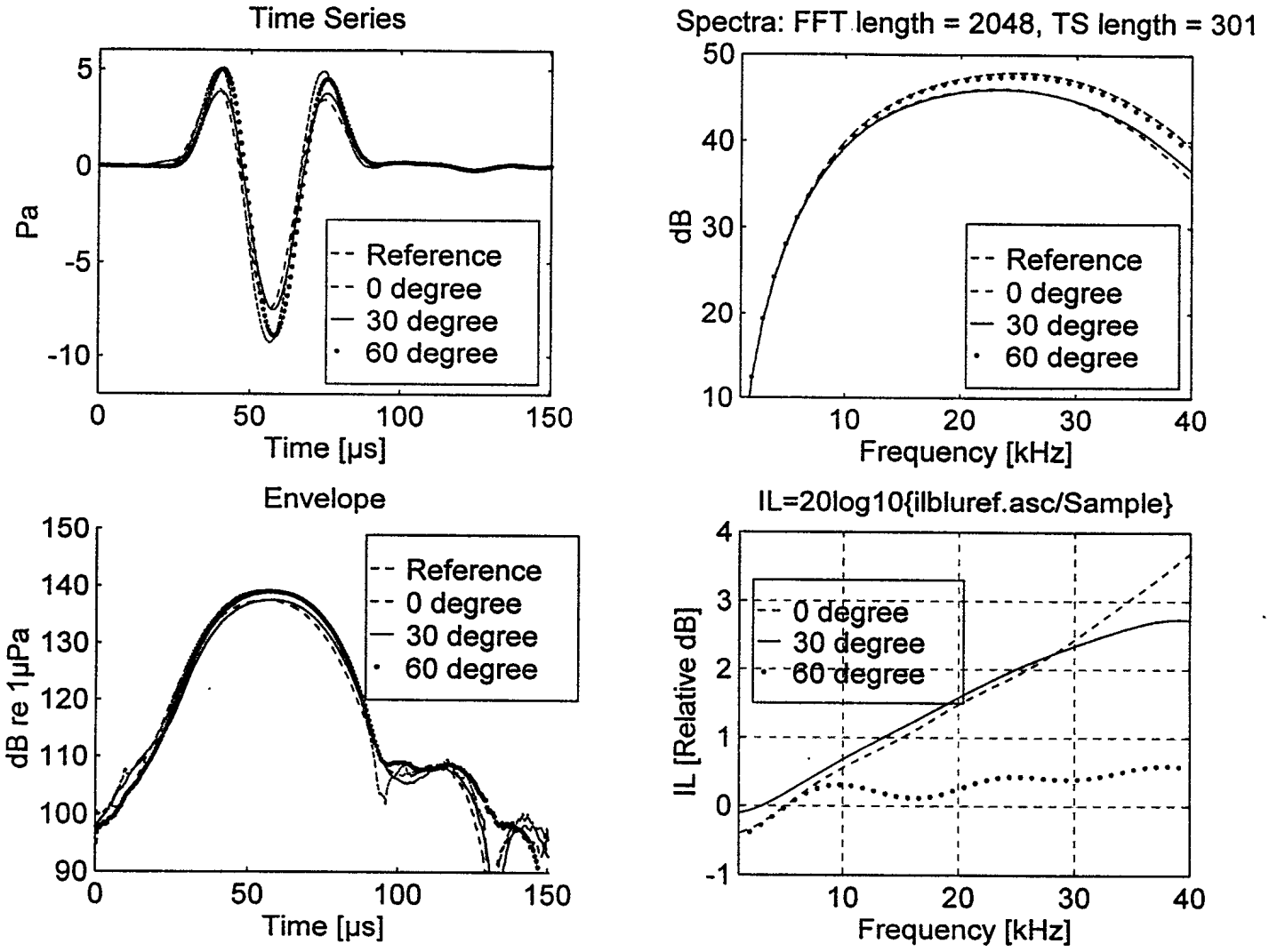

Figure 26. Insertion loss versus angle of incidence for a 10 mm thick epoxy-based 8H GRP panel

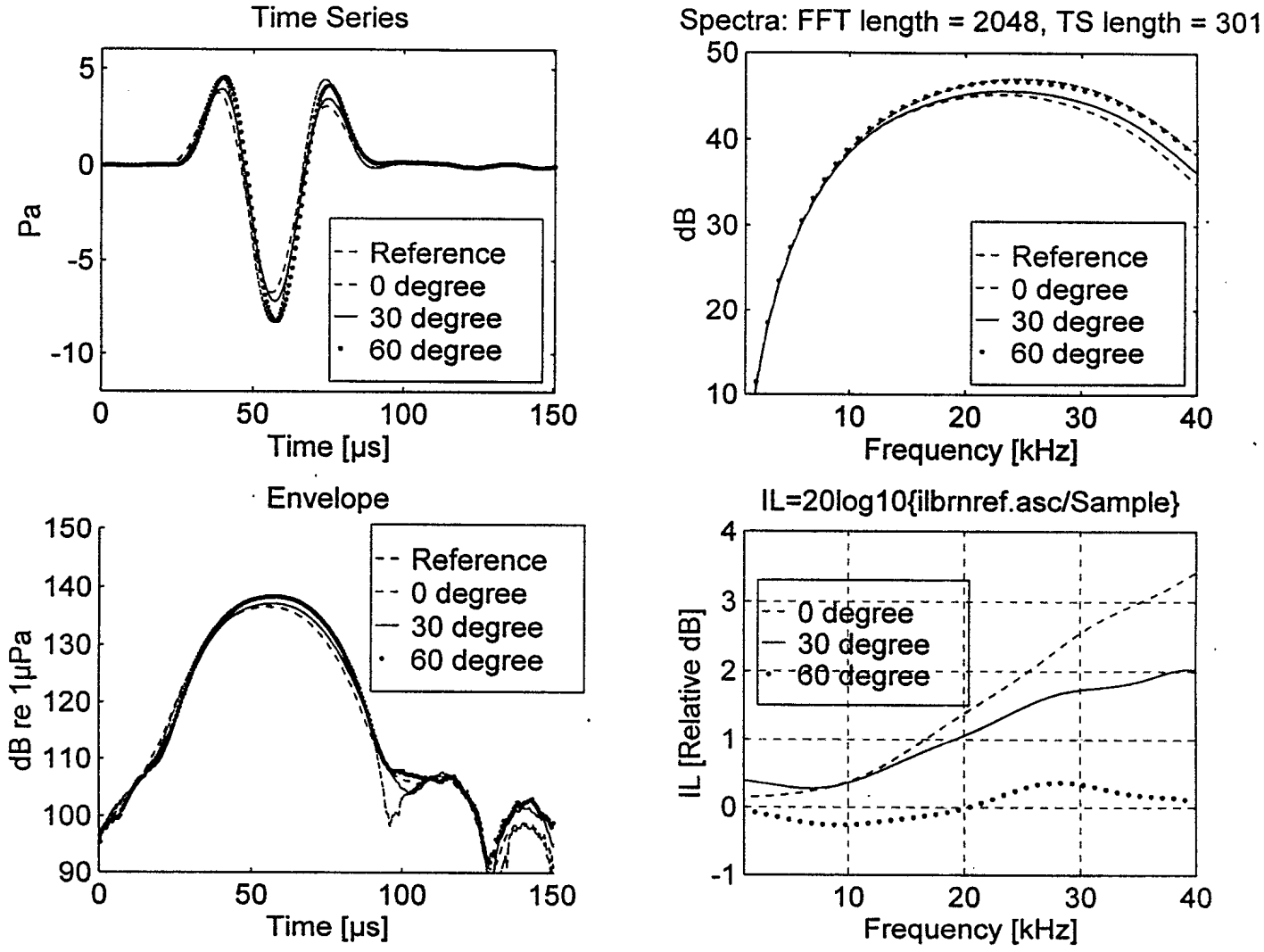

Figure 27. Insertion loss versus angle of incidence for a 10 mm thick cyanate-based 8H GRP panel

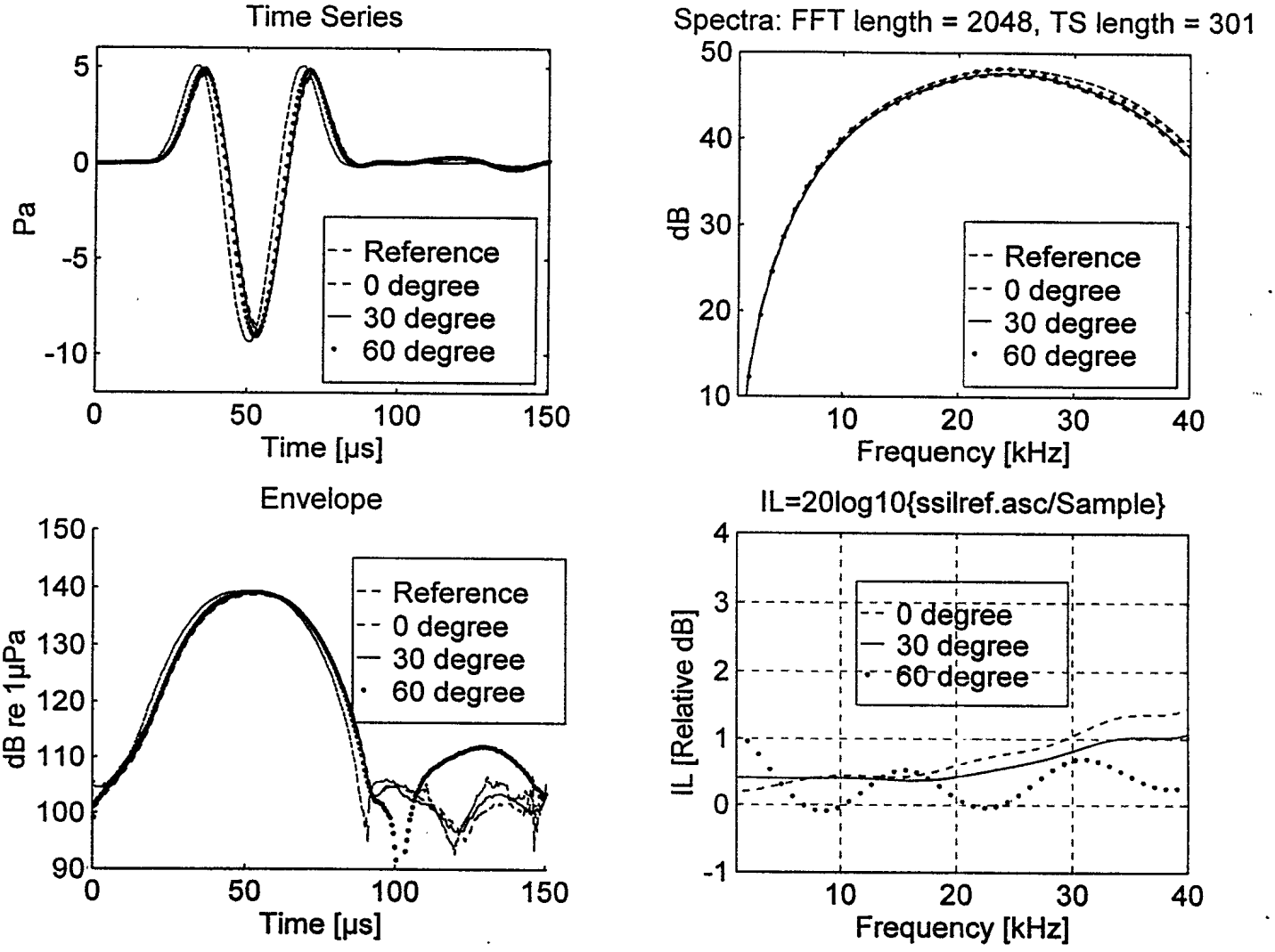

Figure 28. Insertion loss versus angle of incidence for a 20 gauge stainless steel plate

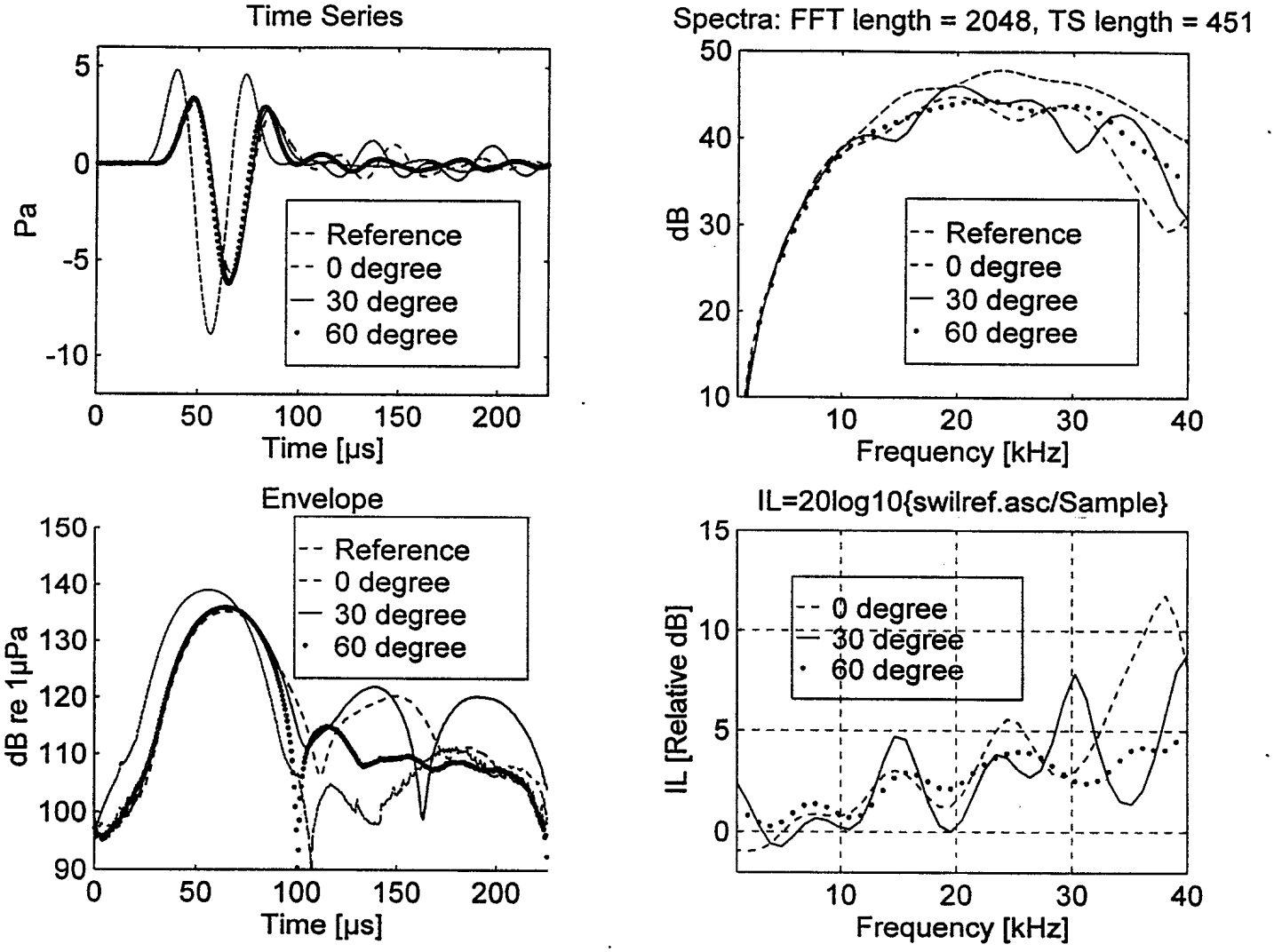

Figure 29. Insertion loss versus angle of incidence for a 60 mm thick double wall stainless steel sonar window

SELF NOISE EVALUATION
OF
AN EPOXY-BASED 8H SPECTRA FIBER COMPOSITE PANEL

Figure 30. Frequency response function and phase of an epoxy-based 8H Spectra Fiber composite panel 61

Figure 31. Pressure, force and radiation measurements of an epoxy-based 8H Spectra Fiber composite panel under pseudo random mode 62

Figure 32. Pressure, force and radiation measurements of an epoxy-based 8H Spectra Fiber composite panel under free run mode 63

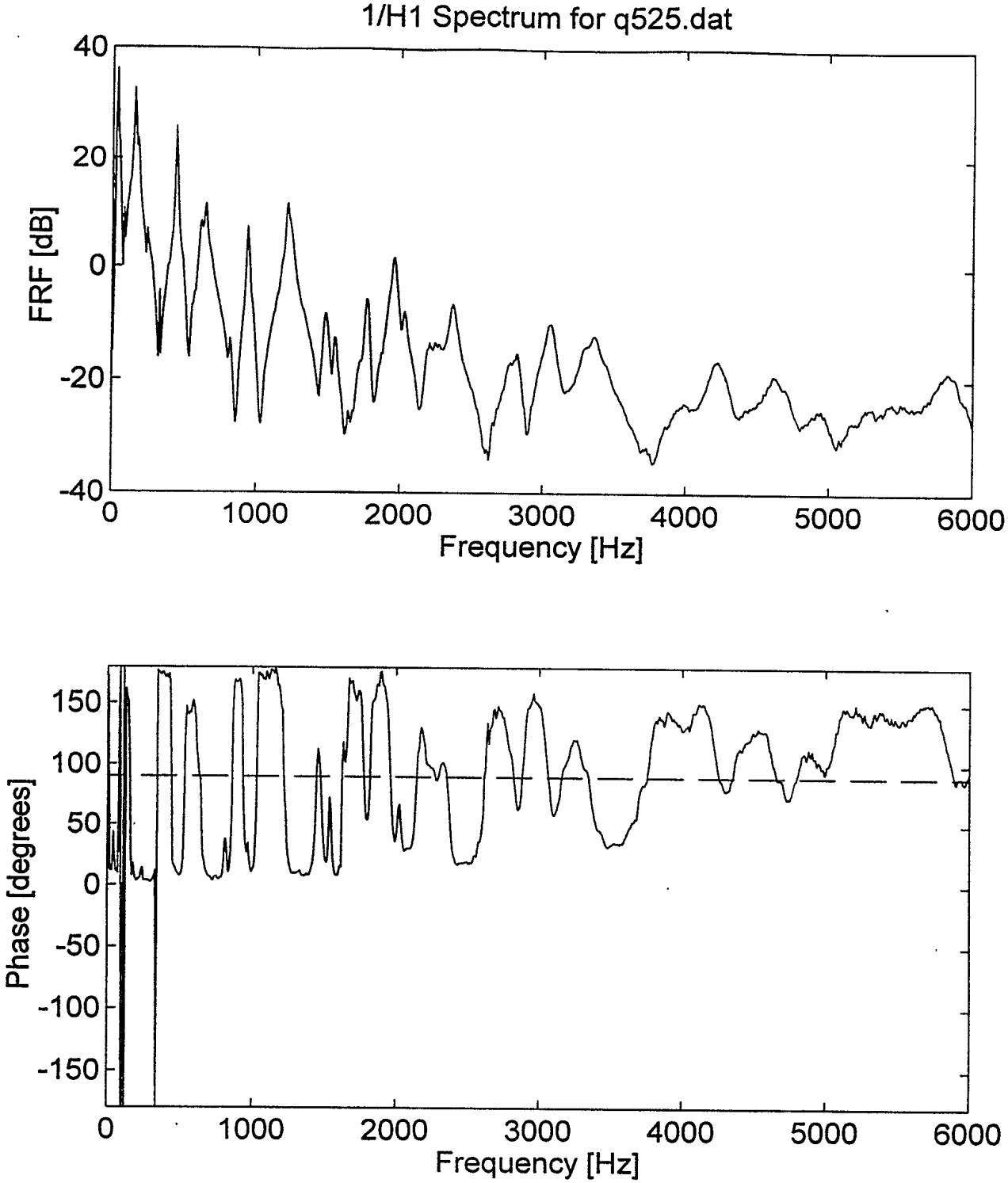

Figure 30. Frequency response function and phase of an epoxy-based 8H Spectra Fiber composite panel

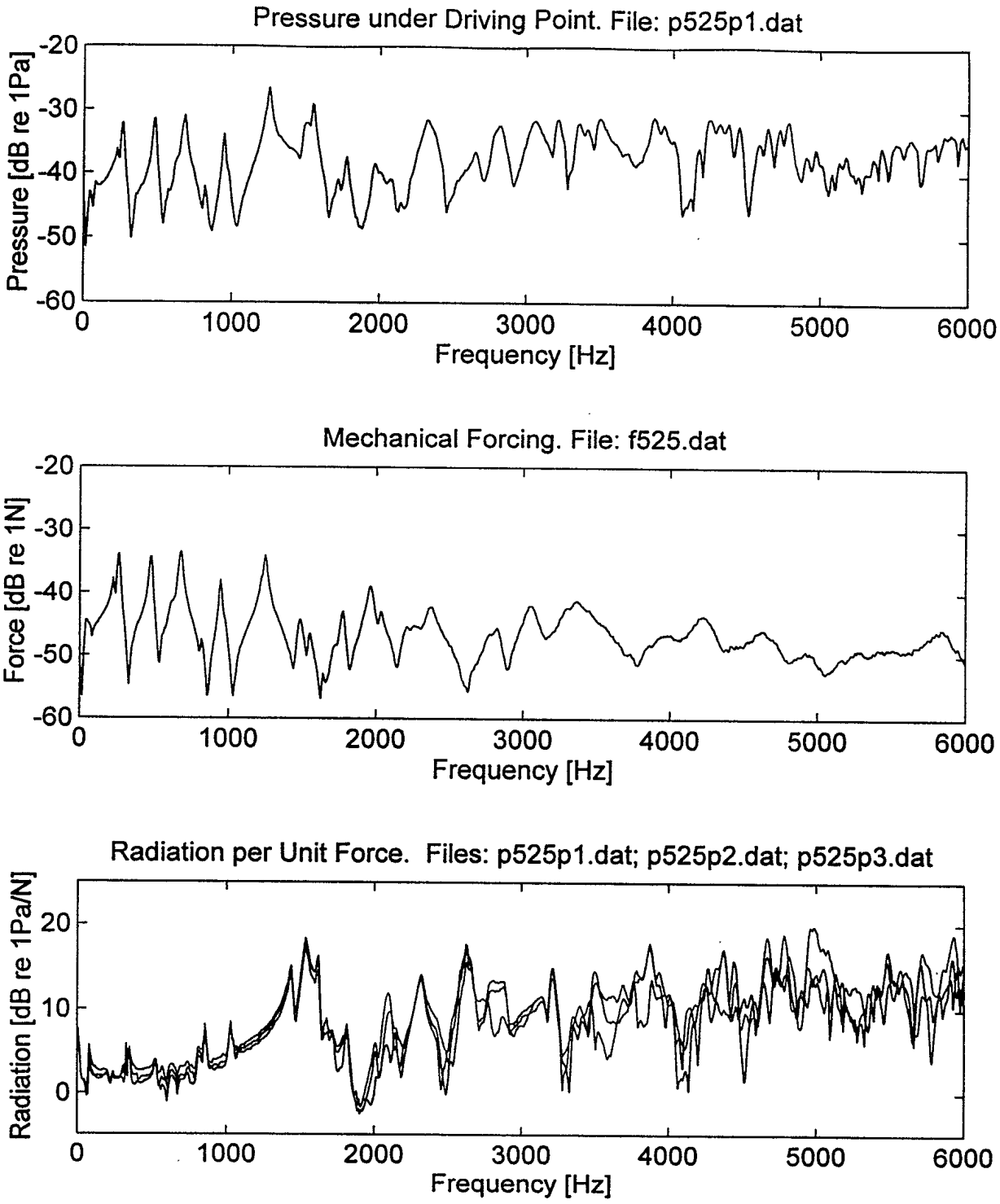

Figure 31. Pressure, force and radiation measurements of an epoxy-based 8H Spectra Fiber composite panel under pseudo random mode

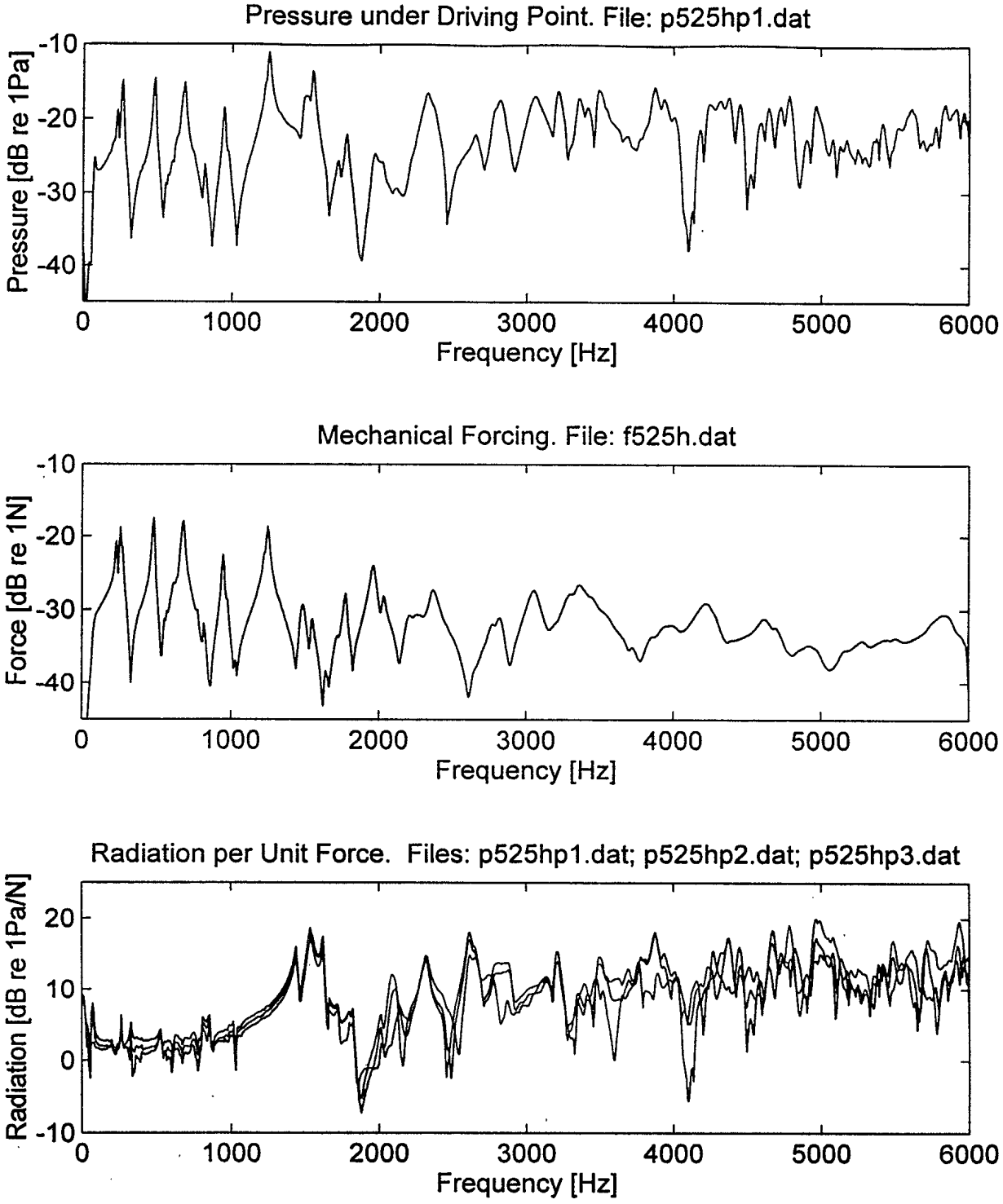

Figure 32. Pressure, force and radiation measurements of an epoxy-based 8H Spectra Fiber composite panel under free run mode

SELF NOISE EVALUATION
OF
AN EPOXY-BASED 4H SPECTRA FIBER COMPOSITE PANEL

Figure 33. Frequency response function and phase of an epoxy-based 4H Spectra Fiber composite panel 65

Figure 34. Pressure, force and radiation measurements of an epoxy-based 4H Spectra Fiber composite panel under pseudo random mode 66

Figure 35. Pressure, force and radiation measurements of an epoxy-based 4H Spectra Fiber composite panel under free run mode 67

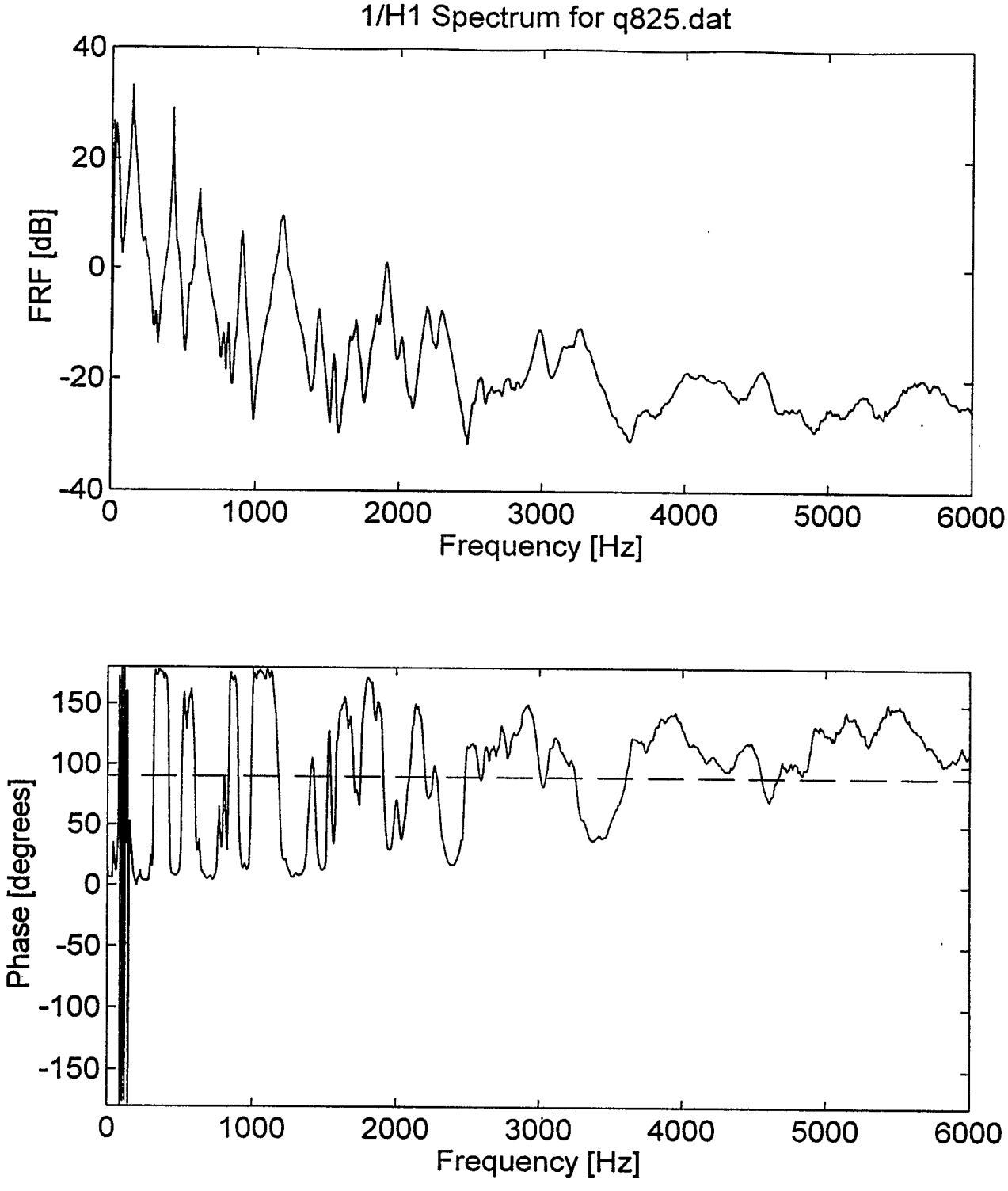

Figure 33. Frequency response function and phase of an epoxy-based 4H Spectra Fiber composite panel

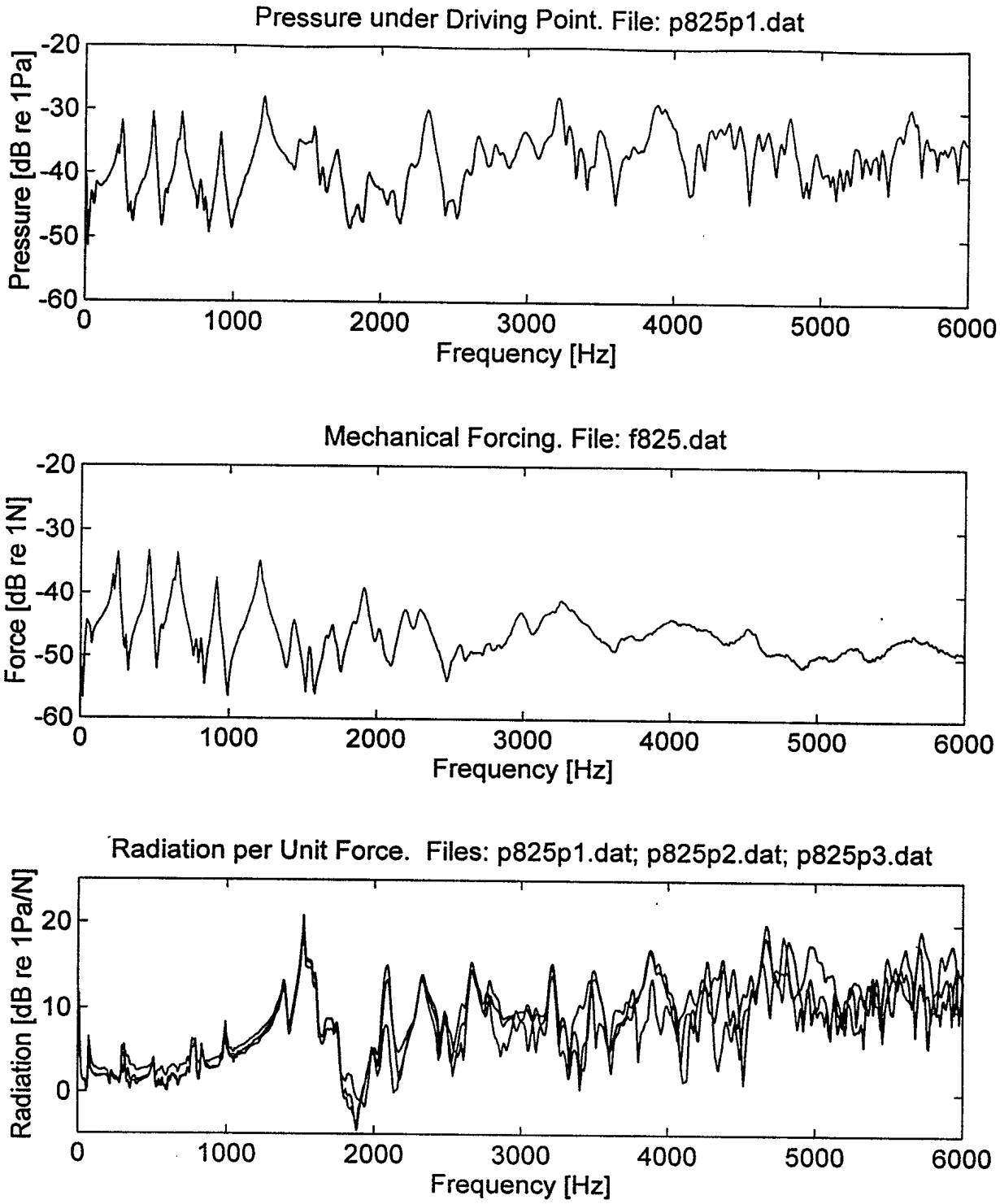

Figure 34. Pressure, force and radiation measurements of an epoxy-based 4H Spectra Fiber composite panel under pseudo random mode

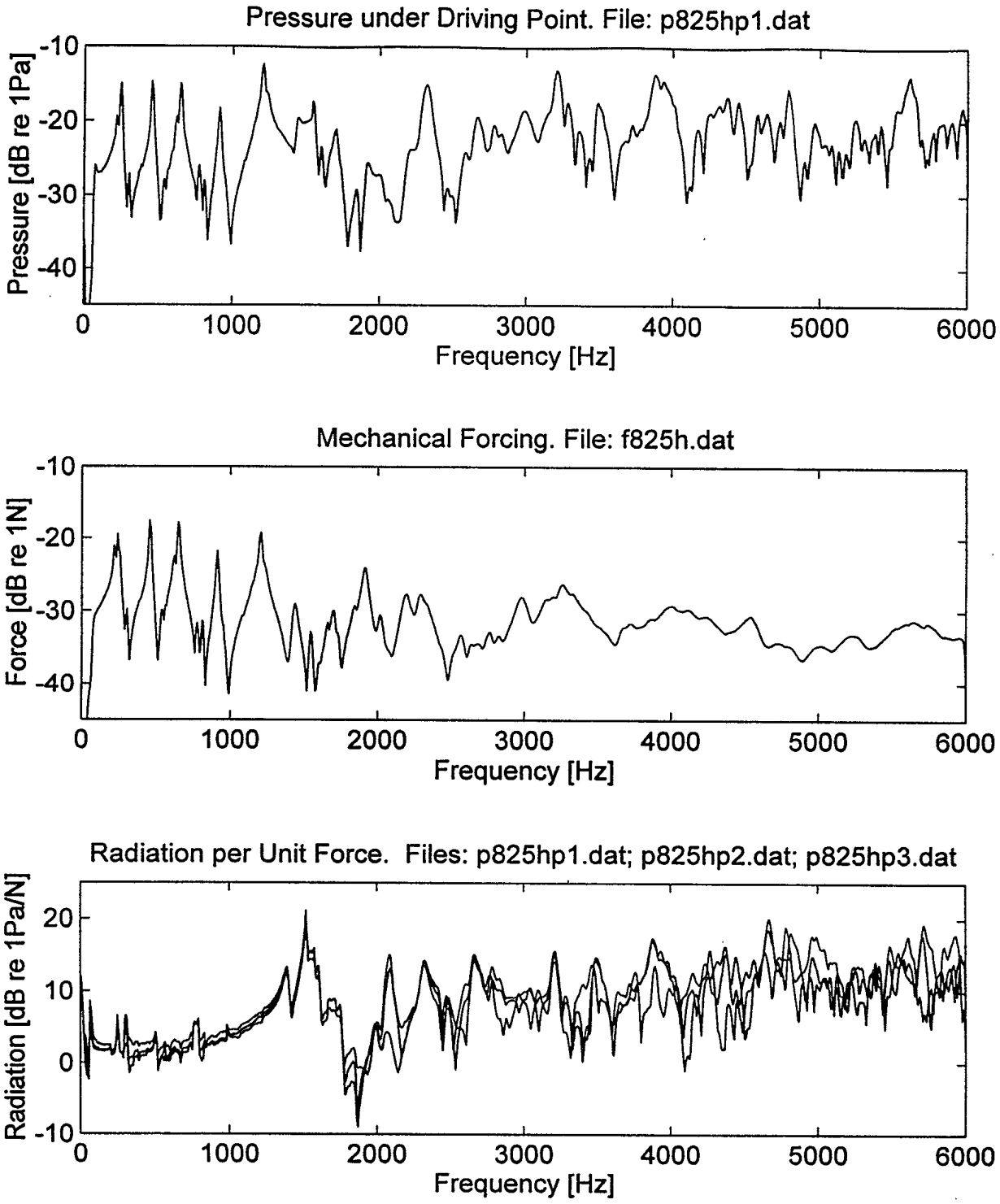

Figure 35. Pressure, force and radiation measurements of an epoxy-based 4H Spectra Fiber composite panel under free run mode

SELF NOISE EVALUATION
OF
A CYANATE-BASED 8H SPECTRA FIBER COMPOSITE PANEL

Figure 36. Frequency response function and phase of a cyanate-based 8H Spectra Fiber composite panel 69

Figure 37. Pressure, force and radiation measurements of a cyanate-based 8H Spectra Fiber composite panel under pseudo random mode 70

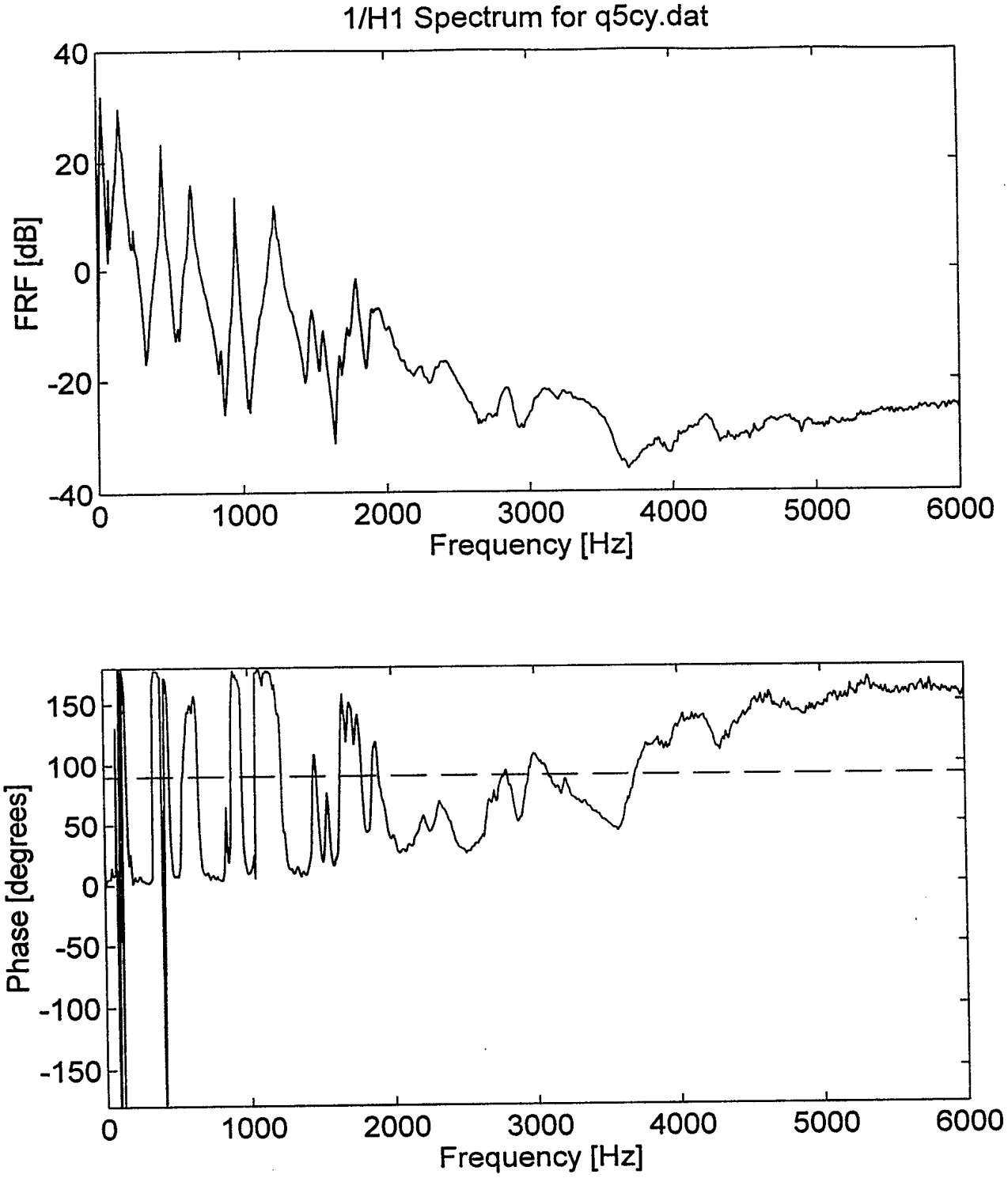

Figure 36. Frequency response function and phase of a cyanate-based 8H Spectra Fiber composite panel

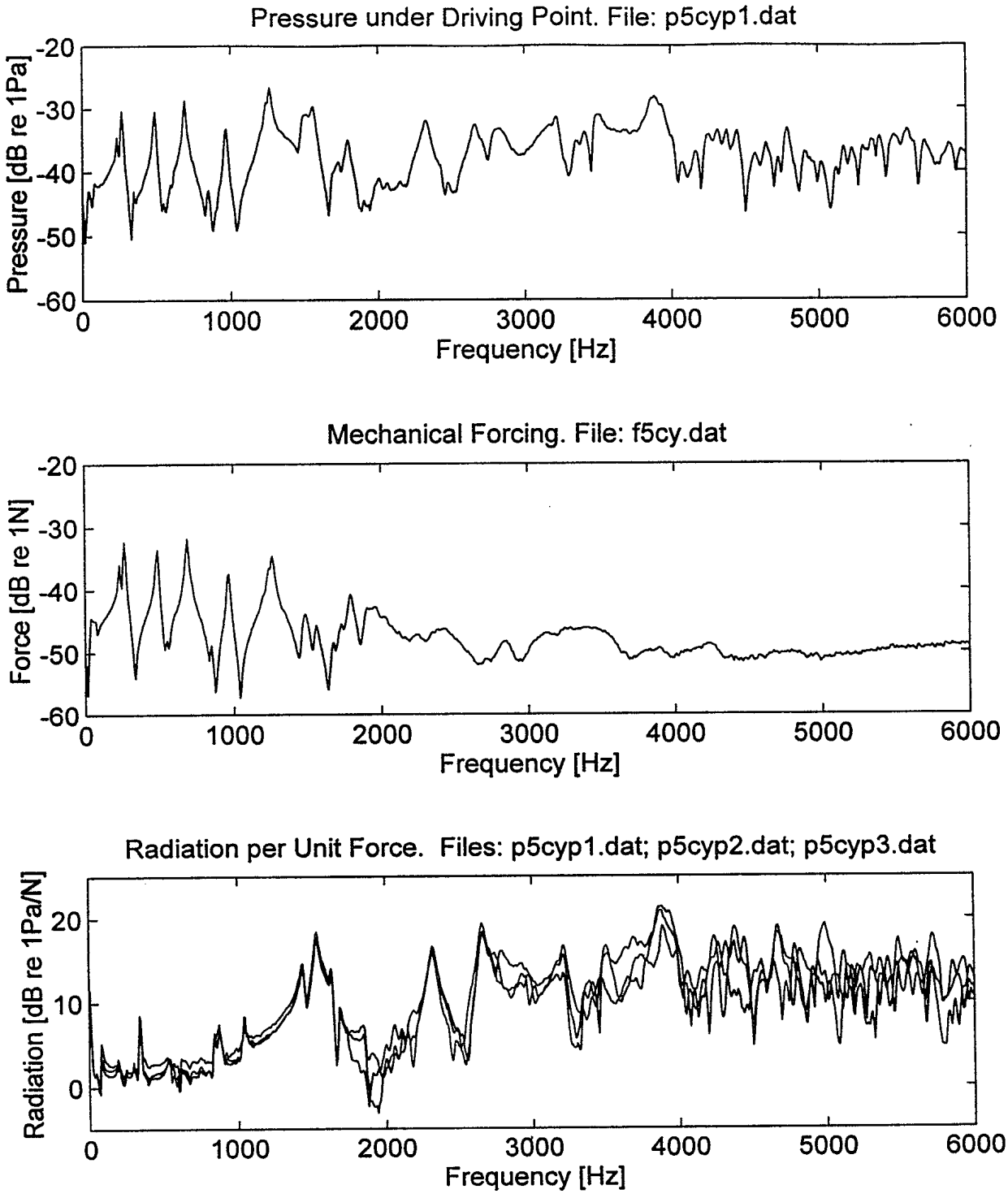

Figure 37. Pressure, force and radiation measurements of a cyanate-based 8H Spectra Fiber composite panel under pseudo random mode

SELF NOISE EVALUATION OF A CYANATE-BASED 4H SPECTRA FIBER COMPOSITE PANEL

Figure 38. Frequency response function and phase of a cyanate-based 4H Spectra Fiber composite panel 72

Figure 39. Pressure, force and radiation measurements of a cyanate-based 4H Spectra Fiber composite panel under pseudo random mode 73

Figure 40. Pressure, force and radiation measurements of a cyanate-based 4H Spectra Fiber composite panel under free run mode 74

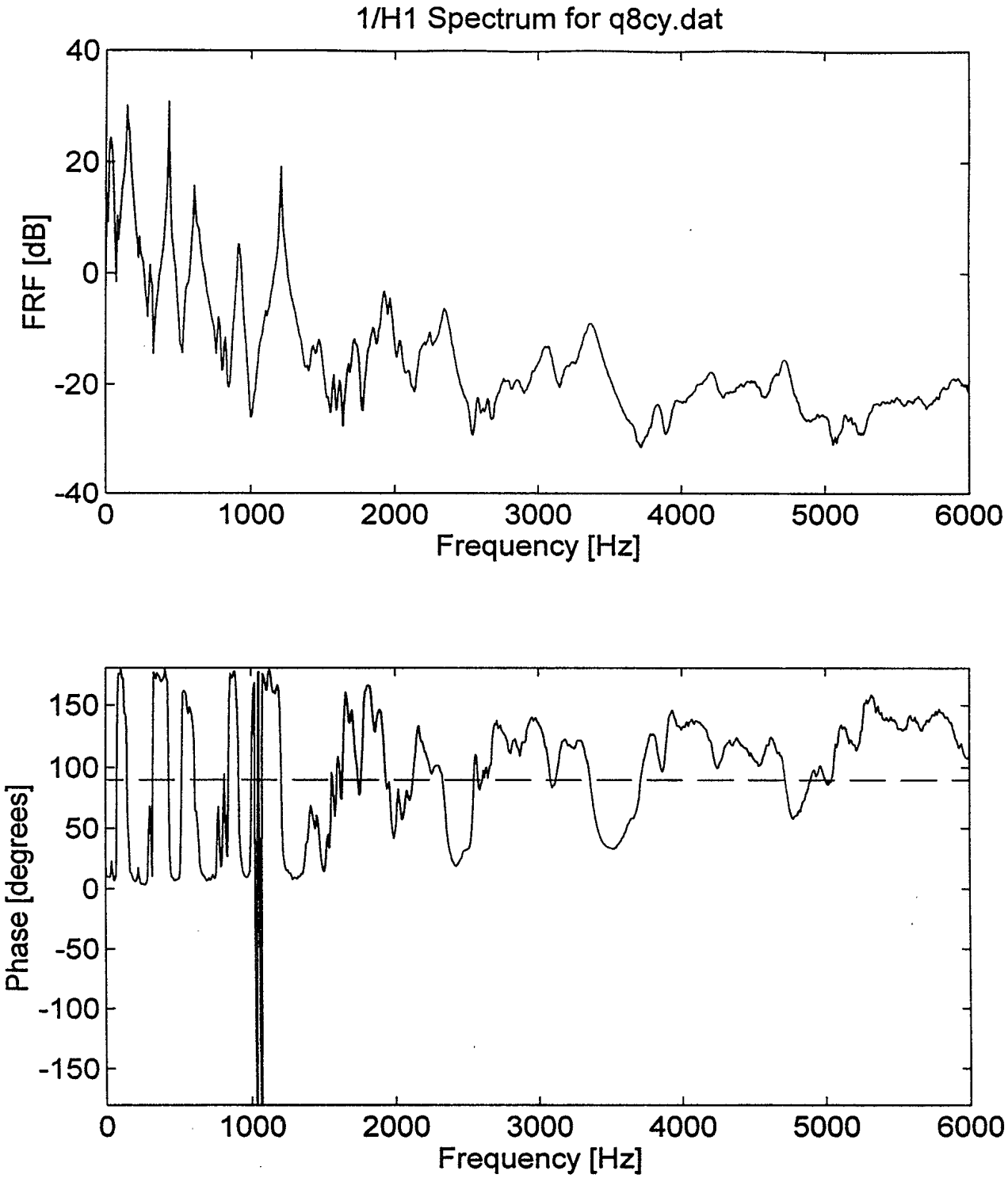

Figure 38. Frequency response function and phase of a cyanate-based 4H Spectra Fiber composite panel

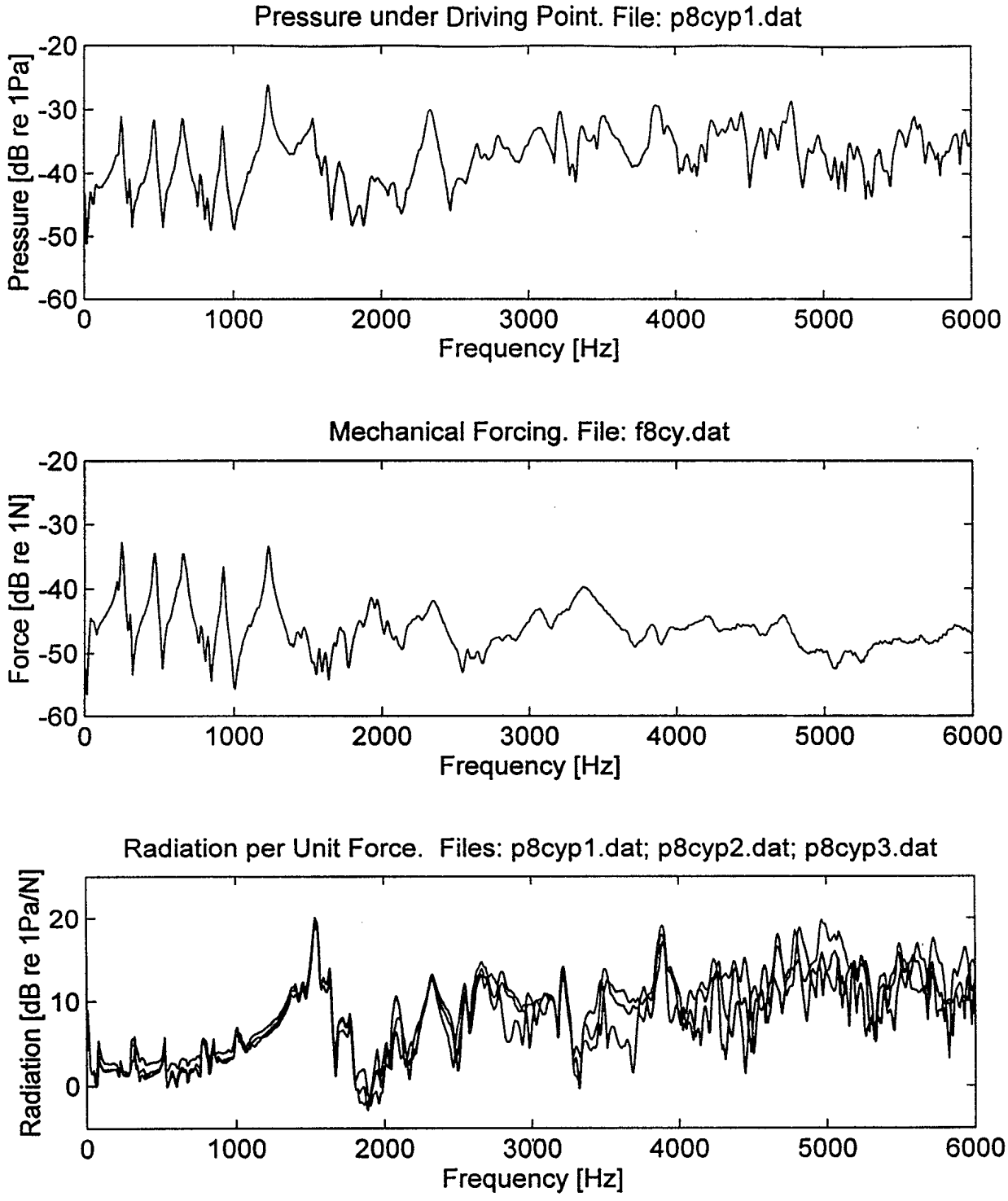

Figure 39. Pressure, force and radiation measurements of a cyanate-based 4H Spectra Fiber composite panel under pseudo random mode

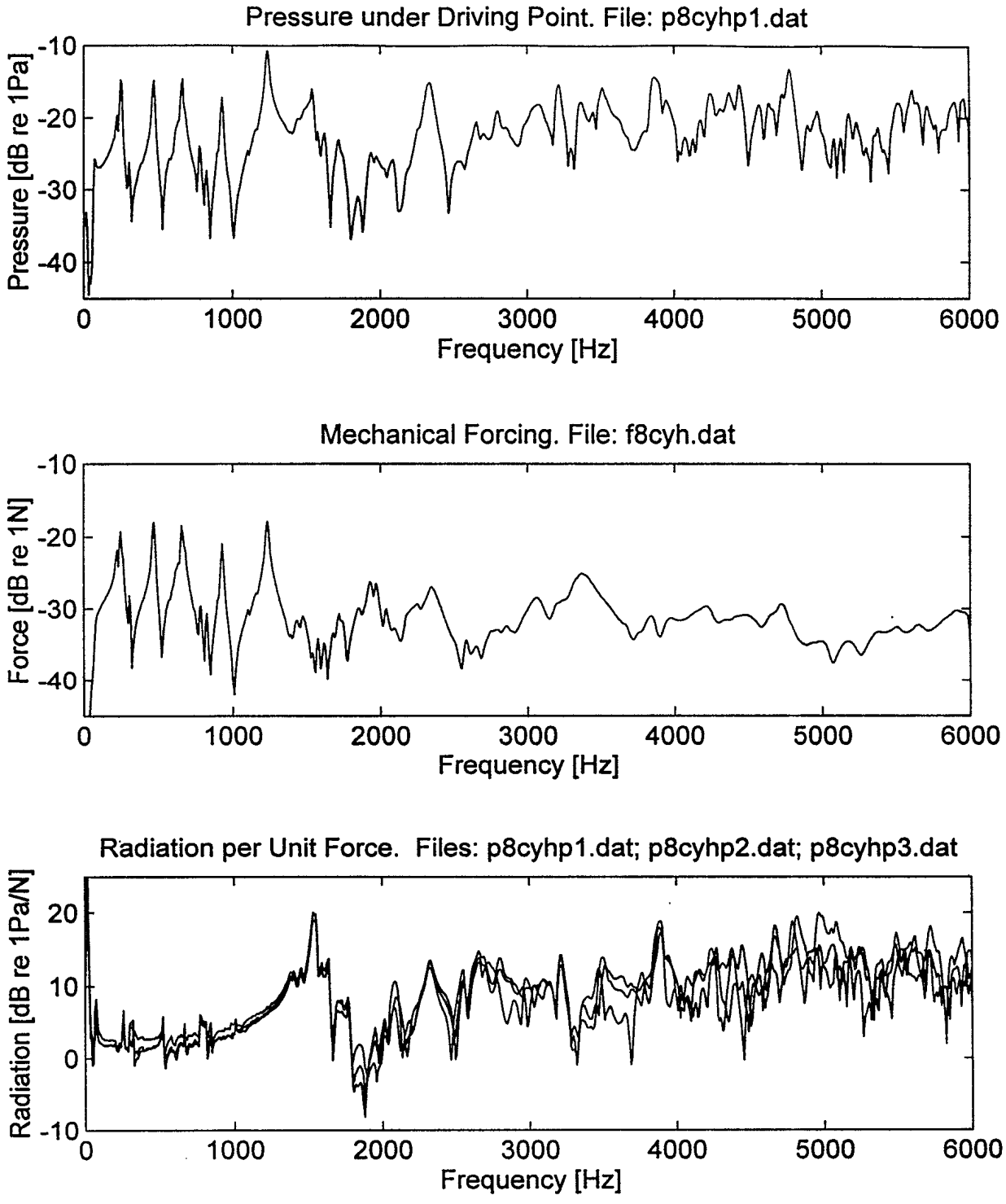

Figure 40. Pressure, force and radiation measurements of a cyanate-based 4H Spectra Fiber composite panel under free run mode

SELF NOISE EVALUATION OF AN EPOXY-BASED 8H GRP PANEL

Figure 41. Frequency response function and phase of an epoxy-based 8H GRP panel 76

Figure 42. Pressure, force and radiation measurements of an epoxy-based 8H GRP panel under pseudo random mode 77

Figure 43. Pressure, force and radiation measurements of an epoxy-based 8H GRP panel under free run mode 78

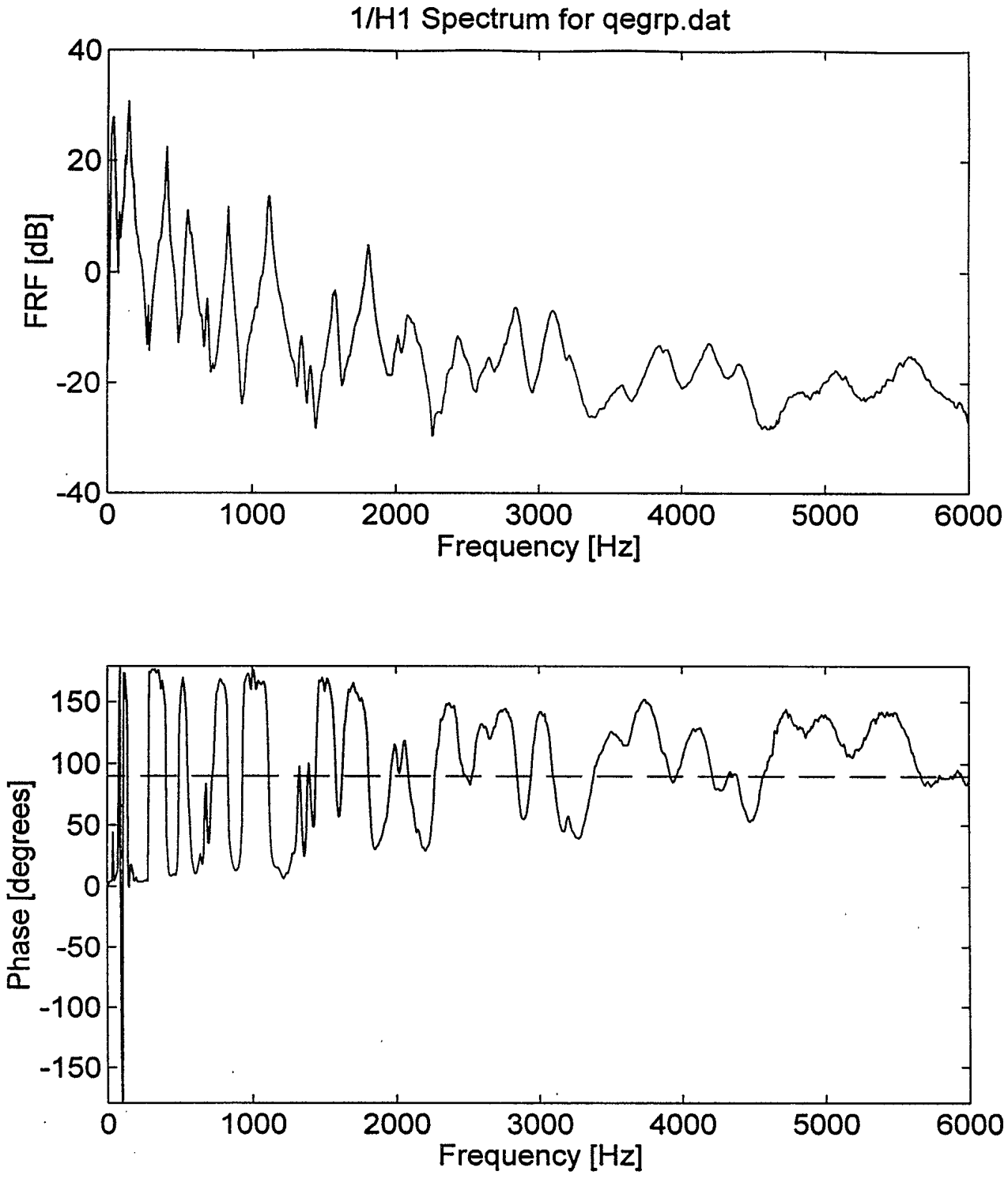

Figure 41. Frequency response function and phase of an epoxy-based 8H GRP panel

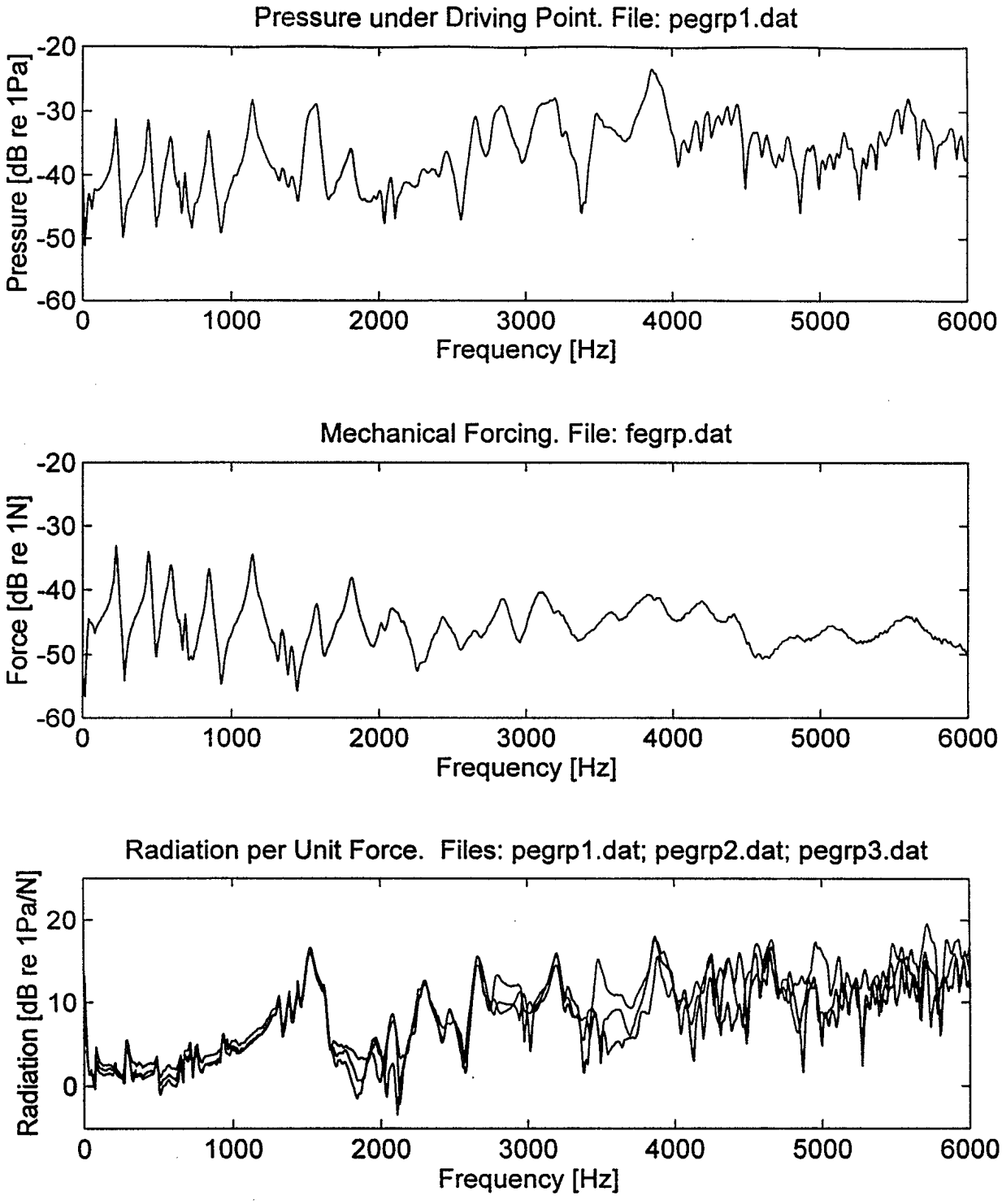

Figure 42. Pressure, force and radiation measurements of an epoxy-based 8H GRP panel under pseudo random mode

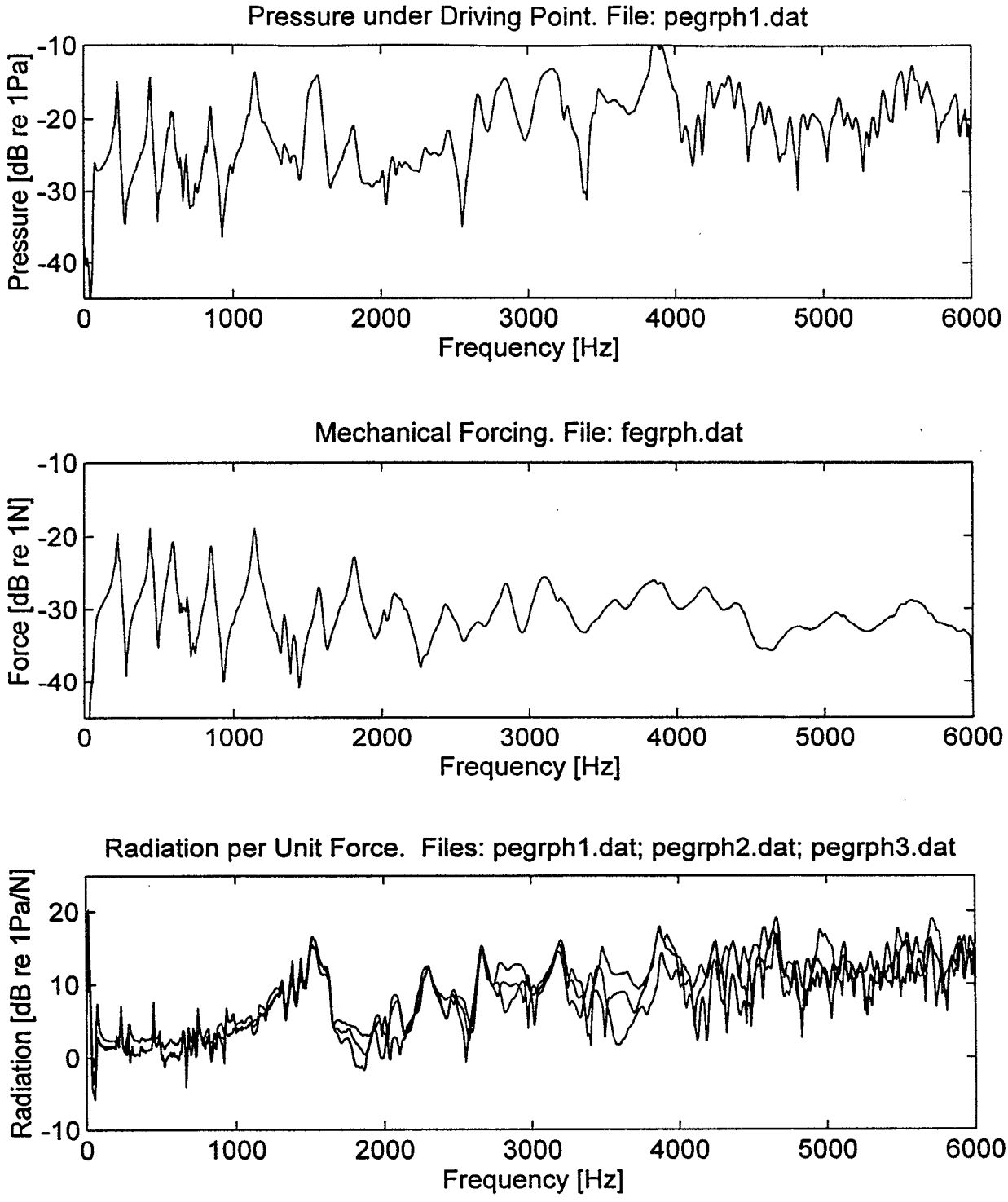

Figure 43. Pressure, force and radiation measurements of an epoxy-based 8H GRP panel under free run mode

SELF NOISE EVALUATION OF A CYANATE-BASED 8H GRP PANEL

Figure 44. Frequency response function and phase of a cyanate-based 8H GRP panel 80

Figure 45. Pressure, force and radiation measurements of a cyanate-based 8H GRP panel under pseudo random mode 81

Figure 46. Pressure, force and radiation measurements of a cyanate-based 8H GRP panel under free run mode 82

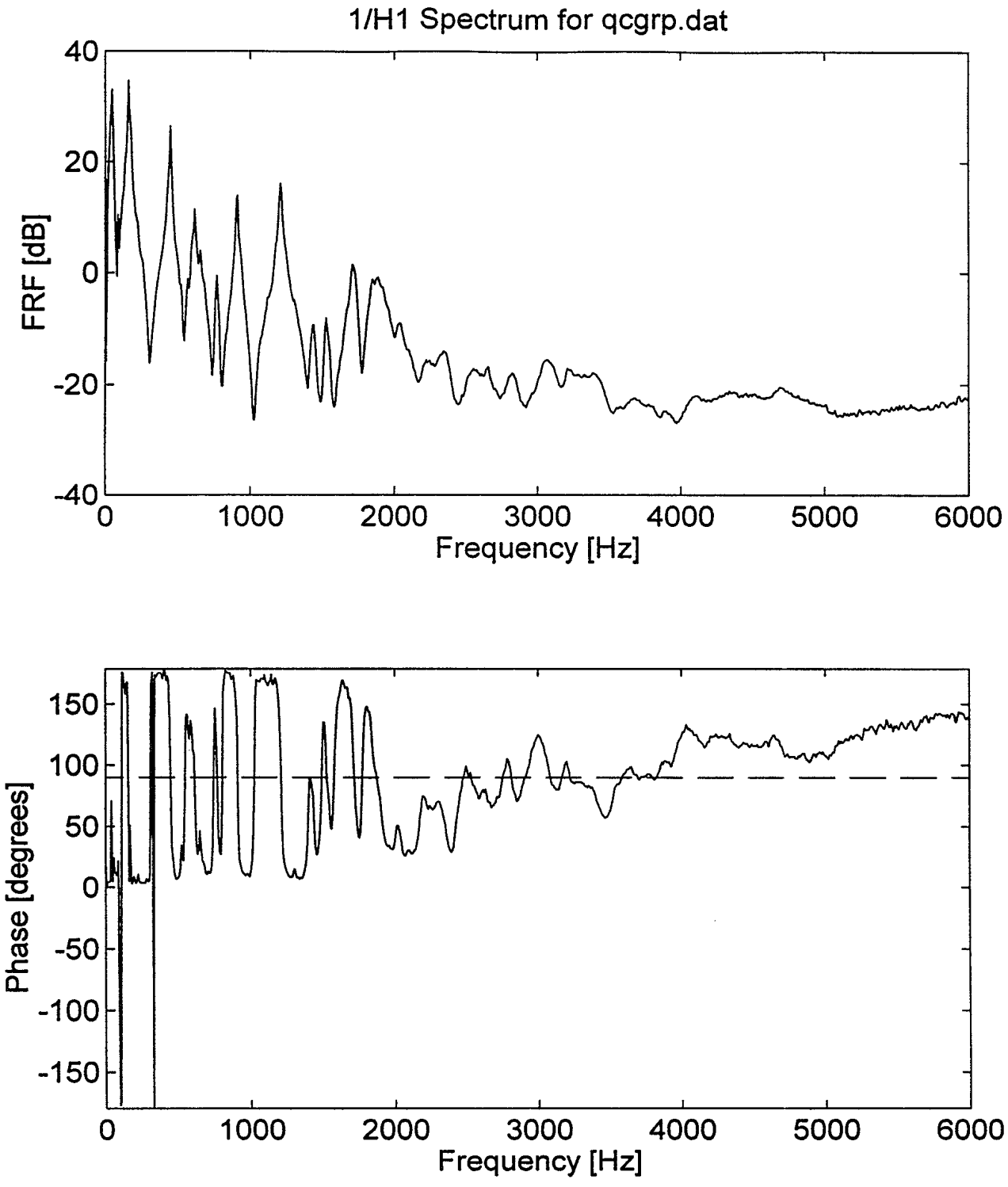

Figure 44. Frequency response function and phase of a cyanate-based 8H GRP panel

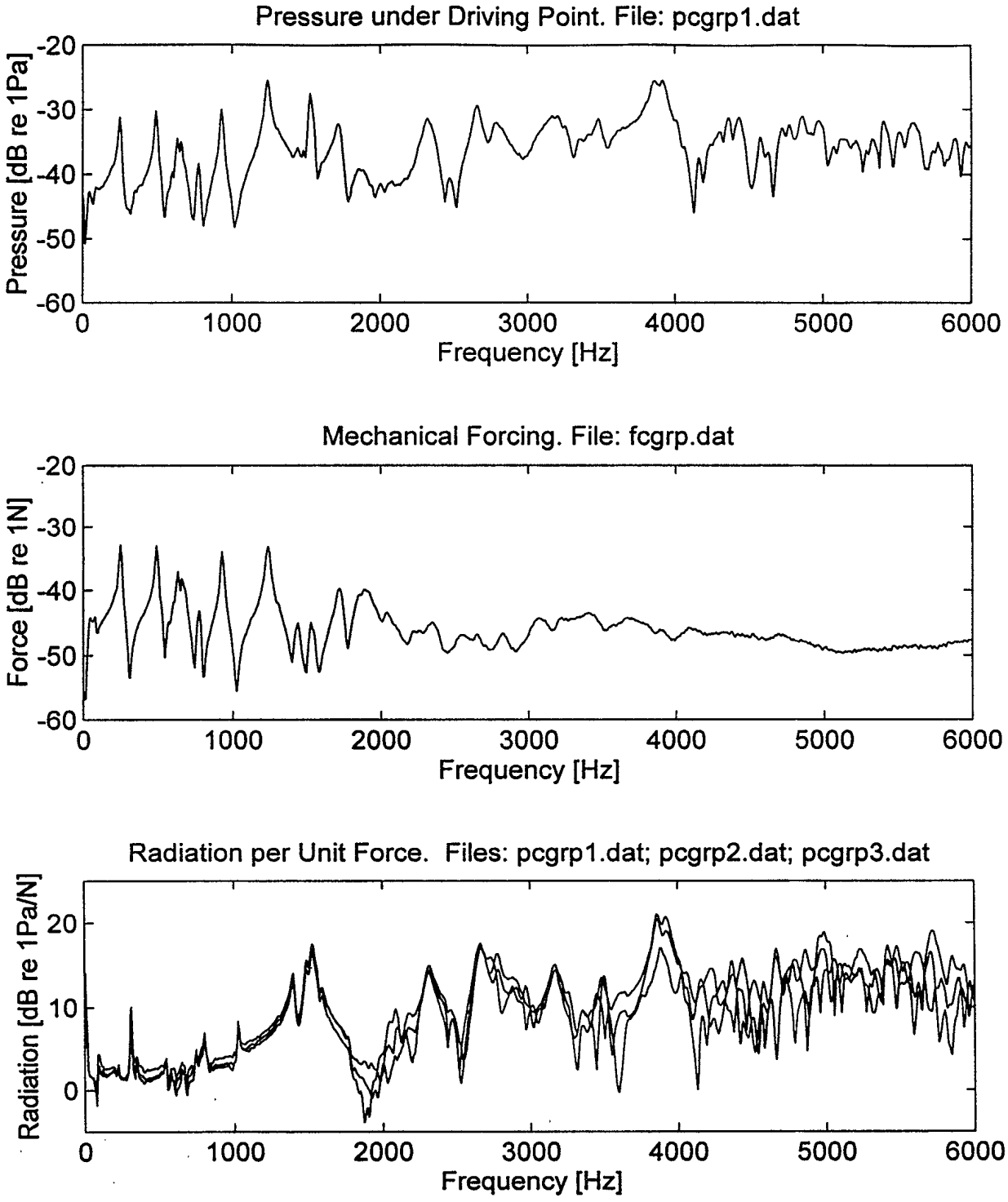

Figure 45. Pressure, force and radiation measurements of a cyanate-based 8H GRP panel under pseudo random mode

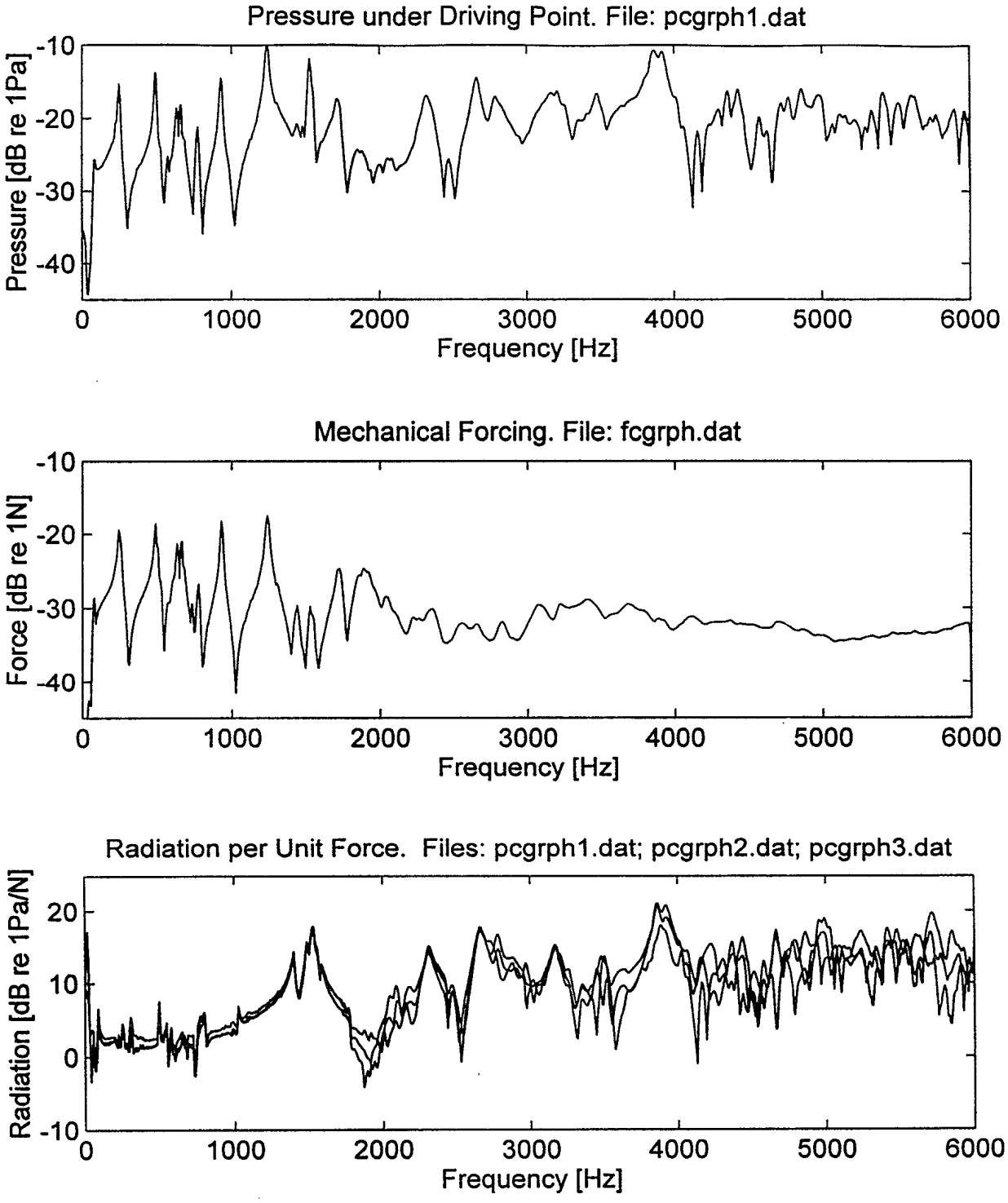

Figure 46. Pressure, force and radiation measurements of a cyanate-based 8H GRP panel under free run mode

SELF NOISE EVALUATION
OF
A DOUBLE WALL STAINLESS STEEL SONAR WINDOW

Figure 47. Frequency response function and phase of a double wall stainless steel sonar window with one wall immersed in water 84

Figure 48. Pressure, force and radiation measurements of a double wall stainless steel sonar window under pseudo random mode with one wall immersed in water 85

Figure 49. Pressure, force and radiation measurements of a double wall stainless steel sonar window under free run mode with one wall immersed in water . 86

Figure 50. Frequency response function and phase of a double wall stainless steel sonar window with two layers of walls immersed in water 87

Figure 51. Pressure, force and radiation measurements of a double wall stainless steel sonar window under pseudo random mode with two layers of walls immersed in water 88

Figure 52. Pressure, force and radiation measurements of a double wall stainless steel sonar window under free run mode with two layers of walls immersed in water 89

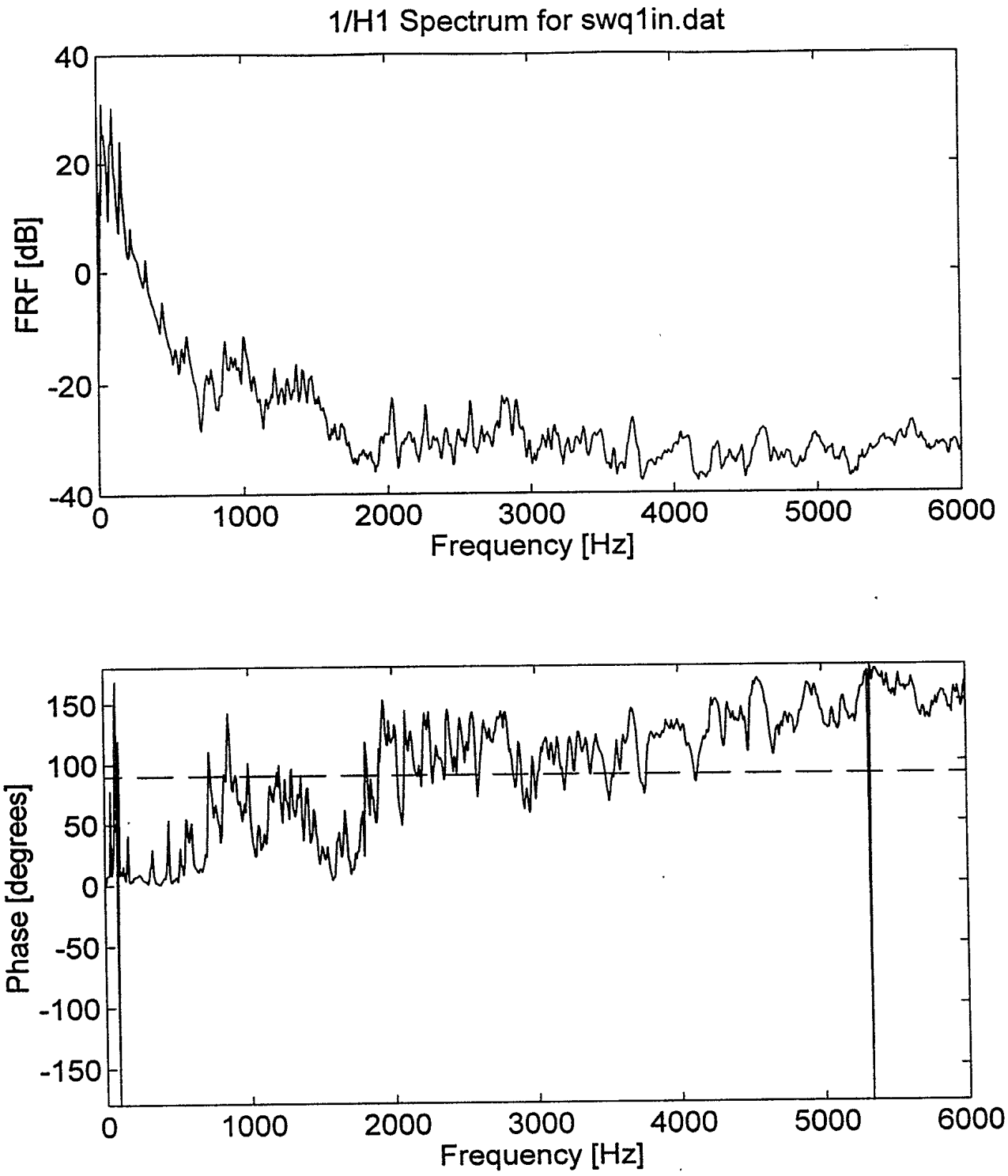

Figure 47. Frequency response function and phase of a double wall stainless steel sonar window with one wall immersed in water

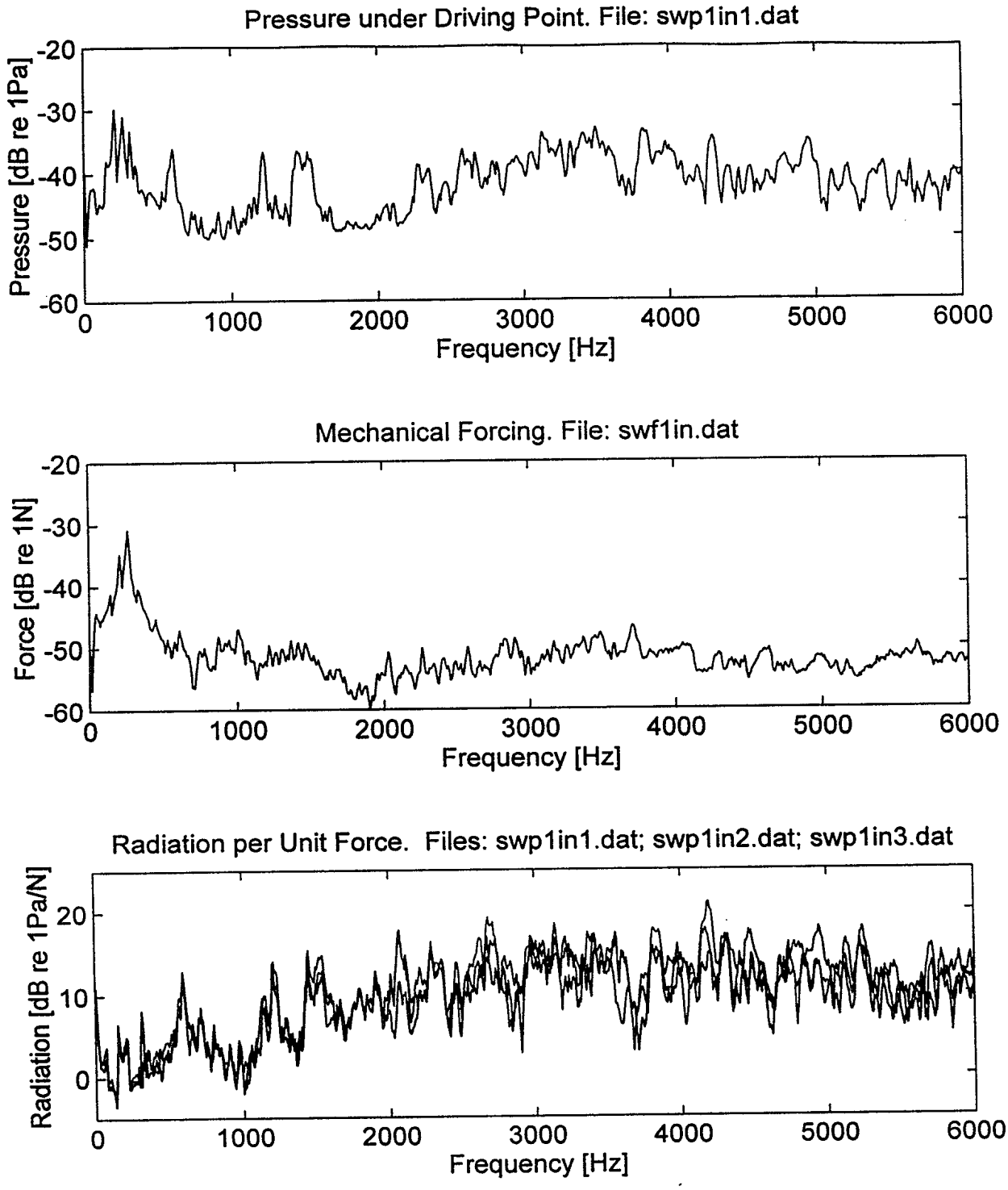

Figure 48. Pressure, force and radiation measurements of a double wall stainless steel sonar window under pseudo random mode with one wall immersed in water

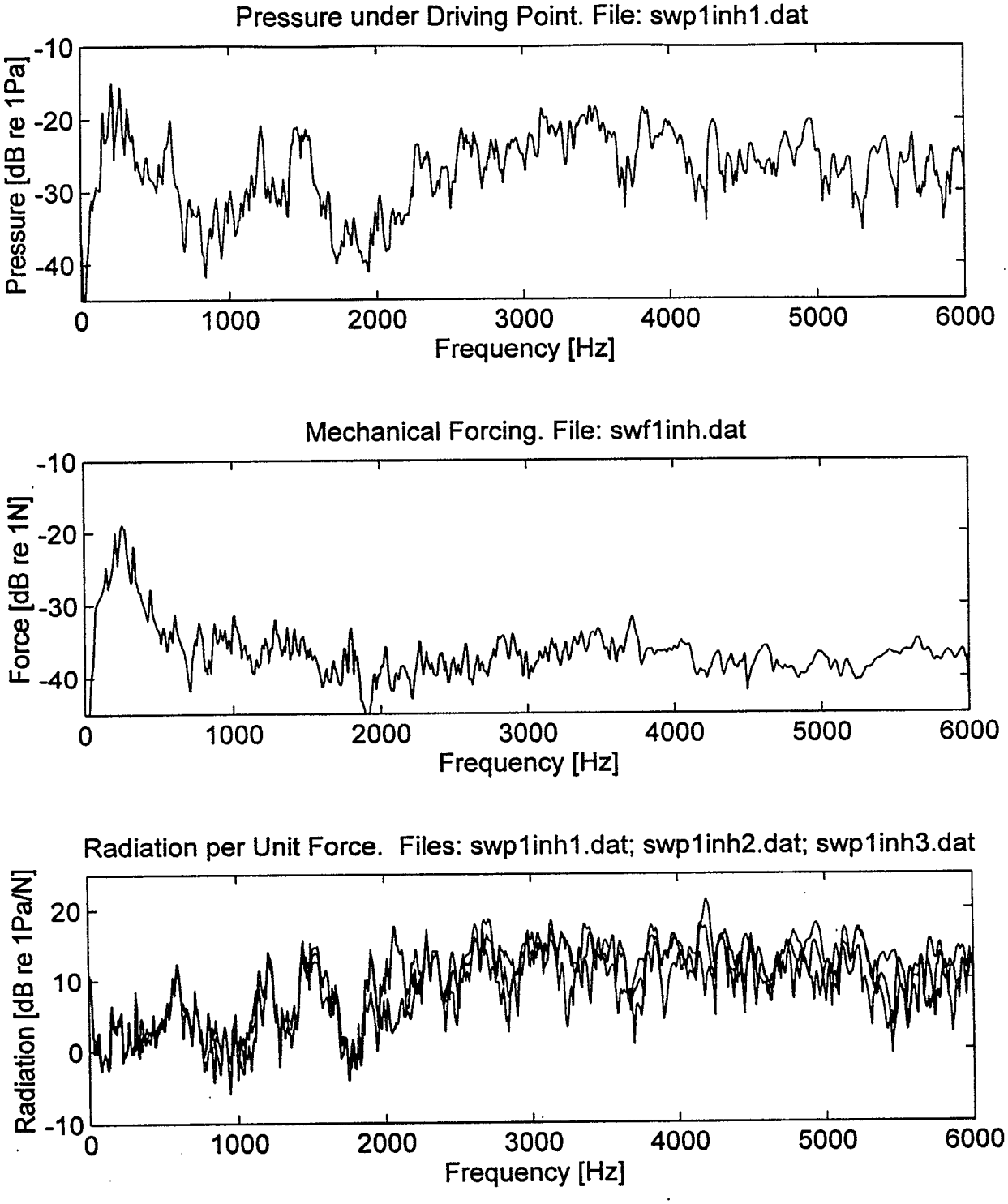

Figure 49. Pressure, force and radiation measurements of a double wall stainless steel sonar window under free run mode with one wall immersed in water

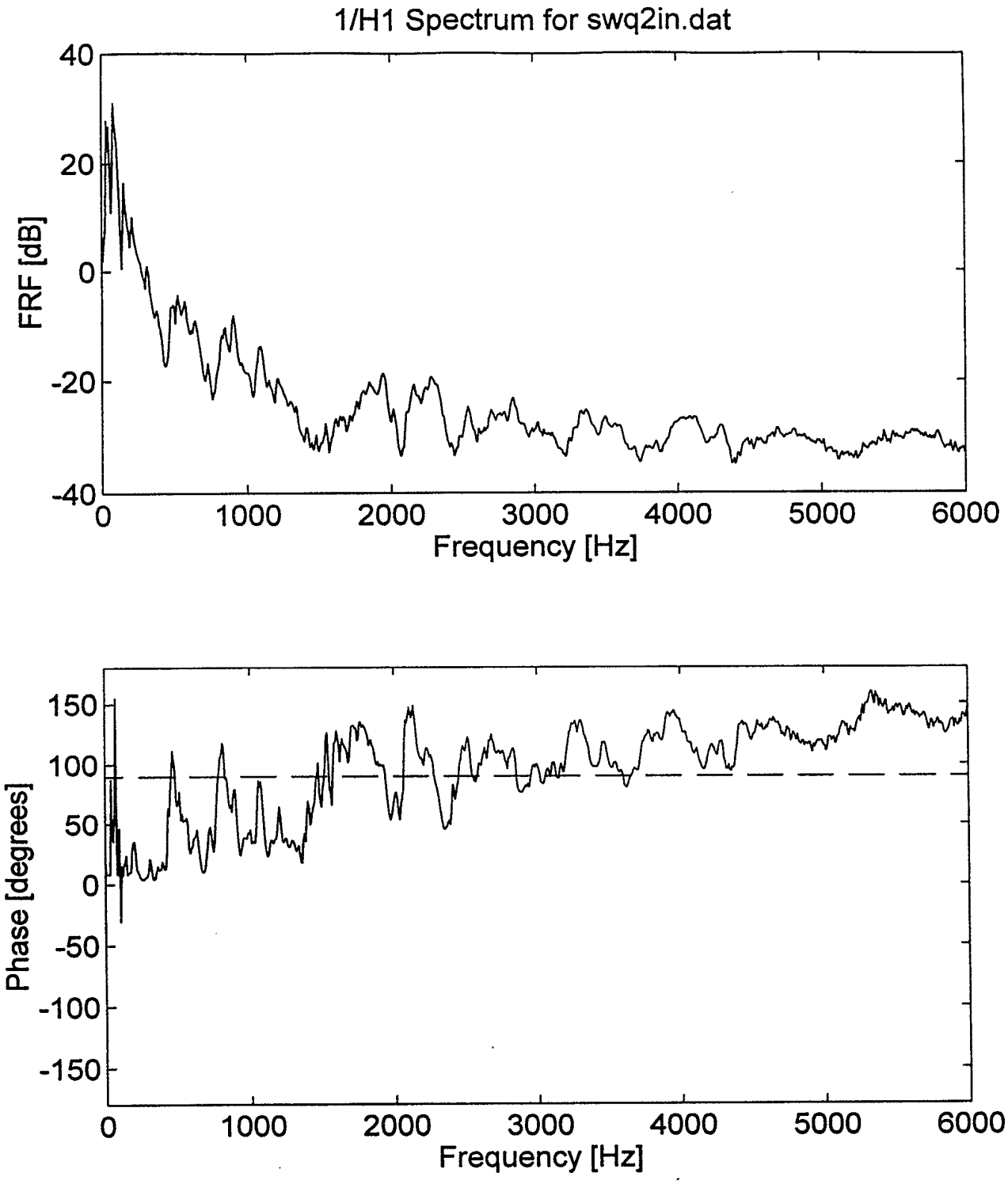

Figure 50. Frequency response function and phase of a double wall stainless steel sonar window with two layers of walls immersed in water

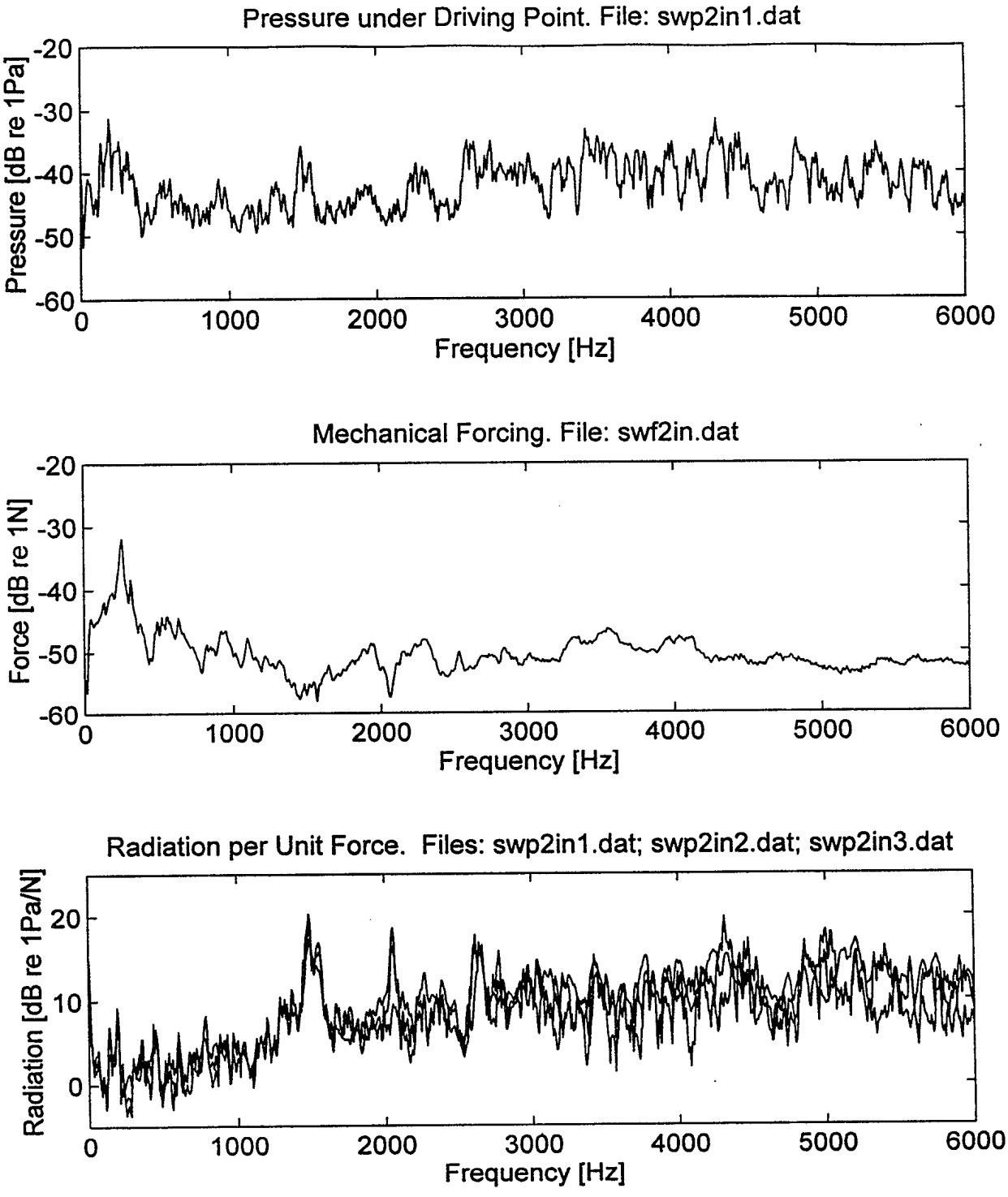

Figure 51. Pressure, force and radiation measurements of a double wall stainless steel sonar window under pseudo random mode with two layers of walls immersed in water

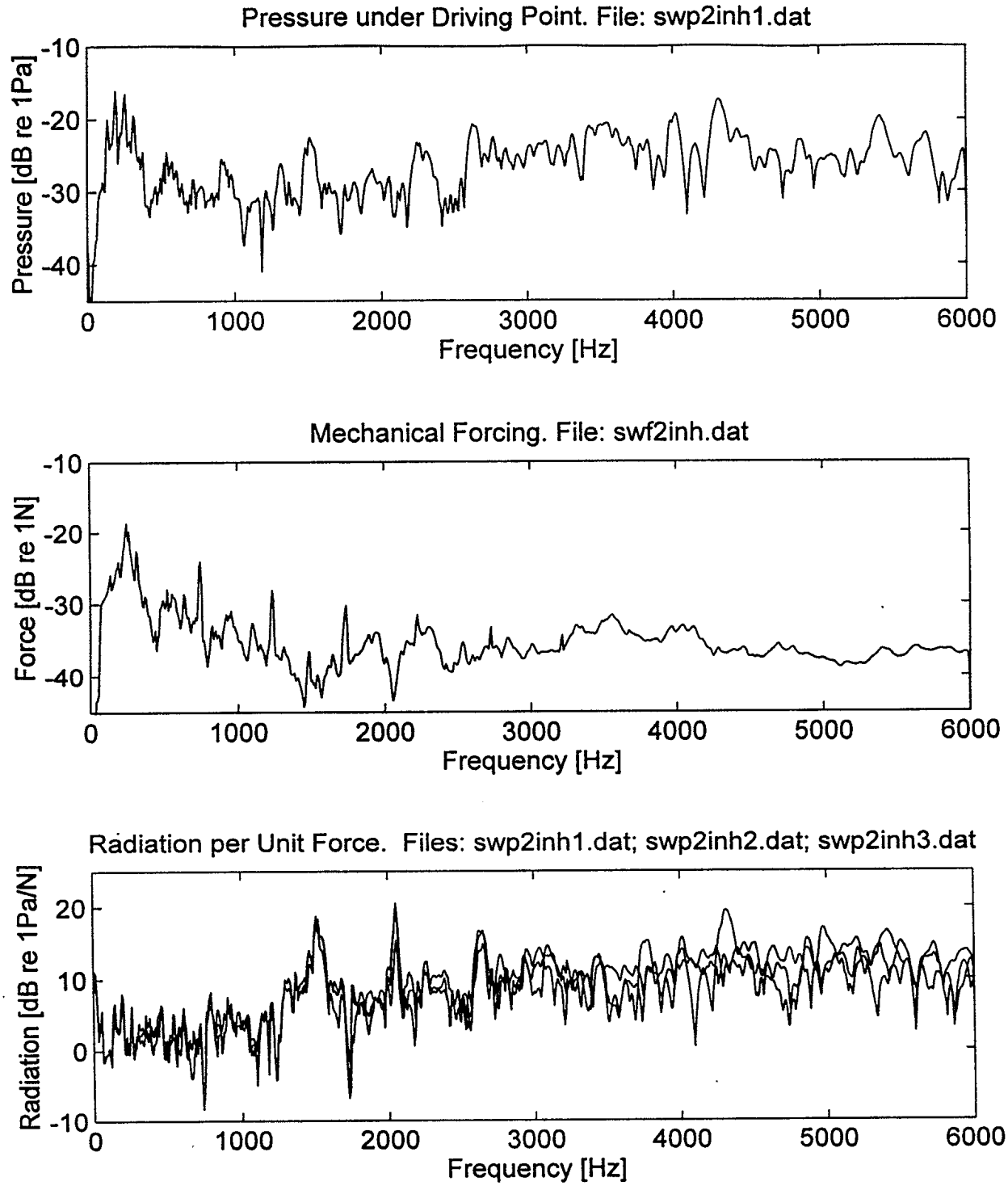

Figure 52. Pressure, force and radiation measurements of a double wall stainless steel sonar window under free run mode with two layers of walls immersed in water

APPENDICES

Appendix A. Calibration chart for B&K hydrophone Type 8103, Serial No. 1049463 . . . 91

Appendix B. Calibration chart for B&K hydrophone Type 8103, Serial No. 1049464 92

Apeendix C. Beam pattern of transmitter GILTX500 after trunctor. Fc=500 kHz, Fm=10 kHz, signal received by a B&K 8103 hydrophone 93

Appendix D. Signal level and distance off truncator, transmitter to truncator distance is 100 cm. Transmitter: GILTX500. Hydrophone: B&K 8103. Fc=500 kHz, Fm=10 kHz 94

Appendix E. System calibration chart for insertion loss measurements 95

P499040.PDF [Page: 105 of 112]

Calibration Chart for Hydrophone Type 8103

Brüel & Kjær

Serial No. 1049463

Nærum Denmark

Reference Sensitivity at 250 Hz* at 23 °C
including 6 m integral cable

Cable Capacitance 95 pF/m typical

Open Circuit Sensitivity:

Voltage Sensitivity:

-211,4 dB re 1 V/μPa**

-91,4 dB re 1 V per Pa or 26,9 μV per Pa

-111,4 dB re 1 V per μbar**

Charge Sensitivity: $95 \cdot 10^{-3}$ pC per Pa

Capacitance (including 6 m cable) 3550 pF

Frequency Response:
Individual Free Field Frequency Response Curve attached.

Date 27-1-83 Signature JD

Summarized Specifications
Usable Frequency Range: 0,1 Hz to 200 kHz (—10 dB)

Linear Frequency Range:
0,1 Hz to 20 kHz ± 1 dB
0,1 Hz to 140 kHz ± 2 dB

Horizontal Directivity 200 kHz: (XY-plane)
typical ± 2 dB

Vertical Directivity 100 kHz: (XZ-plane)
typical ± 4 dB

BC 0084

Physical:

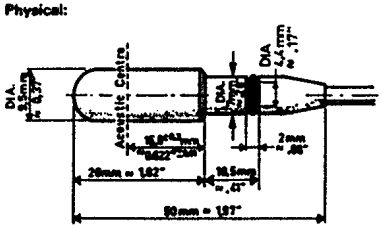

Leakage Resistance:

$> 1 \cdot 10^4$ MΩ at 23 °C

Operating Temperature Range:
—40°C to + 120°C
—40°F to + 248°F

Change of Sensitivity with Temperature:
Charge ≤ 0,03 dB/°C
Voltage ≤ —0,03 dB/°C

Change of Sensitivity with Static Pressure:
3×10^{-7} dB/Pa (0,03 dB/atm)

Temperature Transient Sensitivity: < 50 Pa/°C (ANSI S.2.11-1969); measured with B & K Charge Preamplifier Type 2626, LLF 3 Hz

Allowable Total Radiation Dose: 5×10^7 Rad

Acceleration Sensitivity: < 130 dB re 1 μPa/g

Maximum Operating Static Pressure:
40 atm

Cable:
Double shielded low noise, low capacitance integral cable: 6 m with miniature plug

Weight (incl. cable): 170 g

* Traceable to NBS
** 1 Pascal = 1 N/m² = 10 μbar

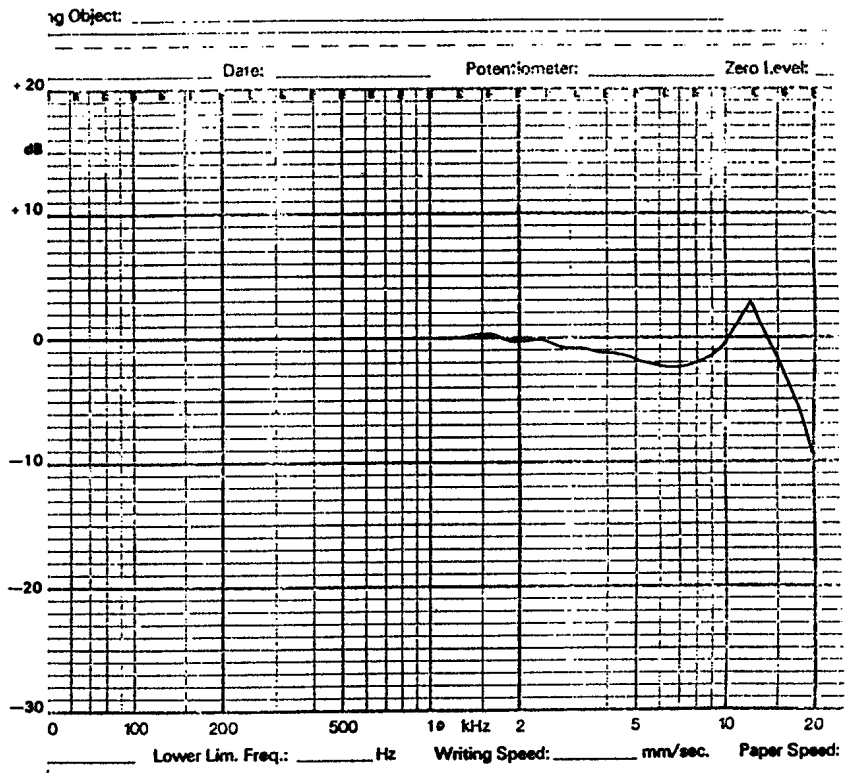

Appendix A. Calibration chart for B&K hydrophone Type 8103, Serial No. 1049463

P499040.PDF [Page: 106 of 112]

Calibration Chart for Hydrophone Type 8103

Brüel & Kjær

Nærum Denmark

Serial No. 1049464

Reference Sensitivity at 250 Hz* at 23 °C
including 6 m integral cable

Cable Capacitance 95 pF/m typical

Open Circuit Sensitivity:

Voltage Sensitivity:

− 211,7 dB re 1 V/μPa**

− 91,7 dB re 1 V per Pa or 24,0 μV per Pa

− 111,7 dB re 1 V per μbar**

Charge Sensitivity: 94 · 10⁻³ pC per Pa

Capacitance (including 6 m cable) 3630 pF

Frequency Response:
Individual Free Field Frequency Response Curve attached.

Date 27-1-83 **Signature** J.A.

Summarized Specifications
Usable Frequency Range: 0,1 Hz to 200 kHz (−10 dB)

Linear Frequency Range:
0,1 Hz to 20 kHz ± 1 dB
0,1 Hz to 140 kHz ± 2 dB

Horizontal Directivity 200 kHz: (XY-plane) typical ± 2 dB

Vertical Directivity 100 kHz: (XZ-plane) typical ± 4 dB

SC 0084

Physical:

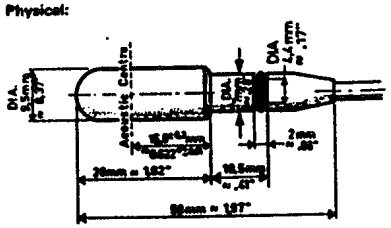

Leakage Resistance:
> 1 · 10⁴ MΩ at 23 °C

Operating Temperature Range:
−40°C to + 120°C
−40°F to + 248°F

Change of Sensitivity with Temperature:
Charge ≤ 0,03 dB/°C
Voltage ≤ −0,03 dB/°C

Change of Sensitivity with Static Pressure:
3 × 10⁻⁷ dB/Pa (0,03 dB/atm)

Temperature Transient Sensitivity: < 50 Pa/°C (ANSI S.2.11-1969); measured with B & K Charge Preamplifier Type 2626, LLF 3 Hz

Allowable Total Radiation Dose: 5×10^7 Rad

Acceleration Sensitivity: < 130 dB re 1 μPa/g

Maximum Operating Static Pressure:
40 atm

Cable:
Double shielded low noise, low capacitance integral cable: 6 m with miniature plug

Weight (incl. cable): 170 g

* Traceable to NBS
** 1 Pascal = 1 N/m² = 10 μbar

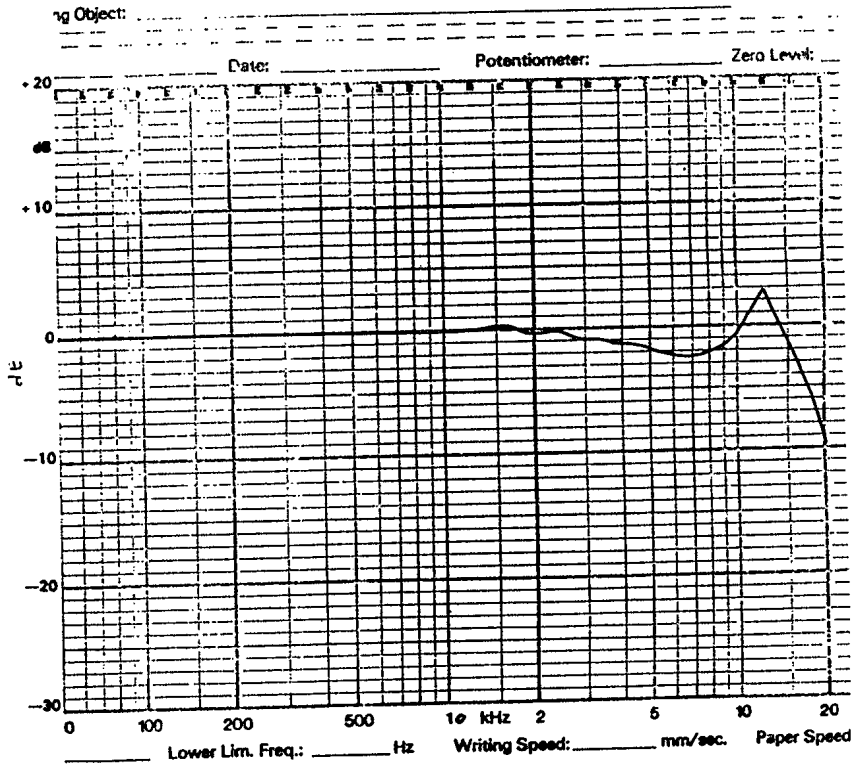

Appendix B. Calibration chart for B&K hydrophone Type 8103, Serial No. 1049464

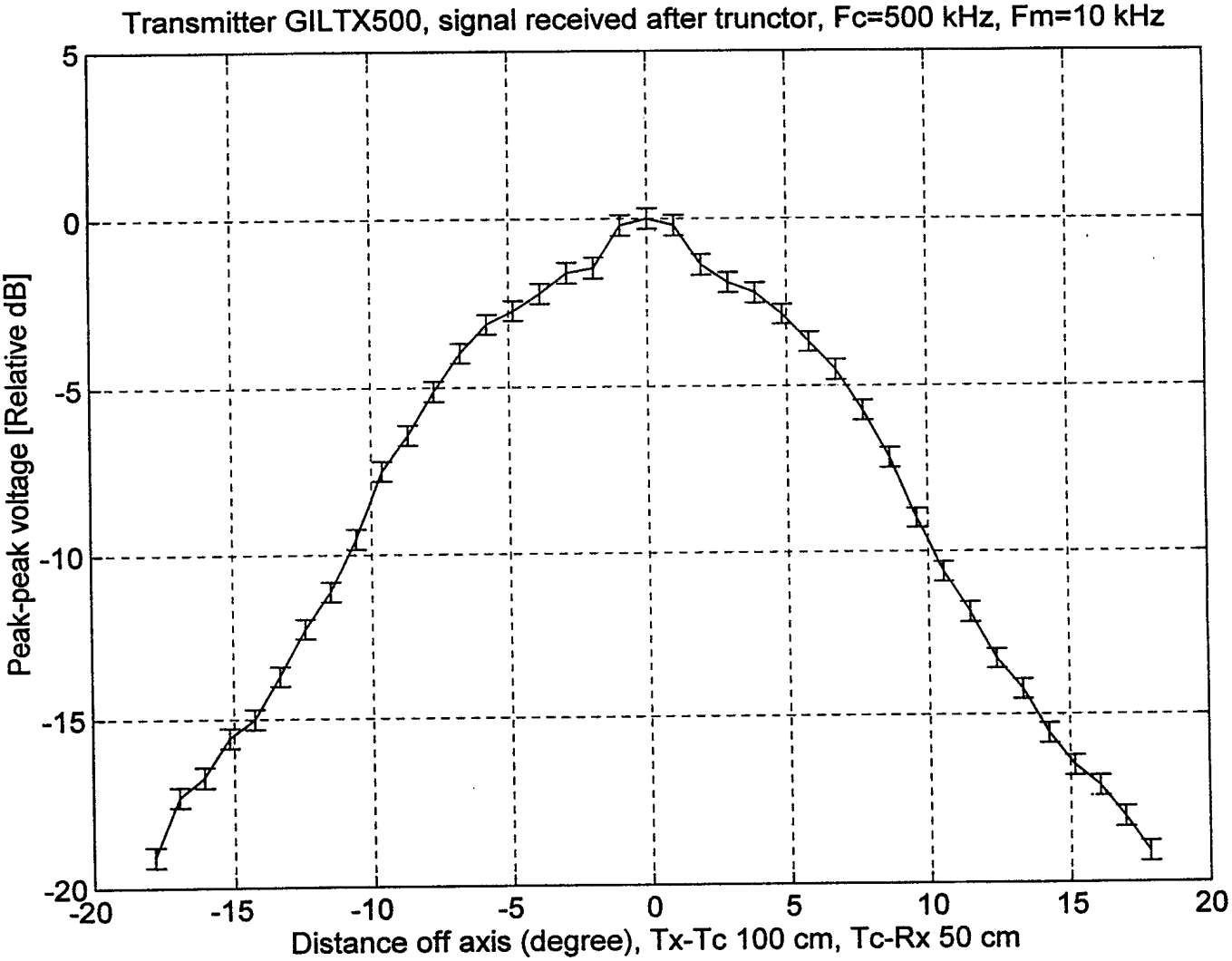

Apeendix C. Beam pattern of transmitter GILTX500 after trunctor. Fc=500 kHz, Fm=10 kHz, Signal received by a B&K 8103 hydrophone

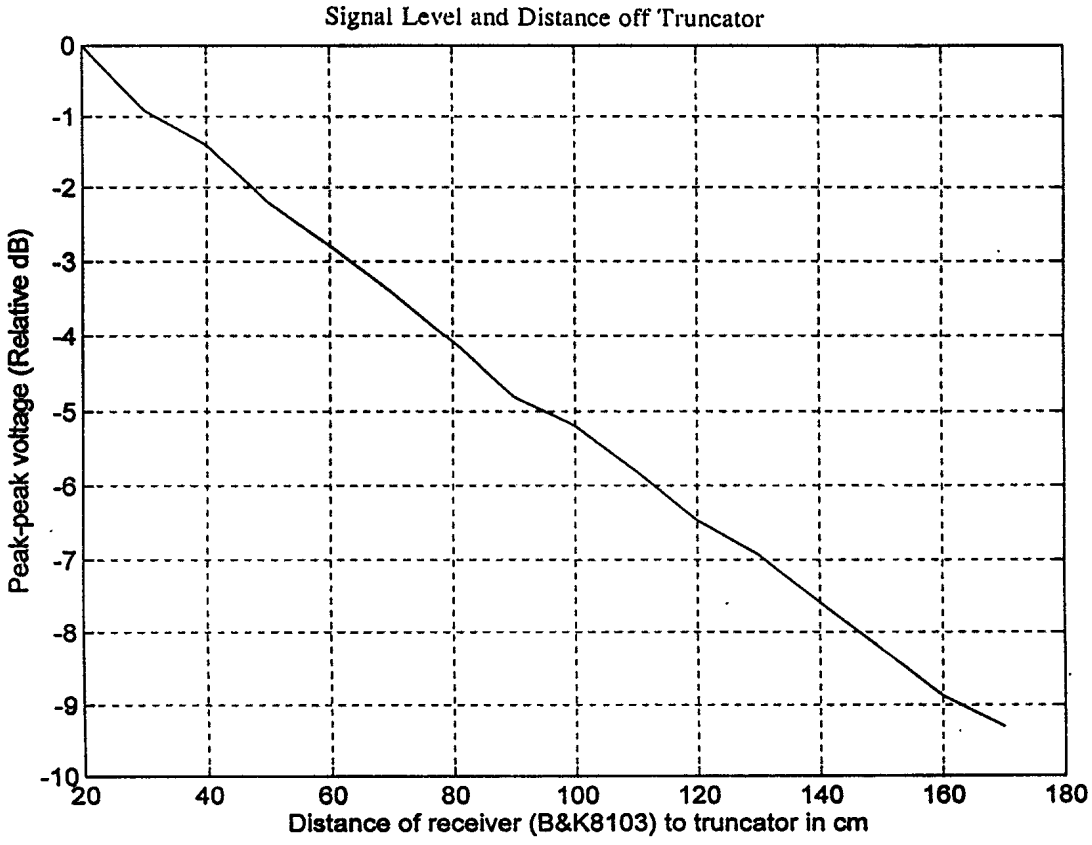

Appendix D. Signal level and distance off truncator, transmitter to truncator distance is 100 cm. Transmitter: GILTX500. Hydrophone: B&K 8103. Fc=500 kHz, Fm=10 kHz

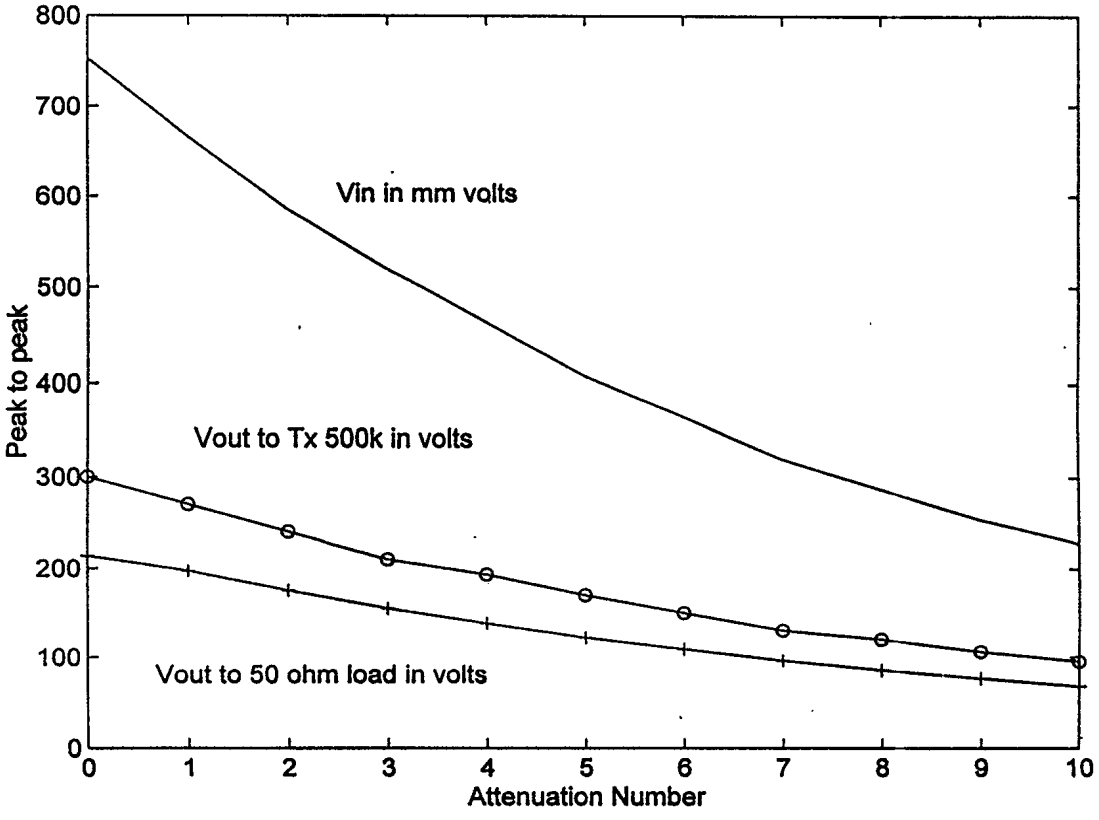

Appendix E. System calibration chart for insertion loss measurements

UNCLASSIFIED
SECURITY CLASSIFICATION OF FORM
(highest classification of Title, Abstract, Keywords)

DOCUMENT CONTROL DATA

(Security classification of title, body of abstract and indexing annotation must be entered when the overall document is classified)

1. ORIGINATOR (the name and address of the organization preparing the document Organizations for whom the document was prepared, e.g. Establishment sponsoring a contractor's report, or tasking agency, are entered in section 8.)

Guigné International Limited
82 St. Thomas Line, P.O. Box 13, Site 21
Paradise, Newfoundland A1L 1C1

2. SECURITY CLASSIFICATION (overall security classification of the document including special warning terms if applicable).

Unclassified

3. TITLE (the complete document title as indicated on the title page. Its classification should be indicated by the appropriate abbreviation (S,C,R or U) in parentheses after the title).

Acoustic Properties of Sonar Dome Materials

4. AUTHORS (Last name, first name, middle initial. If military, show rank, e.g. Doe, Maj. John E.)

Quanshun Liu and Jacques Y. Guigné

5. DATE OF PUBLICATION (month and year of publication of document)

May 1996

6a. NO OF PAGES (total containing information include Annexes, Appendices, etc).

95

6b. NO. OF REFS (total cited in document)

20

7. DESCRIPTIVE NOTES (the category of the document, e.g. technical report, technical note or memorandum. If appropriate, enter the type of report, e.g. interim, progress, summary, annual or final. Give the inclusive dates when a specific reporting period is covered).

DREA Contractor Report

8. SPONSORING ACTIVITY (the name of the department project office or laboratory sponsoring the research and development. Include the address).

Defence Research Establishment Atlantic
P.O. Box 1012
Dartmouth,N.S. B2Y 3Z7

9a. PROJECT OR GRANT NO. (if appropriate, the applicable research and development project or grant number under which the document was written. Please specify whether project or grant).

Project No. 1.f.a

9b. CONTRACT NO. (if appropriate, the applicable number under which the document was written).

W7707-4-2930/01-HAL

10a ORIGINATOR'S DOCUMENT NUMBER (the official document number by which the document is identified by the originating activity. This number must be unique to this document).

DREA/CR/96/420

10b OTHER DOCUMENT NOS. (Any other numbers which may be assigned this document either by the originator or by the sponsor).

11. DOCUMENT AVAILABILITY (any limitations on further dissemination of the document, other than those imposed by security classification)

(X) Unlimited distribution
( ) Distribution limited to defence departments and defence contractors; further distribution only as approved
( ) Distribution limited to defence departments and Canadian defence contractors; further distribution only as approved
( ) Distribution limited to government departments and agencies; further distribution only as approved
( ) Distribution limited to defence departments; further distribution only as approved
( ) Other (please specify):

12. DOCUMENT ANNOUNCEMENT (any limitation to the bibliographic announcement of this document. This will normally correspond to the Document Availability (11). However, where further distribution (beyond the audience specified in 11) is possible, a wider announcement audience may be selected).

Unlimited

UNCLASSIFIED
SECURITY CLASSIFICATION OF FORM

DCD03 2/06/87-M

UNCLASSIFIED
SECURITY CLASSIFICATION OF FORM

13. ABSTRACT (a brief and factual summary of the document. It may also appear elsewhere in the body of the document itself. It is highly desirable that the abstract of classified documents be unclassified. Each paragraph of the abstract shall begin with an indication of the security classification of the information in the paragraph (unless the document itself is unclassified) represented as (S), (C), (R), or (U). It is not necessary to include here abstracts in both official languages unless the text is bilingual).

The acoustic properties of composite panels made from high strength polyethylene Spectra Fiber were compared to conventional glass fiber composites, and to the double walled stainless steel design currently used in the C5 Sonar Dome. Characterization consisted of insertion loss measurements from 0-40 kHz using a parametric array projector, and "self noise" measurements from 0-6 kHz. All the panels but the cyanate-based 4H Spectra Fiber composite panel tested had very low insertion losses (<1 dB) below 10 kHz at normal incidence. Apart from the epoxy-based 4H panel, the Spectra Fiber composite panels had lower insertion losses, and less angular dependence of the insertion loss, than both the glass fiber composites and the double walled stainless steel panel in the 0-40 kHz range. Of the two different resin systems examined, epoxy and cyanate ester, the cyanate ester resin based composite panels had slower water uptake rates than the epoxy panels, but there was no significant difference in the insertion losses below 10 Hz. In general, the angular dependence of the insertion losses below 10 kHz was minimal with the exception of the 4H epoxy Spectra Fiber panel, which had a slightly higher angular dependence. Aging the composite panels in water resulted in some slightly reduced insertion losses, with the exception of the 4H cyanate Spectra Fiber panel. The self noise experiments consisted of measuring the radiated sound produced by a mechanically excited panel placed at the air/water interface in a reverberant tank. Comparison of the composite panels to the stainless steel dome section was complicated by the rigidity of the stainless steel structure, which produced few modes in the frequency range studied.

14. KEYWORDS, DESCRIPTORS or IDENTIFIERS (technically meaningful terms or short phrases that characterize a document and could be helpful in cataloguing the document. They should be selected so that no security classification is required. Identifiers, such as equipment model designation, trade name, military project code name, geographic location may also be included. If possible keywords should be selected from a published thesaurus, e.g. Thesaurus of Engineering and Scientific Terms (TEST) and that thesaurus-identified. If it not possible to select indexing terms which are Unclassified, the classification of each should be indicated as with the title).

sonar dome
Spectra Fiber
insertion loss

P499040.PDF [Page: 112 of 112]

NO. OF COPIES NOMBRE DE COPIES	COPY NO. COPIE N°	INFORMATION SCIENTIST'S INITIALS INITIALES DE L'AGENT D'INFORMATION SCIENTIFIQUE
1	1	JC

AQUISITION ROUTE ▶ FOURNI PAR	DREA
DATE ▶	06 Aug 96
DSIS ACCESSION NO. ▶ NUMÉRO DSIS	

DND 1158 (6-87)

National Defence / Défense nationale

499040

PLEASE RETURN THIS DOCUMENT TO THE FOLLOWING ADDRESS:

DIRECTOR
SCIENTIFIC INFORMATION SERVICES
NATIONAL DEFENCE
HEADQUARTERS
OTTAWA, ONT. - CANADA K1A 0K2

PRIÈRE DE RETOURNER CE DOCUMENT À L'ADRESSE SUIVANTE:

DIRECTEUR
SERVICES D'INFORMATION SCIENTIFIQUES
QUARTIER GÉNÉRAL
DE LA DÉFENSE NATIONALE
OTTAWA, ONT. - CANADA K1A 0K2